Investigation of the metabolic and energetic states of antibody producing CHO cells for process intensification in fed-batch and perfusion cultivations

Dissertation

Von der Fakultät Energie-, Verfahrens- und Biotechnik der Universität Stuttgart zur Erlangung der Würde eines Doktor-Ingenieurs (Dr.-Ing.) genehmigte Abhandlung

Vorgelegt von:

Max Becker

aus Münster

Hauptberichter: Prof. Dr.-Ing. Ralf Takors

Mitberichter: Prof. Dr. Roland Kontermann

Tag der mündlichen Prüfung: 05.12.2019

Institut für Bioverfahrenstechnik

University of Stuttgart
Germany

2019

Für Maike

Danksagung

Zuerst möchte ich Herrn Prof. Dr.-Ing. Ralf Takors für die Möglichkeit danken, meine Promotion mit dieser spannenden Aufgabenstellung am IBVT durchzuführen. Darüber hinaus danke ich ihm für die Diskussionen über offene Fragestellungen und Ergebnisse, aber auch die Freiheiten bei der Durchführung der Arbeit.

Meinen Dank möchte ich auch Herrn Prof. Dr. Roland Kontermann aussprechen für die Übernahme der Mitberichterschaft.

Meinen Ansprechpartnern bei Boehringer Ingelheim Jan Bechmann und Raphael Voges danke ich für die unkomplizierte Zusammenarbeit und die Möglichkeit, mich jederzeit mit neuem Medienbedarf melden zu können.

Bei allen Festangestellten und technischen Mitarbeitern am Institut, die mit Ihrer Unterstützung die täglichen Arbeiten erst möglich gemacht haben und mit ihrer positiven Art immer für einen Plausch zu haben waren, bedanke ich mich: Frau Reu im Sekretariat sowie Alex, Andreas und Salah in technischen Fragen (inklusive guter Sprüche). Darüber hinaus Mira in Sachen HPLC Analytik und Martin für die vielen Anträge an die Verwaltung.

Herzlicher Dank geht an die vielen Kollegen, die zu Freunden geworden sind und die mir die Zeit am Institut über all die Jahre verschönert haben:

Für die schönen Zeiten in unserem abgelegenen Zellkulturlabor, gegenseitige Unterstützung in Sachen Labor und Promotion, sowie Gespräche über jeden Unsinn und das Essen von reichlich Kuchen danke ich all meinen Bürokollegen, aber vor allem Lisa, Vikas, Natascha und Jennifer.

Bei Jurek, Andrés, Annette, Salah, Kraml und Attila bedanke ich mich für die Feierabendbierchen, gemeinsamen Essen oder auch einfach Pausen am Institut, die für die nötige Ablenkung gesorgt haben.

Schwandy, Robert und Sebastian danke ich für die lustigen Abende in der Sportsbar, die Fußballrunden mit dem Institut und Ihren bemühten Einsatz mich beim Managerspiel zu schlagen.

Meinen Studenten Lisa Stepper, Birgit Salzmann und Felix Oster danke ich für ihre erfolgreichen Arbeiten rund um meine Promotion sowie die angenehme Zusammenarbeit.

Zuletzt möchte ich meinen Eltern und meinen Brüdern mitsamt ihren Familien für den Zuspruch und die Ablenkung auch in schwierigen Phasen danken.

Mein ganz besonderer Dank gilt Maike für Ihre Unterstützung und Motivation, aber auch Ihre Gesellschaft in den vielen gemeinsamen Stunden des Schreibens, die mir vieles erleichtert haben.

Contents

Declaration of Originality **VII**

Nomenclature **IX**

List of Figures **XV**

List of Tables **XIX**

Zusammenfassung **1**

Abstract **5**

1 Introduction and Motivation **7**

1.1 Introduction 7

1.2 Motivation 9

2 Theoretical Background **11**

2.1 Chinese hamster ovary cells 11

2.2 Metabolism 13

2.2.1 Main carbon metabolism 13

2.2.2 Energy generation and redox balance 15

2.3 Flux analysis in CHO cells 18

2.4 Fed-batch processes 22

2.4.1 Process overview and performance 23

2.4.2 Parameters influencing process performance 24

2.5 Perfusion processes 25

3 Materials and Methods **31**
3.1 Materials . . . 31
3.1.1 Chemicals . . . 31
3.1.2 Consumables . . . 33
3.1.3 Hardware . . . 34
3.1.4 Software . . . 35
3.1.5 Antibodies for ELISA . . . 36
3.1.6 Buffers and Solutions . . . 36
3.2 Methods . . . 39
3.2.1 Cryoconservation . . . 39
3.2.2 Seed Train . . . 39
3.2.3 Bioreactor Cultivation . . . 40
3.2.4 Analytics . . . 46
3.2.5 Cell specific Rates . . . 50
3.2.6 Flux Balance Analysis . . . 51

4 Results **53**
4.1 Fed-Batch . . . 53
4.1.1 Cellular phenotype and product formation under the influence of pH and pCO_2 . . . 53
4.1.2 Intracellular flux distributions and balancing of ATP and carbon 61
4.1.3 Intracellular pool sizes of glycolysis, TCA and nucleotides in fed-batch phases . . . 70
4.2 Perfusion . . . 75
4.2.1 Growth and metabolic state in reference and glucose-limited steady-states . . . 75
4.2.2 Flux balance analysis and cellular energetic and redox state . . . 79
4.2.3 Intracellular pool sizes of glycolysis, TCA and adenylate nucleotides in perfusion steady-states . . . 85

5 Discussion **89**
5.1 Fed-Batch 89
5.1.1 Early elevated CO_2 and late decreased pH influence growth and induce changes in production kinetics 90
5.1.2 Adjusmtens of intracellular fluxes and energetic state 92
5.1.3 Metabolic adaptations of intracellular pool sizes in different fed-batch phases 95
5.2 Perfusion 97
5.2.1 Impact of glucose availability on cell density and main metabolism 97
5.2.2 Adaptations in ATP formation and cellular redox state and effect on productivity 100
5.2.3 Changes in perfusion mode affect intracellular pool sizes of glycolysis, TCA and adenylate nucleotides 103
5.3 Conclusion 105

References **109**

Appendix A Manuscript I **123**

Appendix B Manuscript II **137**

Appendix C List of Publications and Author Contribution **149**

Declaration of Originality

I declare that the submitted work has been completed by me and that I have not used any other than permitted reference sources or materials. All references and other sources used by me have been appropriately acknowledged in the work.

Hiermit erkläre ich, dass ich die vorliegende Arbeit selbstständig angefertigt habe. Es wurden von mir nur die in der Arbeit ausdrücklich benannten Quellen und Hilfsmittel benutzt. Übernommenes Gedankengut wurde von mir als solches kenntlich gemacht.

Stuttgart, den 10.03.2020
Ort, Datum

Max Becker

Nomenclature

$2PG$	2-Phosphoglyceric acid
$3PG$	3-Phosphoglyceric acid
μ	Growth rate
AA	Amino acids
$Acetyl-CoA$	Acetyl coenzyme A
ADP	Adenosine diphosphate
Ala	Alanine
AMP	Adenosine monophosphate
$AMPK$	AMP-activated protein kinase
Asn	Asparagine
Asp	Aspartate
ATP	Adenosine triphosphate
B	Bleed rate
BHK	Baby hamster kidney
c	Concentration of compound
c^{T}	Transposed vector of weights
CHO	Chinese hamster ovary

cisAco	Cis-aconitate
Cit	Citrate
CO_2	Carbon dioxide
COBRA	Constraint-Based Reconstruction and Analysis
COP	CO_2 stressed fed-batch process
DHAP	Dihydroxyacetone phosphate
DHFR	Dihydrofolate reductase
dMFA	Dynamic metabolic flux analysis
DNA	Deoxyribonucleic acid
EC	Energy charge
ELISA	Enzyme-linked immunosorbent assay
F6P	Fructose 6-phosphate
f_{CO_2}	Fraction of CO_2
$FADH_2$	Flavin adenine dinucleotide
FBA	Flux balance analysis
Fum	Fumarate
G6P	Glucose 6-phosphate
GAP	Glyceraldehyde 3-phosphate
Glc	Glucose
Gln	Glutamine
Glu	Glutamate
Gly	Glycine

*GRP*78	Binding immunoglobulin protein
GS	Glutamine synthethase
GTP	Guanosine triphosphate
HEK	Human embryonic kidney
His	Histidine
HPLC	High-performance liquid chromatography
IgG	Immunoglobulin G
Ile	Isoleucine
Iso	Isocitric acid
KOH	Potassium hydroxide
Lac	Lactate
LC – MS	Liquid chromatography–mass spectrometry
Leu	Leucine
Lys	Lysine
M	Molarity in mol/L
mAb	Monoclonal antibody
Mal	Malate
Met	Methionine
MFA	Metabolic flux analysis
Na_2CO_3	Sodium carbonate
NAD	Nicotinamide adenine dinucleotide (oxidized)
NADH	Nicotinamide adenine dinucleotide

$NADPH$	Nicotinamide adenine dinucleotide phosphate
NOB	Fed-batch process with no base titration
$NS0$	Mouse myeloma
OPA	Ortho-phtaldialdehyde
$Oxal$	Oxaloacetate
P	Perfusion rate
$P/O\ Ratio$	Phosphate/Oxygen Ratio
pCO_2	Partial pressure of carbon dioxide
PEP	Phosphoenolpyruvic acid
Phe	Phenylalanine
pKS	Acidic dissociation constant
PPP	Pentose phosphate pathway
Pyr	Pyruvate
Q	Volumetric production rate
q	Cell specific production or consumption rate
R	Redox variable
$R5P$	Ribose 5-phosphate
REF	Reference fed-batch process
RNA	Ribonucleic acid
rpm	Revolutions per minute
S	Stoichiometric matrix
Ser	Serine

SS	Steady-state
$Succ$	Succinate
$Succinyl-CoA$	Succinyl coenzyme A
TCA	Tricarboxylic acid cycle
TFF	Tangential flow filtration
Thr	Threonine
Trp	Tryptophane
V	Liquid bioreactor volume
v	Flux vector
Val	Valine
VCD	Viable cell density
X_{V}	Viable cell density
Z	Objective function

List of Figures

1.1 Global annual sales for biopharmaceuticals 8

2.1 Percentage of biopharmaceuticals produced in mammalian systems . . . 12
2.2 Simplified scheme of the main carbon metabolism 17
2.3 Workflow of flux balance analysis 21
2.4 Schematic representation of the three main cultivation modes batch, fed-batch and perfusion 22
2.5 Different published cell retention devices used for perfusion processes . 29

3.1 Simplified scheme of the perfusion cultivation 44

4.1 Profiles of pH, pCO_2 and osmolality over the process time for the three settings REF, COP and NOB 55
4.2 Profiles of viable cell density and growth rate over the process time for the three settings REF, COP and NOB 56
4.3 Profiles of antibody concentration and cell specific antibody productivity over the process time for the three settings REF, COP and NOB . . . 57
4.4 Profiles of glucose concentration and cell specific glucose uptake rate over the process time for the three settings REF, COP and NOB 58
4.5 Profiles of lactate concentration and cell specific lactate production rate over the process time for the three settings REF, COP and NOB 59
4.6 Cell specific antibody productivity as a function of growth rate for the three settings REF, COP and NOB 60
4.7 Profile of the volumetric productivity of the antibody over the process time for the three settings REF, COP and NOB 61

4.8 Simplified main carbon metabolism representing the results of the flux balance analysis during the growth phase for the three settings REF, COP and NOB 62
4.9 Simplified main carbon metabolism representing the results of the flux balance analysis during the early stationary phase for the three settings REF, COP and NOB 63
4.10 Simplified main carbon metabolism representing the results of the flux balance analysis during the early decline phase for the three settings REF, COP and NOB 64
4.11 Cell specific ATP production rates during growth phase, early stationary phase and early decline phase for the three settings REF, COP and NOB 66
4.12 Cell specific lactate production rate combined for all three settings REF, COP and NOB as function of the redox variable R 67
4.13 Cell specific antibody productivity combined for all three settings REF, COP and NOB as function of the redox variable R 68
4.14 Carbon balances showing the main fractions for incoming and outgoing carbon during the growth phase for the three settings REF, COP and NOB 69
4.15 Carbon balances showing the main fractions for incoming and outgoing carbon during the early stationary phase for the three settings REF, COP and NOB 70
4.16 Carbon balances showing the main fractions for incoming and outgoing carbon during the early decline phase for the three settings REF, COP and NOB 71
4.17 Intracellular pool sizes of intermediates of glycolysis for the three settings REF, COP and NOB 72
4.18 Intracellular pool sizes of intermediates of TCA for the three settings REF, COP and NOB 73
4.19 Intracellular pool sizes of nucleotides and the corresponding adenylate energy charge for the three settings REF, COP and NOB 74
4.20 Profile of viable cell density over the process time for the three perfusion steady-states 76
4.21 Main cell specific rates for the three perfusion steady-states 79

4.22 Simplified main carbon metabolism representing the results of the flux balance analysis for the three perfusion steady-states 80
4.23 Cell specific ATP production rates for the three perfusion steady-states . 81
4.24 Cell specific antibody productivity and volumetric productivity as a function of ATP formation due to oxidative phosphorylation for the three perfusion steady-states 82
4.25 Carbon balances showing the main fractions for three perfusion steady-states 83
4.26 Cell specific lactate production rate for the three perfusion steady states as function of the redox variable R 84
4.27 Cell specific antibody production rate for the three perfusion steady states as function of the redox variable R 85
4.28 Intracellular pool sizes of intermediates of glycolysis for the three perfusion steady-states 86
4.29 Intracellular pool sizes of intermediates of TCA for the three perfusion steady-states 87
4.30 Intracellular pool sizes of nucleotides and the corresponding adenylate energy charge for the three perfusion steady-states 88

List of Tables

3.1 Chemicals 31
3.2 Consumables 33
3.3 Hardware 34
3.4 Software 35
3.5 Antibodies 36
3.6 Buffers and solutions 36
3.7 Seed train steps and volumes 40
3.8 Parameter setpoints Fed-Batch 41
3.9 Controller settings Fed-Batch 42
3.10 Parameter setpoints Perfusion 43
3.11 Perfusion settings and flowrates 45

4.1 Viable cell density, bioreactor antibody and metabolite concentrations during the three perfusion steady states 77
4.2 pH and partial pressure of CO_2 during perfusion 78

Zusammenfassung

Die heutige biopharmazeutische Industrie verlässt sich hauptsächlich auf großskalige Fed-Batch Prozesse mit tierischen Zellen, um möglichst hohe Produkttiter zu erreichen. Jedoch führen, aufgrund von höheren Mischzeiten in Bioreaktoren im Produktionsmaßstab, Inhomogenitäten zu Zonen vermehrten Stresses und damit schlussendlich zu verminderten volumetrischen Produktivitäten. Leistungsdaten der Zellen wie Wachstum, Produktivität und Nebenproduktbildung werden dabei durch verschiedene Stressfaktoren beeinflusst. Unter anderem bilden der Partialdruck von CO_2 (pCO_2) und der pH-Wert solche Inhomogenitäten, die die Leistung von Produktionsprozessen beeinflussen. Die zugrundeliegenden metabolischen Anpassungen, die dabei letztendlich zu einem Verlust der Produktivität führen, sind bisher noch nicht komplett verstanden. Mögliche Alternativen für übliche Fed-Batch Prozesse können Perfusionsprozesse sein. Als kontinuierliche Prozesse mit Zellrückhaltung können sie Zelldichten erreichen, die ein Vielfaches höher liegen als in Fed-Batch Kultivierungen. Darüber hinaus müssen aber auch zellspezifische Produktivitäten maximiert werden, um bessere volumetrische Produktivitäten zu liefern. Nur dann kann Perfusion intensivierte Prozesse hervorbringen, welche ökonomische Effizienz in deutlich kleinerem Maßstab gewährleisten.

Diese Arbeit soll die metabolischen Anpassungen von CHO Zellen in sowohl Fed-Batch Kultivierungen als auch Perfusionsprozessen unter variierenden Prozessbedingungen aufklären. Die Energieversorgung in Form von ATP wurde dabei als Bindeglied zwischen Metabolismus und zellspezifischer Produktivität genutzt. Für die Fed-Batch Kultivierungen wurde der Einfluss von pCO_2 und pH-Veränderungen verdeutlicht. Früher CO_2 Stress mit Partialdrücken bis zu 200 mbar führte zu einem zeitweisen Anstieg in der zellspezifischen Produktivität bis hin zu 23 pg/Zelle/Tag. Jedoch zeigten die Zellen kurz darauf nur noch eine verringerte intrazelluläre ATP Poolgröße von 2,5 fmol/Zelle. Gleichzeitig stieg die zellspezifische Laktatbildung deutlich (um 80 %) an, während die Produktivität schnell abfiel, obwohl pCO_2 wieder im Bereich der Referenzwerte

lag. In einem zweiten Prozess resultierte eine pH Absenkung in Richtung 6,70 in kontinuierlich ansteigenden zellspezifischen Produktivitäten bis hin zu einem Maximalwert von 20 pg/Zelle/Tag. Zudem wurde keine Laktatbildung beobachtet, da sämtlicher Kohlenstoff aus der Glukose in den TCA geleitet wurde. Interessanterweise waren die damit zusammenhängenden intrazellulären ATP Konzentrationen auch in der stationären Phase konstant bei 4 - 5 fmol/Zelle und damit erhöht im Vergleich zu sowohl dem CO_2 gestressten Prozess (2,5 fmol/Zelle), als auch dem Referenzprozess (weniger als 1 fmol/Zelle). Ebenso zeigte nur der Prozess mit sinkendem pH-Wert über den ganzen Prozess stabile ATP Bildungsraten von 25.000 fmol/Zelle/Tag wie die Flussanalysen zeigten.

Für den Perfusionsprozess wurde Glukoselimitierung als Methode zur Verbesserung der metabolischen Effizienz und der damit zusammenhängenden zellspezifischen Produktivitäten verwandt. Insgesamt wurden in der Perfusion drei verschiedene steady-states verglichen, wobei einer ohne offensichtliche Limitierung zwei glukoselimitierten steady-states gegenüberstand. Demzufolge führte die Glukoselimitierung zu einem vorteilhaften metabolischen Zustand, in dem die Zellen verringerte Glukoseaufnahme (30 %) und Laktatbildung (75 %) zeigten. Darüber hinaus waren die zellspezifischen Produktivitäten über mehrere Tage konstant bei Werten von 15 pg/Zelle/Tag und damit um 50 % erhöht gegenüber dem nicht-limitierten steady-state. Wie in den Fed-Batch Kultivierungen beobachtet, war die zellspezifische Produktivität mit der ATP Versorgung verknüpft. Darüber hinaus konnten aufgrund der verschiedenen steady-state Bedingungen noch genauere Erkenntnisse gewonnen werden: Aufgeschlüsselt auf den Ursprung des ATP zeigte die respiratorische ATP Versorgung starke Korrelationen mit der Antikörperproduktivität. Während der glukoselimitierten steady-states wurde der meiste Kohlenstoff aus der Glukose in den TCA geleitet. Folglich wurde einhergehend mit der niedrigen Laktatbildung mehr NADH in die Mitochondrien für die oxidative Phosphorylierung transportiert. Im Vergleich mit dem steady-state mit Glukose im Überschuss, war die ATP Versorgung aus der oxidativen Phosphorylierung um fast ein Drittel erhöht.

Schlussfolgernd zeigen die Resultate aus Fed-Batch- und Perfusionsprozessen den deutlichen Einfluss der Prozessbedingungen auf den zellulären Metabolismus und die damit zusammenhängende Energieverfügbarkeit. Darüber hinaus ist die resultierende spezifische Produktivität stark abhängig von der ATP Bereitstellung. Wie diese Arbeit zeigt, ist die ATP Versorgung anfällig für Veränderungen in pCO_2 und pH-Wert, so-

dass bereits Zellen, welche nur kurzzeitig Inhomogenitäten nach dem Scale-up erleben, die Prozessleistung beeinflussen können. Auf der anderen Seite kann die Glukoselimitierung für die Prozessintensivierung im Perfusionsbetrieb genutzt werden, da sie die Effizienz Kohlenstoff betreffend und damit auch die ATP Bereitstellung aus der oxidativen Phosphorylierung erhöht. Dadurch wird die zellspezifische Produktivität gesteigert, sodass infolgedessen Perfusionsprozesse mit bereits hohen Zelldichten verbesserte volumetrische Produktivitäten erreichen.

Abstract

Today's biopharmaceutical industry mostly relies on large-scale fed-batch processes with mammalian cells to reach highest possible product titers. However, due to higher mixing times in production scale bioreactors, inhomogeneities lead to zones of increased stress inside the bioreactor and consequently to diminished volumetric productivities. Especially cellular performance parameters like growth, productivity and by-product formation are influenced by various stress factors. Among others, the partial pressure of CO_2 (pCO_2) and pH are known to form such inhomogeneities influencing the performance of production processes. The underlying metabolic adaptations finally leading to the loss in productivity are not yet fully understood. Possible alternatives for common fed-batch processes can be perfusion processes. As continuous processes using cell retention they can reach cell densities multiple times higher than in fed-batch cultivations. But additionally, cell specific productivities have to be maximized to yield superior volumetric productivities. Only then, perfusion can provide intensified processes which guarantee economic efficiency in much smaller scale.

This thesis aims at unraveling metabolic adaptations made by CHO cells in both fed-batch cultivations and perfusion processes under varying process conditions. The energy supply in form of ATP was used as link from metabolism to cell specific antibody productivities. For the fed-batch cultivations the impact of pCO_2 and pH shifts were elucidated, typical for cells experiencing large scale inhomogeneities. Early CO_2 stress with partial pressures of up to 200 mbar led to a temporary increase in cell specific producitivity towards 23 pg/cell/day. However, shortly after cells showed diminishing intracellular ATP pool sizes towards 2.5 fmol/cell. Simultaneously, cell specific lactate production increased severely (80 %), while the productivity fell quickly although pCO_2 was back to reference values. On the other side, a pH down-shift towards pH 6.70 resulted in continuously rising cell specific productivities to peak values of 20 pg/cell/day. Additionally, no lactate formation was observed since all carbon from glucose was fueling

the TCA cycle. Interestingly, related intracellular ATP concentrations were constant at 4-5 fmol/cell even in the stationary phase and therefore elevated compared to both CO_2 stressed (2.5 fmol/cell) and reference conditions (below 1 fmol/cell). Likewise, only the pH shifted process showed stable ATP formation rates of about 25,000 fmol/cell/day throughout the process as flux analysis revealed.

For the perfusion glucose limitation was applied as method to improve metabolic efficiency and the interrelated cell specific productivities. In total, three different perfusion steady states were compared, where one steady state without any apparent limitation contrasted two glucose-limited steady states. As a result, glucose limitation led to a beneficial metabolic state where cells showed decreased glucose uptake (30 %) and lactate formation (75 %). Furthermore, cell specific productivities were constant at about 15 pg/cell/day for several days. Therefore, the values were increased by 50 % compared to the non-limited steady-state. Like observed in the fed-batch cultivations, the cell specific productivity was connected to the ATP supply. Moreover, due to the different steady state conditions even more precise findings could be made: Broken down to the origin of ATP, respiratory ATP supply showed strong correlation to the antibody productivity. During the glucose limited steady states most of the carbon coming from glucose was fueled into TCA. Consequently, along with the lower lactate formation, more NADH was transported into mitochondria for oxidative phosphorylation. In comparison to the steady state with excess glucose ATP supply from oxidative phosphorylation was increased by almost one third.

In conclusion, the results from both fed-batch and perfusion processes show the strong influence of process conditions on the cellular metabolism and the interrelated energy availability. Furthermore, the resulting specific productivity is strongly dependent on ATP supply. As this work shows, ATP supply is prone to variations in pCO_2 and pH, so that cells experiencing only short term inhomogeneities after scale-up can alter the overall process performance. On the other side, glucose limitation can be used for process intensification in perfusion mode as it significantly increases the carbon efficiency and therefore the ATP supply from oxidative phosphorylation. Hereby, the cell specific productivity is boosted and consequently perfusion processes, already having high cell densities, can reach enhanced volumetric productivities.

1 Introduction and Motivation

1.1 Introduction

The global market for biopharmaceutical products is continually growing. Concurrently increasing annual sales provide a major reason for the development of optimized production processes (Gaughan, 2016; Walsh, 2014; Morrison & Lähteenmäki, 2017). From 2010 to 2016 the global annual sales nearly doubled from 107 to 202 Billion US-$, while the sales for the top 10 biopharmaceuticals alone increased by about a third to 76 Billion US-$ (figure 1.1, Walsh (2014); Morrison and Lähteenmäki (2017)). The biopharmaceutical products comprise many categories like antibodies, blood factors, hormones, fusion proteins, vaccines and many more (Aggarwal, 2014). However, monoclonal antibodies produced by Chinese hamster ovary (CHO) cells have a major share of the top-selling drugs in the past decade (Ecker, Jones, & Levine, 2015). In the past years, an increasing number of expiring patent protections and the resulting emergence of biosimilar products have put pressure on current first-generation production processes (Mullard, 2012; Gaughan, 2016).

As typical large-scale production processes for biopharmaceuticals, fed-batch cultivations remain in the focus of process optimization. Accordingly, maximum cell densities and product titers in current fed-batch processes have increased substantially up to $30x10^6$ cells/mL and more than 10 g/L (Wurm, 2004; Kunert & Reinhart, 2016; Zboray et al., 2015). After successful cell line engineering and media optimization, numerous process parameters can still influence the volumetric productivity (Birch & Racher, 2006; Shukla & Thömmes, 2010; Seth, Hossler, Yee, & Hu, 2006). Especially during large-scale cultivations several parameters can cause inhomogeneities inside the bioreactor, eventually leading to deterioration in overall performance concering cellular growth and productivity. Identification of these parameters and their impact on process performance is therefore crucial for the success of large-scale production processes.

Alternatively to large-scale fed-batch processes, an economic production of biopharmaceuticals can also be achieved by the intensification of production processes, aiming at higher volumetric productivities in smaller production scales. By applying cell retention in continuous mode, perfusion processes can provide long-term operation at high cell densities (Clincke, Molleryd, Zhang, et al., 2013; Clincke, Molleryd, Samani, et al., 2013; Voisard, Meuwly, Ruffieux, Baer, & Kadouri, 2003; Bielser, Wolf, Souquet, Broly, & Morbidelli, 2018). In comparison to fed-batch processes, multiple times higher viable cell densities of more than $100x10^6$ cells/mL are possible (Clincke, Molleryd, Zhang, et al., 2013; Clincke, Molleryd, Samani, et al., 2013; Warikoo et al., 2012). Therefore, elevated volumetric productivities make production processes in medium-scale economically feasible (Croughan, Konstantinov, & Cooney, 2015). However, cell specific productivities need to remain high throughout the long-term perfusion to maximize volumetric productivity and to compete with established fed-batch processes (Steinebach et al., 2017; Bausch, Schultheiss, & Sieck, 2018). Optimization strategies for culture conditions which enhance the cellular productivity can therefore contribute to perfusion as an intensified biopharmaceuticals production alternative.

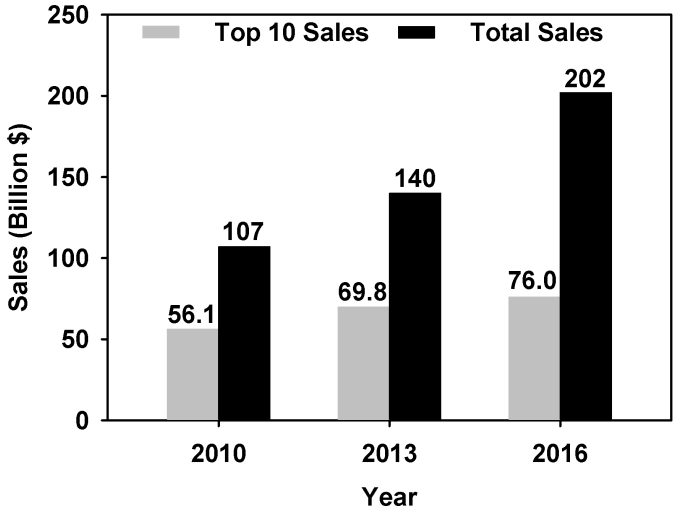

Figure 1.1: Global annual sales for biopharmaceuticals for the years 2010, 2013 and 2016 in billion US-$, divided into total sales and sales of the 10 biopharmaceuticals with the highest sales numbers (data from Walsh (2014); Morrison and Lähteenmäki (2017))

.

1.2 Motivation

Although media and feeding strategies in large-scale fed-batch processes have been subject to optimization (Birch & Racher, 2006; Shukla & Thömmes, 2010), the occurrence of local gradients cannot be completely prevented due to larger volumes and increased mixing times. Accordingly, typical gradients emerging in production scale bioreactors result from gassing, the addition of feed solutions, or titration agents for pH control (Xu et al., 2018). Since the pH in cell culture systems is mostly controlled via the addition of CO_2 in the ingas stream as an acid and Na_2CO_3 solution as base, local accumulation of these agents and resulting inhomogeneities of the pH correlate and have to be considered during scale-up (Xing, Kenty, Li, & Lee, 2009; Sieblist et al., 2011). Presence and negative influence of these gradients have been shown before (Xing et al., 2009; Osman, Birch, & Varley, 2001; Langheinrich & Nienow, 1999). As scale-down models proved, growth and productivity of mammalian cells are often diminished, while by-product formation in form of lactate can significantly increase in zones with higher pH or elevated partial pressure of CO_2 (Gray, Chen, Howarth, Inlow, & Maiorella, 1996; Goudar et al., 2007; Darja et al., 2016; Brunner, Fricke, Kroll, & Herwig, 2017; Brunner, Doppler, Klein, Herwig, & Fricke, 2018; Ivarsson, Noh, Morbidelli, & Soos, 2015). However, effects on metabolic flux distributions and the underlying energy metabolism have been adressed seldom, although the impact on energy demanding cellular productivity is substantial (Brunner et al., 2018; Russell, 2007; Dickson, 2014).

Similarly, cellular productivity is crucial for the performance of perfusion processes (Bausch et al., 2018; Steinebach et al., 2017). However, most studies in the past decade investigated the maximization of cell densities (Clincke, Molleryd, Zhang, et al., 2013) or the characterization of cell retention devices with a recent focus on hollow fiber modules (Karst, Serra, Villiger, Soos, & Morbidelli, 2016; Clincke, Molleryd, Zhang, et al., 2013; Kelly et al., 2014). Individual approaches for the optimization of cellular metabolism and productivity in particular included temperature reduction (Wolf et al., 2018) or glucose limitation (Takuma, Hirashima, & Piret, 2007). Especially glucose limitation can be a potential tool to increase metabolic efficiency and reduce by-product formation by limiting carbon availability. Until now, similar effects were only observed in late batch or fed-batch phases (Mulukutla, Gramer, & Hu, 2012; Ivarsson et al., 2015;

Martínez et al., 2013). However, possible effects of glucose limitation on flux distributions and energy availability have not been analyzed for perfusion, yet.

Consequently, the scope of this thesis can be divided into two parts, both focusing on the optimization of antibody production processes with CHO cells:

- In the fed-batch part the impact of the typical scale-up sensitive parameters Na_2CO_3 addition and partial pressure of CO_2 (pCO_2) was investigated in comparison to an industrial reference process of the project partner Boehringer Ingelheim.
- In the perfusion part the effect of glucose limitation as a process intensification approach was analyzed during steady state cultivation in comparison to a non glucose limited reference steady state.

Main objective for both parts was to unravel the connection of extracellular process settings and intracellular state. Extracellular rates calculation, quantification of intracellular metabolite pool sizes and modelling of metabolic fluxes were performed to gain insight into cellular adaptations to the current conditions. Special focus was put on the connection between energy availability in terms of ATP and cell specific antibody productivity. Consequently, the resulting volumetric productivities were used as indicators for identifying the most efficient cellular state by either avoiding detrimental effects of stress factors in fed-batch mode or by introducing measures to increase efficiency of carbon usage in perfusion mode.

2 Theoretical Background

2.1 Chinese hamster ovary cells

Several well characterized mammalian cells lines like chinese hamster ovary (CHO), baby hamster kidney (BHK), mouse myeloma (NS0) or human embryonic kidney (HEK) have been studied extensively and are available for use in both research and industry. All of them are capable to express recombinant proteins which are correctly folded and posttranslationaly modified to be applied in the human body (J. Y. Kim, Kim, & Lee, 2012). Therefore, solubility, stability and biologic activity are guaranteed. Typical products derived from mammalian cells are antibodies, therapeutic proteins or viral vaccines which cannot be correctly synthesized by bacteria due to the missing glycosylation abilities. Despite the broad range of available mammalian cell lines, the main production hosts for biopharmaceuticals nowadays remain chinese hamster ovary cells (figure 2.1). 61 % of biopharmaceuticals with mammalian producer cells are expressed by CHO cells (Ecker et al., 2015; Kantardjieff & Zhou, 2013). First, the chinese hamster (Cricetulus griseus) was only used as laboratory animal since the early 1900s. In the 1950s, cells were isolated from the hamsters' ovaries and successfully cultivated in vitro for the first time, leading to various further researches in the following decades (Puck, Cieciura, & Robinson, 1958).

In the 1980s, CHO cells became the host for the first therapeutic protein approved for use on the pharmaceutical market: the human tissue plasminogen activator (Wurm, 2004). Decisive for the development of such an industrial process was the creation of highly productive cells by the application of gene amplification systems. Gene amplification systems using dihydrofolate reductase (DHFR) or glutamine synthetase (GS) are the most widely used today. Urlaub, Käs, Carothers, and Chasin (1983); Urlaub et al. (1986) generated the precursors of todays main CHO production cell lines by introducing DHFR deficiency into the cells for the first time in the 1980s. The cells are

transfected with the gene for the target product along with an amplifiable gene for either DHFR or GS, depending on the system. In absence of the according metabolites hypoxanthine and thymidine (DHFR) or glutamine (GS) only transfected cells are capable of surviving (Butler, 2005). Accordingly, the product of interest is expressed in the remaining viable cells. After the selection process, screening is performed to find clones with a stable expression behaviour and the highest cell-specific productivity. In the following process development, the cellular behavior is characterized and optimal production conditions are found regarding pH, dissolved oxygen, nutrient availability and various further parameters. Consequently, not only the mode of cultivation (see sections 2.4 and 2.5) is decisive but also the medium composition and the resulting metabolic adaptations of the cell. Finally, the scale-up in production size bioreactors is the last step in the generation of current biopharmaceutical production processes using CHO cells as manufacturing organisms besides the regulatory requirements for market approval (Wurm, 2004).

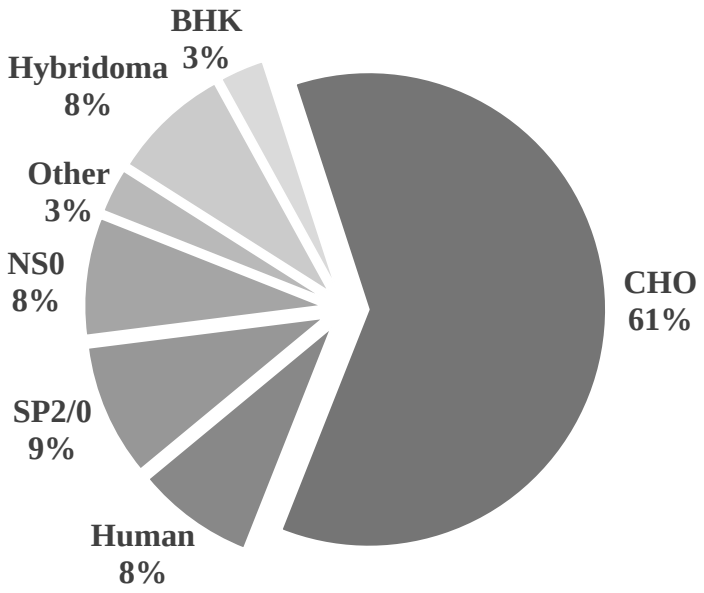

Figure 2.1: Percentage of biopharmaceuticals produced in mammalian systems sorted by cell line in the year 2012 (data from (Kantardjieff & Zhou, 2013))

.

2.2 Metabolism

2.2.1 Main carbon metabolism

The main carbon metabolism of mammalian cells comprises multiple pathways (compare figure 2.2). The main anabolic and catabolic pathways providing cellular building blocks and energy, respectively, are the glycolysis, the pentose phosphate pathway (PPP), the tricarboxylic acid cycle (TCA), the oxidative phosphorylation, the glutaminolysis and the metabolism for the remaining amino acids.

As the starting point of the glycolysis, glucose is the main substrate and the backbone for energy generation (figure 2.2). Glucose uptake is achieved by transporters in the cellular membrane and is based on the present concentration gradient (S. Ozturk & Hu, 2005). The first glycolysis intermediate glucose-6-phosphate is not solely used in the glycolysis. Additionally, it is converted to ribulose-5-phosphate in the first step of the pentose phosphate pathway under the generation of 2 NADPH. The fraction of carbon derived from glucose entering the PPP can vary substantially depending on the cell line and process conditions. For CHO cell lines values between 0.3 and 20 % have been reported (Carinhas et al., 2013; Templeton, Dean, Reddy, & Young, 2013; Martínez et al., 2013). All PPP reactions are located in the cytosol. Ribulose-5-phosphate is a precursor for nucleotides such as DNA and RNA. Therefore, the pentose phosphate pathway is especially important for cell replication, biomass generation and growth. Additionally, nucleotides and coenzymes like ATP or NAD are formed out of ribulose-5-phosphate.
The remaining glucose-6-phosphate is transformed in the further course of glycolysis which is located in the cytosol and consists of several single reactions. Taken together, reactions of glycolysis yield two molecules of pyruvate out of every single molecule glucose taken up by the cells. During the conversion of glucose to pyruvate 2 molecules of ATP are generated directly and 2 molecules of NAD^+ are reduced to NADH (Pörtner, 2009; Berg, Tymoczko, Stryer, et al., 2012).

Excess intracellular pyruvate concentrations can result in the by-product formation of lactate, especially under conditions of high glucose availability as part of overflow metabolism (Luo et al., 2012). Lactate is directly formed by reducing pyruvate via the

lactate dehydrogenase under the regeneration of NAD^+. Lactate accumulating in the medium can lead to decreased pH and therefore increased base titration and osmolality but also direct inhibition of growth and productivity (K. Chen, Liu, Xie, Sharp, & Wang, 2001). Inhibiting concentrations of more than 60 mM especially occur in fed-batch processes with prolonged process times and high glucose availabilities (Lao & Toth, 1997). Previously secreted lactate can be taken up by the cells again. The metabolic switch from lactate formation to uptake has been the focus of several studies. Clearly, lactate can be consumed as alternative carbon source once glucose is depleted, especially in batch cultures (Martínez et al., 2013; S. S. Ozturk, Riley, & Palsson, 1992). Furthermore, changing process conditions like limiting glucose availability (Xie & Wang, 1994), using different carbon sources (Altamirano, Paredes, Illanes, Cairo, & Godia, 2004) or applying pH (Ivarsson et al., 2015) or temperature shifts (Sou et al., 2015) has shown to lead to lactate consumption by the cells although glucose is still present in the medium. The redox (NAD/NADH) balance also plays a significant role in the formation of lactate and is interrelated with the ATP formation (see section 2.2.2). However, not all mechanisms and origins of triggering lactate consumption have been completely elucidated, yet.

Despite the possible by-product formation from lactate, the major part of pyruvate resulting from glycolysis is transported into mitochondria and fuels the TCA (figure 2.2). Depending on the cell line and culture conditions, fractions of pyruvate entering the TCA may differ. For CHO cells lowest published values were 20 % (Templeton et al., 2013) but can go up to 100 % or even more if lactate is consumed and thereby additionally fueling the TCA via pyruvate (Templeton et al., 2013; Carinhas et al., 2013). In the first step of TCA, pyruvate is oxidatively decarbonized to acetyl-CoA under formation of NADH. Together with the resulting oxaloacetate from the previous TCA circulation acetyl-CoA is transformed to citrate and further to alpha-ketoglutarate yielding NADH. More NAD is reduced to NADH in the transformation of alpha-ketoglutarate to succinyl-CoA. In the next step GTP is formed (depicted as energy equivalent to ATP in figure 2.2) when succinyl-CoA is transformed to succinate. This is oxidized to fumarate which is hydrated to malate. Eventually, malate is oxidized to form oxaloacetate fueling a new circulation of the TCA in combination with acetyl-CoA. Taken together, the TCA finally yields 1 molecule of ATP and 3 molecules of NADH per circulation of

pyruvate and double the amount per molecule of glucose (Berg et al., 2012; S. Ozturk & Hu, 2005). Additionally, one molecule of NADH is generated prior, when one molecule pyruvate is being transformed to acetyl-CoA.

The second main substrate for CHO cells is the amino acid glutamine which is both carbon and nitrogen source. Glutamine uptake sums up to about 10 % to 20 % compared to glucose uptake, depending on the concentration in the medium (Wahrheit, Nicolae, & Heinzle, 2014; Nolan & Lee, 2011). Via glutaminolysis glutamine is transformed to alpha-ketoglutarate in two steps and thereby fuels the TCA (figure 2.2). In the first step glutamine is transformed to glutamate under the formation of ammonia followed by the second step in which glutamate is transformed to alpha-ketoglutarate. Alternatively, the glutamate resulting from the first step can be secreted by the cells. Glutamine overflow metabolism can lead to ammonia accumulation due to the formation of ammonia during the first step of glutaminolysis. Ammonia is the second major by-product with inhibiting effects besides lactate. Negative effects on growth and product formation were observed for concentrations of about 6-8 mM or higher (Hassell, Gleave, & Butler, 1991; P. Chen & Harcum, 2006; Schneider, Marison, & von Stockar, 1996).

2.2.2 Energy generation and redox balance

The energy generation is most important for both biomass generation and cellular antibody production. CHO cells can metabolize their main energy source glucose in multiple ways with different efficiencies. One is the transformation to lactate via glycolysis. The transformation of glucose to lactate yields 2 molecules of ATP. More efficient is the complete oxidation of glucose via glycolysis, TCA and the subsequent oxidative phosphorylation to CO_2 where 36 molecules of ATP can be produced theoretically (Warburg, 1956; Glacken, 1988). The cofactors NADH and $FADH_2$ contribute to ATP synthesis via electron transport chain and oxidative phosphorylation. The resulting number of molecules of ATP produced per NADH or $FADH_2$, respectively, is defined as P/O ratio. The ratio describes the efficiency of oxidative phosphorylation and the previous electron transport chain and depends on the used cofactor. For NADH and $FADH_2$ P/O ratios of 2.5 and 1.5 were described (Hinkle, 2005).

Accordingly, the redox (NAD/NADH) balance is of major importance for the ATP formation. As introduced in section 2.2.1, pyruvate plays a crucial role in the redox balance since lactate is produced under the regeneration of NAD+, therefore representing a sink for NADH. By contrast, pyruvate fueling the TCA eventually yields 3 molecules of NADH, providing a major source of NADH. Hence, lactate formation prevents larger fractions of NADH from being transported into mitochondria. Under the ideal metabolic state of no lactate formation the complete NADH from glycolysis and TCA is subsequently used in oxidative phosphorylation for the generation of ATP (Nolan & Lee, 2011). Consequently, interrelation of the redox balance and the cell-specific lactate formation has been found for results of intracellular flux analyses (Nolan & Lee, 2011; Brunner et al., 2017).

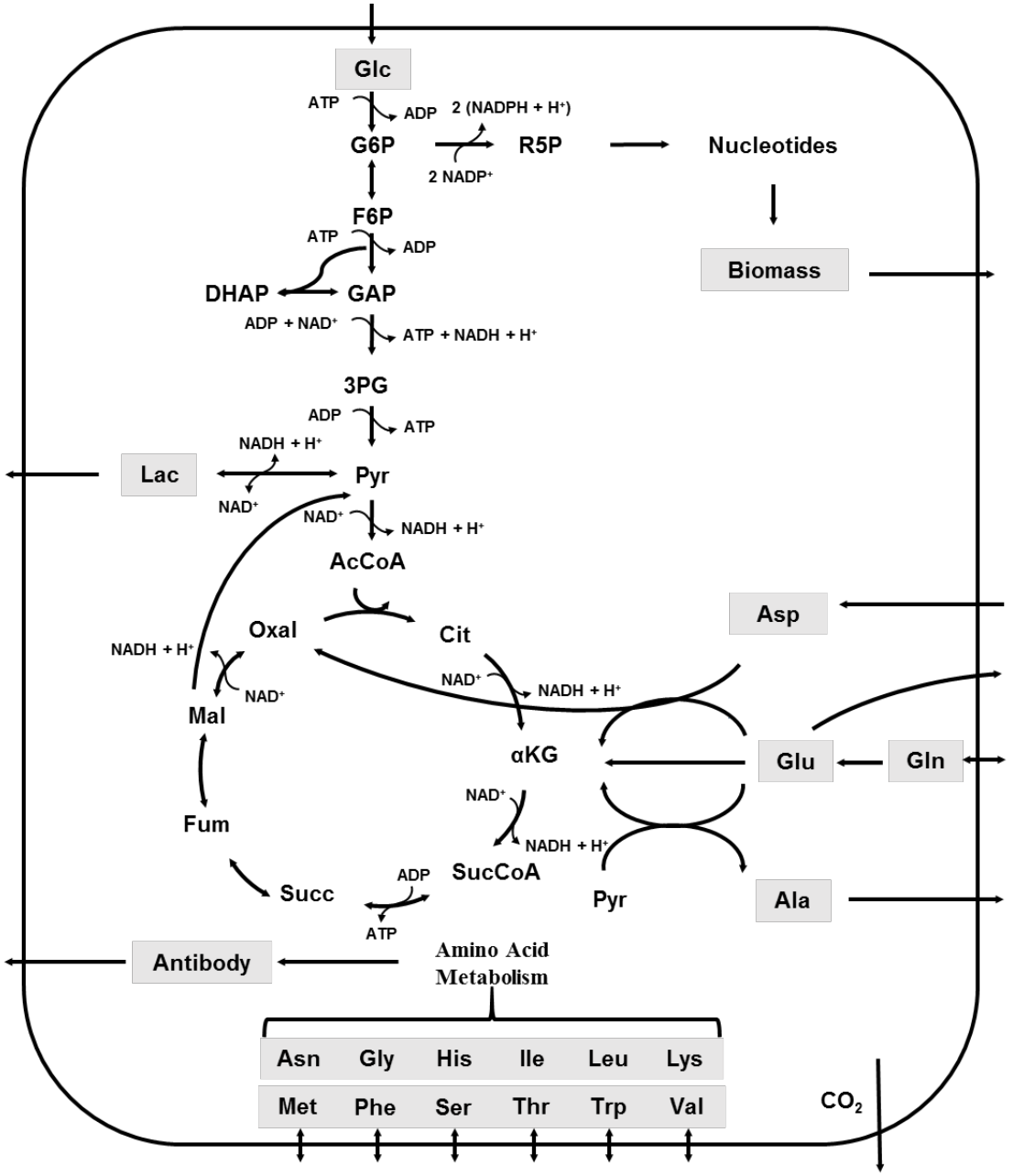

Figure 2.2: Simplified scheme of the main carbon metabolism. Depicted are the main metabolites of glycolysis and tricarboxylic acid cycle including the ATP and NADH generation. Simplifications were made for the pentose phosphate pathway leading to biomass precursors and the amino acid metabolism yielding the monoclonal antibody. Compartmentalization regarding mitochondrial department was neglected. Metabolites with a grey background were quantified extracellularly in the experimental part of this work.

2.3 Flux analysis in CHO cells

The analysis of intracellular fluxes can provide a thorough understanding of metabolic states and adaptations during production processes using both microbial and mammalian host systems. Intracellular flux distributions can hardly be measured and are therefore calculated based on a model representing the cellular metabolism. The reconstruction of the cellular metabolism and implementation into a model structure is mostly done with the help of biochemical databases (Thiele, Price, Vo, & Palsson, 2005). Simplifications are often made to improve clarity of the results and to decrease efforts during both model preparation and flux computation. Two approaches are mostly applied to calculate intracellular flux distributions: metabolic flux analysis (MFA) and flux balance analysis (FBA) (Stephanopoulos, Aristidou, & Nielsen, 1998; Orth, Thiele, & Palsson, 2010). In both approaches a pseudo steady-state is assumed for the intracellular metabolic state, equivalent to no accumulation or depletion of metabolites.

$$S \cdot v = 0$$

The metabolic reactions and the involved metabolites are stored in a stoichiometric matrix S. The rows in S correspond to metabolites and the columns to reactions. The matrix is then combined with a vector v containing the corresponding flux values for measured and non-measured fluxes to be determined

For MFA the metabolic model is simplified by focusing on the main pathways and most significant reactions. Therefore, the total number of reactions is assessable to such an extent, that measured extracellular uptake and production rates are sufficient to calculate all intracellular fluxes. Consequently, the system can be described as determined, yielding a unique solution of the small-scale metabolic network (Niklas & Heinzle, 2011). Analysis is often performed in distinct states of the process such as the growth or the stationary phase where cell-specific rates stay almost constant and can be averaged over longer periods of time. Alternatively, time resolved flux distributions can be gained by performing dynamic metabolic flux analysis (dMFA) where systems dynamics are taken into account by the combination with either a kinetic model or time-series data analysis (Ahn & Antoniewicz, 2012).

For FBA mostly larger models are used, ranging up to genome-scale size with hundreds of reactions included (Feist & Palsson, 2008). Therefore, FBA is used for models classified as underdetermined due to the large reaction numbers and comparably small number of measured rates. Instead of simplifying the model by reducing the reaction number, upper and lower flux bounds which are derived from measured extracellular uptake and production rates are introduced as constraints (Z. Huang, Lee, & Yoon, 2017; Orth et al., 2010) (see figure 2.3). Furthermore, an objective function like maximization of growth or ATP production is chosen and imposed on the system based on biological coherency and state of the culture to gain a reasonable solution (Feist & Palsson, 2010; Orth et al., 2010).

$$Z = c^{\mathrm{T}} \cdot v$$

The objective function Z is a linear combination of fluxes with the vector of weights c. Thereby, the reactions contributing to the objective are chosen. Hence, FBA can also be used for different approaches like media or strain optimization before experimental validation. However, depending on the size of the solution space and chosen constraints multiple solutions could potentially maximize the objective (Z. Huang et al., 2017; Orth et al., 2010).

Software solutions like the *Constraint-Based Reconstruction and Analysis* (COBRA) toolbox enable quickly implemented flux analysis (Schellenberger et al., 2011). Therefore, multiple cell lines and a wide scope of cultivation settings have been analyzed with flux analysis. Applications in the field of biopharmaceuticals production with CHO cells have been diverse in the past few years but contribute to the understanding of various process optimization approaches. As following examples show, investigations cover different cultivation modes but especially multiple approaches to analyze and intensify production processes on a metabolic level:

The investigation of the switch from lactate production to consumption is an important metabolic event not yet fully understood. However, studies showed higher TCA influx and elevated energetic efficiency for lactate consuming cells using flux analysis (Mulukutla et al., 2012; Martínez et al., 2013). When comparing different cultivation phases increased glycolytic and pentose phosphate fluxes were found in early stages

when growth was high in contrast to later stages when TCA flux was high and growth reduced (Templeton et al., 2013) Decreased temperature led to higher productivity but remarkably decreased fluxes of carbon in all pathways (Sou et al., 2015). Ivarsson et al. (2015) found decreased lactate uptake and increased TCA cycle fluxes for lower pH values during batch fermentation. Consequently, the resulting origin of ATP differed among varying pH values. Another approach included the addition of the histone deacetylase inhibitor butyrate, which has been shown to have positive effect on the specific productivity in CHO cells (Jiang & Sharfstein, 2008). Flux analyses revealed that butyrate treatment led to an overall increase in intracellular fluxes even in stationary phase when fluxes in the previously mentioned studies were lower (Carinhas et al., 2013). Templeton, Xu, Roush, and Chen (2017) compared industrial fed-batch and perfusion processes using flux analysis and found minor differences in the intracellular flux distributions but major deviations in underlying protein production concerning the fractionation of biomass and antibody production.

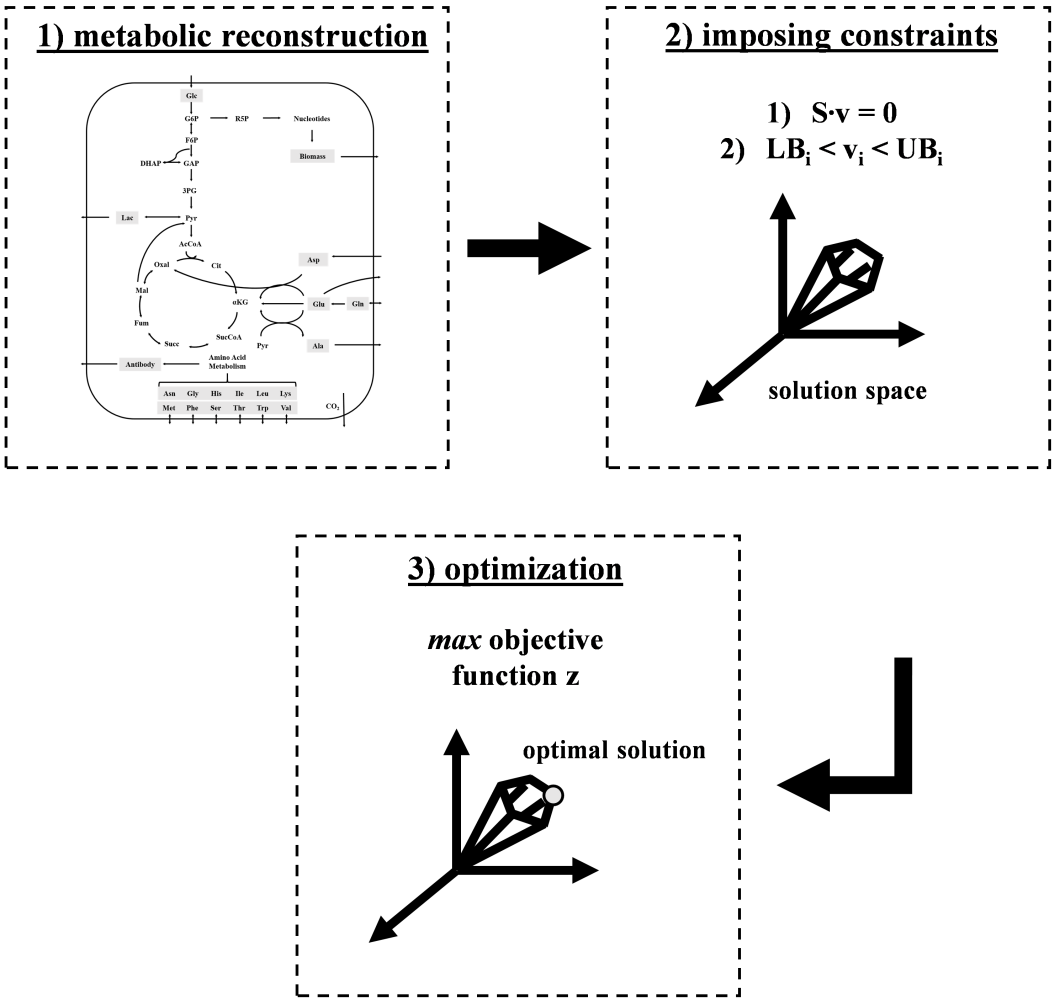

Figure 2.3: Workflow of flux balance analysis including 1) the generation of a stochiometric model of the cellular metabolism from databases and publications, 2) the transfer of the reactions to the stochiometric matrix S and the imposition of constraints (lower bounds LB and upper bounds UB) for the cell-specific rates v whereby the solution space is constrained and 3) the optimization of the fluxes using an objective function z and identification of an optimal flux distribution solution within the constrained solution space.

2.4 Fed-batch processes

Among the three main cultivation modes (figure 2.4), fed-batch processes are the most commonly used cultivation mode in industrial production of biopharmaceuticals. In contrast to simple batch processes without volume change after inoculation, fed-batch processes show prolonged cultivation times and increasing volume due to the addition of growth supporting feed media during the cultivation. Performance parameters and recent approaches for process optimization are discussed in the following section.

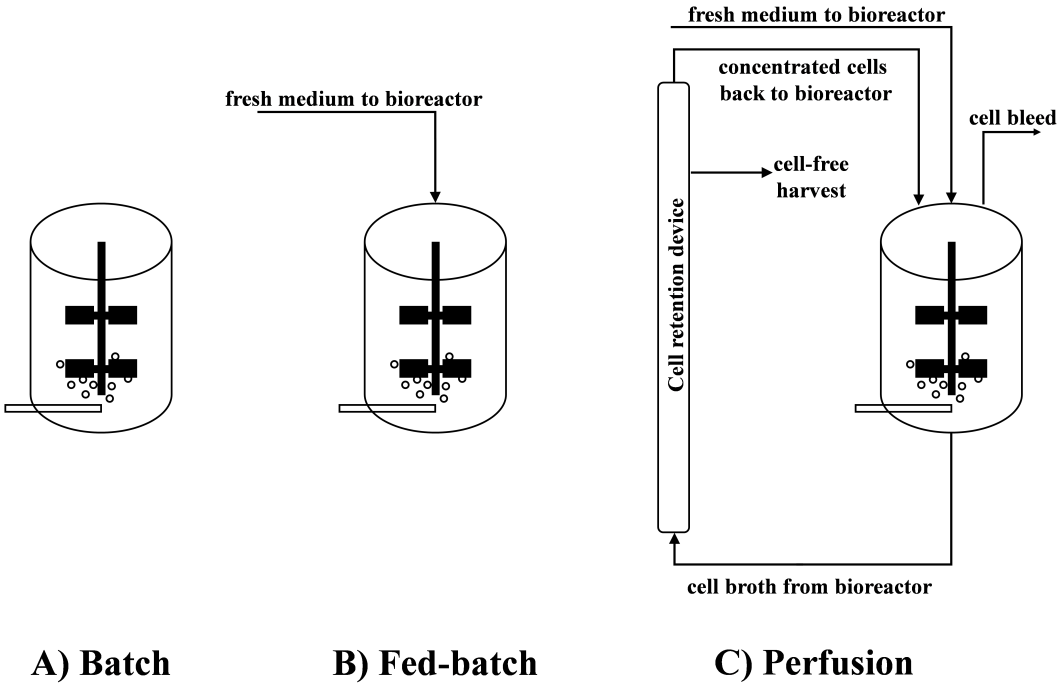

Figure 2.4: Schematic representation of the three main cultivation modes. The batch in A) is a closed system with no addition of medium and constant liquid volume after inoculation. The fed-batch in B) is supplied with an enriched feed-medium after inoculation without removal of the spent medium and therefore has an increasing liquid volume. The perfusion setup in C) is characterized by an additional cell retention system and continuous addition and withdrawal of medium and therefore constant liquid volume. Feed-medium is added to the bioreactor while spent medium is pumped out via the cell retention device which retains the cells within the system. Consequently, cell densities can reach much higher levels in perfusion culture.

2.4.1 Process overview and performance

Typical values for viable cell densities in published CHO fed-batch cultivations in the past decade range from 20 - 30 x 10^6 cells/mL (Y.-M. Huang et al., 2010; Reinhart, Kaisermayer, Damjanovic, & Kunert, 2013), whereas maximum cell specific productivities can reach values around 50 pg/cell/day with resulting final titers of up to 10 g/L (Zboray et al., 2015; Reinhart et al., 2013). Simple batch processes are therefore outperformed by approximately the factor of three in terms of viable cell density and by the factor of two in cultivation time. Consequently, titers are significantly increased in fed-batch processes (Kunert & Reinhart, 2016).

To avoid excessive increase in liquid volume and therefore unwanted dilution of cell density and the product of interest, the added feed is concentrated multiple times (about 10 - 15 x) compared to the batch medium. Possible feeding strategies may be based on previously determined consumption rates or feedback loops regarding continuously measured bioprocess parameters (Wlaschin & Hu, 2006; L. Zhang, Shen, & Zhang, 2004). The feeding routine can be realized by either bolus addition of the feed medium (mostly done once or twice daily) or a continuous feeding thereof. The first option is simple and based on measured substrate concentrations shortly before the feeding but can contribute to the increased accumulation of inhibitory by-products. Lactate, resulting from carbon metabolism, and ammonia, resulting from nitrogen metabolism (compare section 2.2.1), may be produced in overflow due to the increased nutrient availability to ensure sufficient substrate supply until the next bolus feedings. Bolus feeding is often used in large scale biopharmaceutical production processes because of the ease of operation (Li, Vijayasankaran, Shen, Kiss, & Amanullah, 2010). On the contrary, the introduction of a more sophisticated continuous feeding, respectively the variation of the feed rate, and therefore the minimization of the substrate availability can consequently contribute to the reduction of by-product formation (Luo et al., 2012; Ljunggren & Häggström, 1992). The concentration ranges of half saturation constants for glucose (0.4 mmol/L) and glutamine (0.1 mmol/L) can be used as setpoints to avoid lactate and ammonia accumulation although feeding strategies have to be precise to avoid limitation effects (Chee Furng Wong, Tin Kam Wong, Tang Goh, Kiat Heng, &

Gek Sim Yap, 2005; Abu-Absi et al., 2013). Possible consequences may be losses in cell viability or product quality once nutrient limitation becomes too pronounced.

Nevertheless, because of superior volumetric productivities compared to batch processes and the simplicity of operation compared to perfusion processes (see section 2.5) fed-batch processes are the main biopharmaceutical production mode and remain in the focus of process optimization studies.

2.4.2 Parameters influencing process performance

Several process parameters like temperature, pH, osmolality, partial pressure of CO_2 (pCO_2) or metabolite concentrations may influence the performance of the cultivation by altering growth, productivity or metabolism of the cells. Although specific effects may vary depending on the cell line, especially in large scale cultivations inhomogeneities can lead to deviations in cellular performance.

The partial pressure of CO_2 is one of multiple parameters showing both formation of inhomogeneities in large scale and influence on cellular metabolism (Gray et al., 1996; Xu et al., 2018). Furthermore, the pCO_2 often increases during the course of a cultivation due to the increasing cell densities but also through the accumulation of inorganic carbon species as a consequence of base addition (Goudar et al., 2007). Increased CO_2 stress is critical because it is known to hinder both cellular growth and productivity but is nevertheless necessary in smaller fractions to mimic the physiological environment the cells were originally obtained from (Mostafa & Gu, 2003; Gray et al., 1996; Brunner et al., 2018).

Likewise, osmolality rises towards the end of a fed-batch cultivation. While the starting values reach up to 300 mOsm/kg and therefore similar to cytoplasmic osmolalities (Mortimer & Müller, 2001), an increase is mainly caused by the accumulation of salts and ions through the feeding but also through base addition. Consequently, with increasing process time osmolalities above 450 mOsm/kg can contribute to a loss in growth and viability and an increasing number of lysing cells and therefore the begin of the stationary or decline phase. Furthermore, glucose uptake and lactate formation is increased (Pfizenmaier, Matuszczyk, & Takors, 2015; Han, Koo, & Lee, 2009; N. S. Kim & Lee, 2002; Zhu et al., 2005). Cell lysis itself increases osmolality further and foaming starts

due to released cellular proteins. However, beneficial effects on cell specific productivity for osmolalities have been observed for osmolalities of about 350 mOsm/kg coinciding with cell cycle arrest (D. Shen et al., 2010; Pfizenmaier et al., 2015; Pfizenmaier, Junghans, Teleki, & Takors, 2016).

Temperature is normally held constant at the physiological value of 37.0 °C to support optimal growth. However, shifts downwards can be used for cell cycle arrest and prolongation of the stationary phase in late fed-batch stages when the cell density already reached its maximum value. Hereby, growth and by-product formation are substantially slowed down while productivity remains on a constant level or is even increased as shown by several authors (Yoon, Choi, Song, & Lee, 2005; Kaufmann, Mazur, Fussenegger, & Bailey, 1999; Furukawa & Ohsuye, 1999).

Interrelated with CO_2 and base addition, pH values may be distributed inhomogeneously in large scale cultivations. Numerous proteins with roles in diverse cellular functions are sensitive to the H^+ concentration (Casey, Grinstein, & Orlowski, 2010). Likewise, the pH has been shown to substantially affect the lactate formation of CHO cells. Several authors showed decreasing trends of lactate formation rates with the pH value decreasing towards 6.8. Potential reasons for the reduction in lactate formation at lower pH values were the avoidance of a further decrease in extra- and intracellular pH, different activities of glycolytic enzymes and redox balancing (Ivarsson et al., 2015; Trummer et al., 2006; Liste-Calleja et al., 2015; Yoon et al., 2005).

Besides the actual substrate concentrations (see section 2.2.1), substitution of the substrate glucose with alternative sugars such as galactose or mannose can also lead to the reduction of by-product formation. However, overall performance in terms of growth and product formation may be hampered in comparison to the use of glucose (Altamirano et al., 2001, 2004; Berrios, Altamirano, Osses, & Gonzalez, 2011).

2.5 Perfusion processes

Besides fed-batch cultivations perfusion cultivations (see figure 2.4) are emerging in biopharmaceuticals production as intensified processes using a smaller volume but higher cell densities. Perfusion describes a continuous culture where the same amount of used medium is withdrawn as fresh medium is added and therefore the cultivation volume remains constant. Additionally, a cell retention device is connected to the bioreactor to

avoid the wash-out of cells as experienced in simple continuous cultures. The perfusion rate can be adjusted in subsequent processes or even within a single process. Hereby, substrate supply and by-product removal can be controlled (Chotteau, 2015). Consequently, cell densities much higher than during fed-batch cultivations can be reached. Published values range up to 200 x 10^6 cells/mL (Clincke, Molleryd, Zhang, et al., 2013). Through the continuous mode of operation the process time can theoretically be extended for weeks to months depending on both biological and technical factors. The cell line has to prove stability in growth and productivity over several generations while the stability of the set-up but especially the cell retention device is crucial for the continuous operation. Although titers are not necessarily higher than in fed-batch mode due to the constant wash out of the product of interest, the volumetric productivity is increased because of the high cell densities. Furthermore, the cell retention devices facilitate the introduction of subsequent continuous downstreaming operation since the product is already separated from the cells (Steinebach et al., 2017; Warikoo et al., 2012). Alternatively, perfusion can also be used for cell bank generation (Clincke, Molleryd, Samani, et al., 2013) or in seed reactors (Pohlscheidt et al., 2013) to quickly reach high inoculation densities for the main reactor.

An overview of different cell retention devices is depicted schematically in figure 2.5. Depending on the device it is either placed inside the bioreactor or connected externally. However, the mode of action of all cell retention devices is based on differences in size or density between medium components and cells.

Filtration techniques retain cells by their size. Limitations can occur once the pores start clogging with biological material and flow is reduced. However, various different devices have been characterized and published in the recent decades like external hollow fibers for tangential flow filtration (figure 2.5 A) (Clincke, Molleryd, Zhang, et al., 2013; Clincke, Molleryd, Samani, et al., 2013; Karst et al., 2017; Kelly et al., 2014) or alternating flow filtration (Karst et al., 2016; Clincke, Molleryd, Zhang, et al., 2013; Clincke, Molleryd, Samani, et al., 2013). Here, the pores of the hollow fibers are flushed either tangentially or by introducing a backflush in certain time intervals. This is supposed to ensure long-time application without membrane fouling. Alternatively, spin filters (figure 2.5 B) are predominantly integrated on the agitator shaft, where the

constant rotational movement is supposed to reduce fouling (Komolpis, Udomchokmongkol, Phutong, & Palaga, 2010; Vallez-Chetreanu, Ferreira, Rabe, von Stockar, & Marison, 2007).

Inclined settlers use the principle of sedimentation for the separation of cells (figure 2.5 C). The cell broth is added to the settler and the sedimenting cells are withdrawn at the bottom and sent back to the bioreactor while the spent medium is slowly pumped from the top. Using sedimentation almost no shear stress acts on the cells. On the other side, long residence times within the settler might limit cells in substrate or oxygen availability (Wen, Teng, & Chen, 2000; Y. Shen & Yanagimachi, 2011; Choo et al., 2007). The labile antihemophilic factor VIII is produced in large-scale using gravitational settlers (X. Zhang, Wen, & Yang, 2011).

Furthermore, several alternative cell retention devices have been described in literature. Among them are acoustic separators applying an acoustic resonance field (figure 2.5 E). Here, the cells agglomerate in standing acoustic waves and can be led back into the bioreactor while the medium is removed. Drawback may be the increased shear applied to the cells by the acoustic field (Ryll et al., 2000; Shirgaonkar, Lanthier, & Kamen, 2004; Gorenflo, Smith, Dedinsky, Persson, & Piret, 2002). In Hydrocyclones the cell suspension from the bioreactor is separated into an underflow and an overflow (figure 2.5 D). Since the cells have a higher density they are carried out of the hydrocyclone via the underflow and led back to the reactor. The spent medium is rising inside the hydrocyclone and leaving as cell-free harvest through the overflow. Again, shear sensitive cells could be affected by the applied forces (Pinto, Medronho, & Castilho, 2008; Elsayed, Medronho, Wagner, & Deckwer, 2006). Centrifugal forces can be used by connecting a centrifuge to the bioreactor as done by B. J. Kim, Oh, and Chang (2008) (figure 2.5 F). Sterile single-use inlets can be inserted to simplify the handling in between different runs. Although the separation settings can be varied dynamically, the long-term robustness could be decreased due to the mechanical complexity of the centrifugal set-up.

In the recent years cell retention systems using either sedimentation, tangential flow filtration or alternating flow filtration devices have become the most applied set-ups in

industry. The aforementioned devices are favored due to the scalability of the systems and the low shear stress applied (S. Ozturk & Hu, 2005).

Regarding process optimization results from process parameter investigations can only partly be transferred from fed-batch cultivations to perfusion systems (see section 2.4.2). Temperature decrease for example can be used similarly for perfusion process as described in section 2.4.2, as a recent study by Wolf et al. (2018) showed. Partial pressure of CO_2 can be more pronounced because of the much higher cell densities (Goudar et al., 2007) whereas osmolalities can increase as a result of highly concentrated perfusion media but are restricted in maximum values by the constant wash-out. Additionally, when adjusting process parameters long-term stability has to be considered in terms of stable growth respective viability due to the continuous mode of operation. Consequently, perfusion rates may have to be changed after process parameter variation.

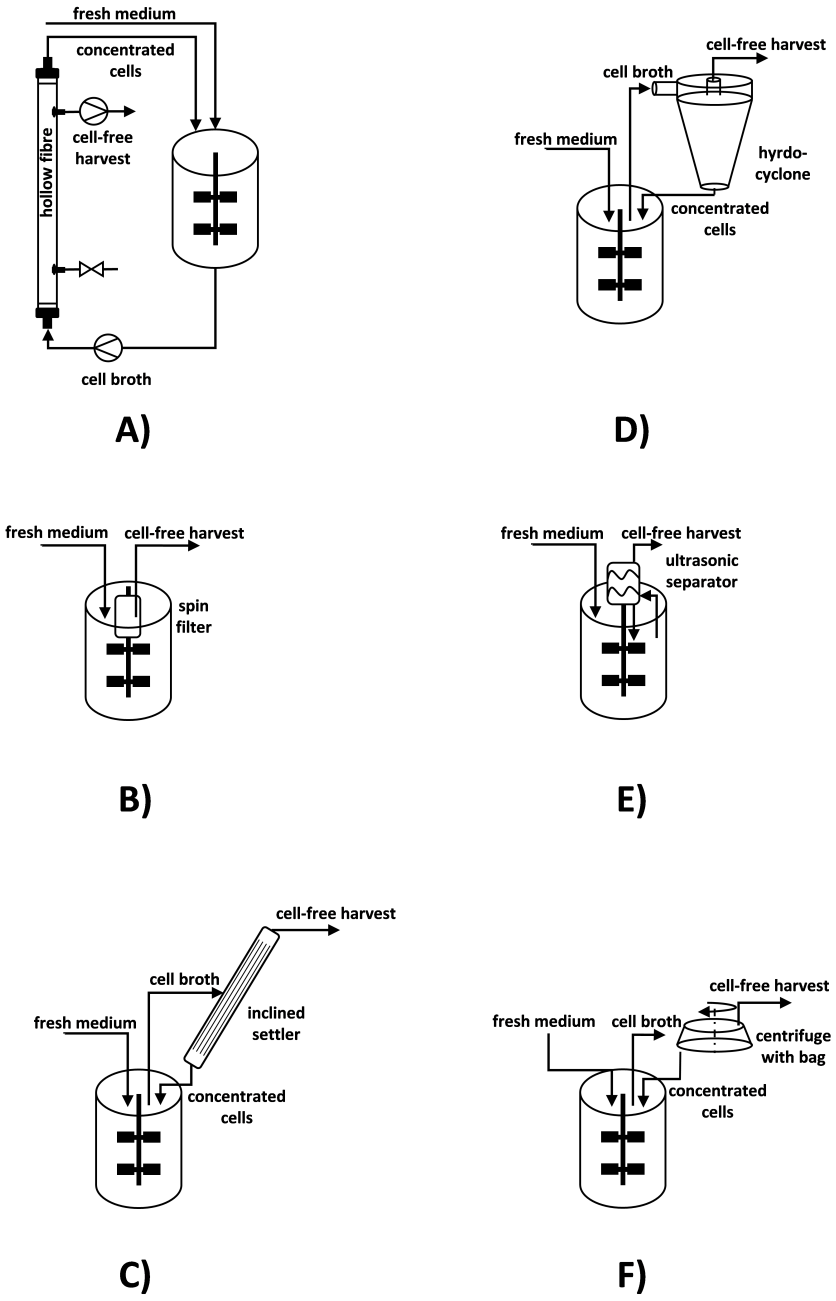

Figure 2.5: Schemes for different published cell retention devices used for perfusion processes. Devices can be divided into bioreactor internal and external. A) tangential flow filtration with an external hollow fiber module, B) internal spin filter, C) external gravity settler, D) external hydrocyclone, E) external ultrasonic separator, F) external centrifuge

3 Materials and Methods

3.1 Materials

3.1.1 Chemicals

Table 3.1: Chemicals

Chemical	Manufacturer
3-mercaptopropionic acid	Sigma-Aldrich, USA
300 mOsm/kg standard	Gonotec, Germany
500 mOsm/kg standard	Gonotec, Germany
9-fluorenylmethyl chloroformate	Sigma-Aldrich, USA
Acetonitrile $\geq$ 99.9 %	VWR, Germany
Buffer solution LaboTrace	TraceAnalytics, Germany
Cis-aconitate $\geq$ 98 %	Sigma-Aldrich, USA
Adenosine diphosphate disodium salt	Gerbu, Germany
Adenosine monophosphate disodium salt	Fluka, USA
Adenosine triphosphate disodium salt	Gerbu, Germany
Algal lyophilized cells U-^{13}C $\geq$ 99 %	Sigma-Aldrich, USA
Amino acid standard	Sigma-Aldrich, USA
Antifoam (proprietary)	Boehringer Ingelheim AG & Co. KG, Germany
Basal medium (proprietary)	Boehringer Ingelheim AG & Co. KG, Germany
Boric acid	Merck, Germany
Bovine sermum albumin	VWR, Germany
Choloroform $\geq$ 98 %	Sigma-Aldrich, USA

Chemicals - continued

Chemical	**Manufacturer**
Dimethyl sulfxoide	Sigma-Aldrich, USA
Ethanol $\geq$ 96 %	Carl Roth, Germany
Ethylenediaminetetraacetic acid	Carl Roth, Germany
Feed medium (proprietary)	Boehringer Ingelheim AG & Co. KG, Germany
Fructose-6-phosphate $\geq$ 98 %	Sigma-Aldrich, USA
Glucose-6-phosphate $\geq$ 98%	Sigma-Aldrich
Glucose and lactate standard	TraceAnalytics, Germany
Hydrochloric acid	Carl Roth, Germany
L-asparagine $\geq$ 99 %	Sigma-Aldrich, USA
L-glutamine $\geq$ 99 %	Carl Roth, Germany
L-ornithine $\geq$ 99%	Sigma-Aldrich, USA
L-tryptophane $\geq$ 99 %	Fluka, USA
Methanol $\geq$ 99.8 %	VWR, Germany
Ortho-phtaldialdehyde	Fluka, USA
pH 4.00 buffer solution	Carl Roth, Germany
pH 7.00 buffer solution	Carl Roth, Germany
pH 9.00 buffer solution	Carl Roth, Germany
Phosphoric acid	Fluka, USA
Potassium hydroxide 45 %	Sigma-Aldrich, USA
Potassium phosphate dibasic	Sigma-Aldrich, USA
Potassium phosphate monobasic	Sigma-Aldrich, USA
Preculture medium (proprietary)	Boehringer Ingelheim AG & Co. KG, Germany
Pyruvate $\geq$ 99 %	Sigma-Aldrich, USA
SeramunBlau	Seramun Diagnostica, Germany
Sodium azide	Sigma-Aldrich, USA
Sodium carbonate	Carl Roth, Germany
Sodium chloride $\geq$ 99.8 %	Carl Roth, Germany

Chemicals - continued

Chemical	Manufacturer
Sodium hydrogen carbonate	Carl Roth, Germany
Sodium hydroxide	Carl Roth, Germany
Sodium phosphate dibasic	Carl Roth, Germany
Sodium tetraborate decahydrate	Sigma-Aldrich, USA
Sulfuric acid $\geq$ 98 %	Carl Roth, Germany
Tetrabutylammonium bisulfate	Fluka, USA
Tris(hyroxymethyl)aminomethane	Carl Roth, Germany
Trypan blue solution 0.4 %	Sigma-Aldrich, USA
Tween 20	Fluka, USA
Water LC-MS grade	VWR, Germany

3.1.2 Consumables

Table 3.2: Consumables

Consumable	Manufacturer
96 well plate, F-bottom	Greiner, Germany
Cedex smart slides	Roche, Germany
Cryo vials	Greiner, Germany
Filter 0.22 μm	Carl Roth, Germany
Filter Sartolab P-20 0.2 μm	Sartorius, Germany
Glass fiber filter A/D	Pall, USA
Hollow fiber module CFP-4-E-3X2MA	GE Healthcare, Germany
HPLC glas vials	VWR, Germany
Luer lock connectors	Carl Roth, Germany
Metrigard filter	Pall, USA
Microtiter Plates	Greiner, USA
Pipet tips	Sarstedt, Germany
Reaction tubes	Sarstedt, Germany

Consumables - continued

Consumable	Manufacturer
Reaction tubes safe lock	Eppendorf, Germany
Sequant ZIC-pHILIC	Di2chrom, Germany
Serological pipets	Sarstedt, Germany
Shake flasks	Corning, USA
Supelcosil LC18	Sigma-Aldrich, USA
Syringe Omnifix with luer lock	Braun Melsungen, Germany
Tube for Osmomat 030	Gonotec, Germany
Vial Inserts	VWR, Germany
Zorbax Eclipse Plus C18/250 x 4.6 mm	Agilent Technologies, USA

3.1.3 Hardware

Table 3.3: Hardware

Hardware	Manufacturer
Avanti J-25 centrifuge	Beckman Coulter, USA
Bioblock	DASGIP, Germany
Bioreactor DS1500ODSS	DASGIP, Germany
Cedex XS analyzer	Roche, Germany
Cryoboy	Nalgene, USA
Cryostat F3	Haake, Germany
Diode array detector	Agilent Technologies, USA
Fluorescence detector	Agilent Technologies, USA
Gas mixing module	DASGIP, Germany
HPLC 1200	Agilent Technologies, USA
Incubator Minitron	Infors, Switzerland
LaboTrace	TraceAnalytics, Germany
Megafuge 1.0R	Heraeus, Germany
Microcentrifuge 5417R	Eppendorf, Germany

Hardware - continued

Hardware	Manufacturer
Microplate reader Synergy	BioTek, USA
Nanopure II	Barnstead, USA
Osmomat 030	Gonotec, Germany
Oxygen probe	Mettler Toledo, USA
Peristaltic pump 101u	Watson Marlow, UK
Peristaltic pump 505s	Watson Marlow, UK
pH probe	Mettler Toledo, USA
pH/DO module	DASGIP, Germany
Pipet boy acu	Integra Biosciences, Switzerland
Pump module	DASGIP, Germany
Research pipets	Eppendorf, Germany
Temperature/agitation module	DASGIP, Germany
Thermomixer comfort	Eppendorf, Germany
Total carbon analyzer Multi N/C 2100s	Analytik Jena, Germany
Triple Quad mass spectrometer 6410B	Agilent Technologies
Vacuum incubator RVC 2-33	Martin Christ, Germany
Vacuum pump	Vaccubrand, Germany

3.1.4 Software

Table 3.4: Software

Software	Manufacturer
Chemstation	Agilent Technologies, USA
DASGIP control 4.0	DASGIP, Germany
Mass Hunter B.04.00	Agilent Technolgies, USA
Matlab 2013a	Mathworks, USA
Microsoft Office	Microsoft, USA

3.1.5 Antibodies for ELISA

Table 3.5: Antibodies

Antibody	Manufacturer
Anti-human IgG F(c) goat antibody	Biomol, Germany
Anti-human kappa chain goat antibody peroxidase conjugated	Biomol, Germany
IgG1 standard (proprietary)	Boehringer Ingelheim AG & Co. KG, Germany

3.1.6 Buffers and Solutions

Table 3.6: Buffers and solutions

Buffer or solution			Compound
Agent for amino acid analysis	2.5	mg	9-fluorenylmethyl chloroformate
	1	mL	acetonitrile
Blocking solution ELISA	1	L	Tris buffered saline
	10	g	Bovine serum albumine
Coating buffer ELISA	3.7	g	Sodium hydrogen carbonate
	0.64	g	Sodium carbonate
	ad 1.0	L	Nanopure water
Cryo medium	10	%	Dimethyl sulfxoide
	90	%	Culture medium
Dilution buffer ELISA	1	L	Tris buffered saline
	10	g	Bovine serum albumine
	5	mL	Tween 20 (10 %)
Elution buffer A for HPLC (amino acids)	10	mM	Sodium phosphate dibasic
	10	mM	Sodium tetraborate decahydrate

Buffers and solutions - continued

Buffer or solution			**Compound**
	0.5	mM	Sodium azide
Elution buffer A for HPLC (nucleotides)	100	mM	Potassium phosphate monobasic
	100	mM	Potassium phosphate dibasic
	4	mM	Tetrabutylammonium bisulfate
Elution buffer A for LC-MS/MS (polar metabolites)	10	%	Ammonium acetate buffer (10 mM)
	90	%	acetontrile
Elution buffer A for LC-MS/MS (alpha keto acids)	0.1	%	formic acid
Elution buffer B for HPLC (amino acids)	45	%	acetonitrile
	45	%	methanol
	10	%	Water LC-MS grade
Elution buffer B for HPLC (nucleotides)	70	%	Elution buffer A (nucleotides)
	30	%	methanol
Elution buffer A for LC-MS/MS (polar metabolites)	90	%	Ammonium acetate buffer (10 mM)
	10	%	acetontrile
Elution buffer A for LC-MS/MS (alpha keto acids)	0.1	%	formic acid
	90	%	acetontrile
Filtration buffer: pH = 6.95, 330 mOsm/kg	3.5	mM	Potassium phosphate monobasic
	6.7	mM	Potassium phosphate dibasic
	165	mM	Sodium chloride
OPA reagant for amino acid	10	mg	Ortho-phtaldialdehyde

Buffers and solutions - continued

Buffer or solution			**Compound**
analysis	1	mL	potassium borate (0.4 M)
	8.2	L	3-mercaptopropionic acid
Phosphate buffered saline	1.0	mM	Potassium phosphate monobasic
	5.6	mM	Sodium phosphate dibasic
	154.0	mM	Sodium chloride
Tris buffered saline for ELISA	6.1	g	Tris(hyroxymethyl) aminomethane
	8.2	g	Sodium Chloride
	6.0	mL	Hydrochloric acid (6 mM)
	ad 1.0	L	Nanopure water
Tween 20 (10%)	10	%	Tween 20
Washing solution for ELISA	1	L	Tris buffered saline
	5	mL	Tween 20 (10 %)

3.2 Methods

3.2.1 Cryoconservation

Working cell banks of the proprietary CHO cell line (provided by Boehringer-Ingelheim Pharma GmbH Co. KG, Germany) were prepared using the cryo medium (section 3.1.6) to conserve cells of similar origin as a starting point. Therefore, the cryo medium was mixed together and stored at 2 - 8 °C. Cells from the master cell bank were expanded in shake flasks (Corning, USA) and harvested during exponential growth phase with high viabilites above 90 %. After determination of the viable cell density, the cell suspension was transfered to sterile centrifuge tubes (Sarstedt, Germany) and centrifuged at 180 g for 7 minutes in a Megafuge 1.0R (Heraeus, Germany) at room temperature. The old medium was discarded and chilled cryo medium was added to yield a final cell density of 1 x 10^7 viable cells/mL. Aliquots of 1 mL were filled into each cryo vial (Greiner, Germany). The cryo vials were then placed in a controlled-rate freezing apparatus Cryoboy (Nalgene, USA) with a temperature decrease of 1 °C/min and stored in a -70 °C freezer. After 24 h the frozen cryo vials were transferred to the vapor phase of a liquid nitrogen container for long-term storage.

3.2.2 Seed Train

For thawing the cells and reaching a cell density of 0.4 x 10^6 cells/mL, 25 mL of preculture medium were heated to 36.5 °C and then added to a 125 mL shake flask. The cryo vial was thawed at 36.5 °C in water as fast as possible. Once the cells and cryo medium were thawed they were transferred to the prepared shake flask under the hood. The seed train (table 3.7) for the bioreactor cultivations consisted of a sequence of shake flasks with volumes ranging from 125 mL to 1000 mL to expand the biomass until the bioreactors could be inoculated. Each time the inoculation density was 0.4 x 10^6 cells/mL. Passaging of the cells to fresh medium and/or shake flasks with larger volume was done three times each week. The final step in the seed train for a fourfold bioreactor cultivation were four 1000 mL shake flasks with a culture volume of 250 mL each. Cultivation time was about 72 h prior to bioreactor inoculation to reach cell densities of 3 - 4 x 10^6 cells/mL. Incubator (Infors, Switzerland) settings during seed train cultivations were 36.5 °C at 5 % CO_2 and 120 rpm.

Table 3.7: Seed train steps and volumes

Time [h]	Shake flask volume [mL]	Liquid volume [mL]
0	125	25
72	125	50
120	125	50
168	250	100
240	2 x 1000	2 x 250
288	4 x 1000	4 x 250
360	4 x bioreactor	4 x 1000

3.2.3 Bioreactor Cultivation

The following subsections describe the procedure of bioreactor cultivation from inoculation and controller adjustment to both intra- and extracellular sampling. All cultivations were performed in a fourfold DASGIP DS1500ODSS bioreactor system (DASGIP, Germany) equipped with a rushton turbine in the bottom and a pitch-bladed impeller above. Aeration was performed with a gas mixing station (DASGIP, Germany) connected to a L-sparger inside the bioreactor. Temperature, dissolved oxygen and pH were monitored by probes (Mettler Toledo, USA). Two pump modules (DASGIP, Germany) with four peristaltic pumps each were connected for the addition of feeds and base. DASGIP control 4.0 (DASGIP, Germany) was used as process control system.

3.2.3.1 Inoculation

After running the seed train (section 3.2.2), inoculation was done by transferring exponentially growing cells into the bioreactor. The used volume of preculture was determined by calculating a resulting seed density of 0.7 x 10^6 cells/mL for both fed-batch and perfusion cultivations. The according volume of preculture was then centrifuged at 180 g for 7 minutes in a Megafuge 1.0R (Heraeus, Germany) and the cell pellet resuspended in the batch medium. Sterile addition of the inoculum to the autoclaved bioreactor was done by adding the cell suspension to an inoculum flask connected to the bioreactor under the clean bench.

3.2.3.2 Fed-Batch Mode

The cultivations in fed-batch mode were performed using the DASGIP four parallel bioreactor system and can be divided in three different process types explained later in this section. Starting volume for all processes was 1.0 L with an initial batch phase of 24 h. After that, the constant feed was started, so that the final volume after 14 days of cultivation was about 1.4 - 1.5 L. Glucose stock solution with 350 g/L was autoclaved to serve as bolus addition in case of glucose concentrations falling below 11 mM during cultivation. In this case, the glucose concentration was set to 22 mM by adding the according volume of glucose stock solution additional to the constant feed. Setpoints of temperature, pH, dissolved oxygen and agitation were the same for the three different process types and are listed in table 3.8. Prior to cultivation 1 M sodium carbonate solution was prepared as base and filtered for sterilization while CO_2 addition in the ingas was used as acid. Elevated CO_2 aeration was performed mainly in the beginning of the process because of the high initial medium pH of 7.2. Due to increasing cell densities and therefore CO_2 and lactate formation by the cells, the pH controller switched to base addition while CO_2 was held at the overlay value of 3 %.

Table 3.8: Parameter setpoints Fed-Batch for the reference process (REF), the CO_2 stressed process (COP) and the Process with no base addition (NOB)

Process	REF	COP	NOB
Temperature [°C]	36.5	36.5	36.5
pH < 48 h [-]	6.95	6.95	6.95
pH > 48 h [-]	6.80	6.80	6.80
Dissolved oxygen [%]	60	60	60
Agitation [rpm]	200	200	200
CO_2 overlay [%]	3	3	3

The industrial reference process (REF) (provided by Boehringer Ingelheim AG Co. KG) was compared to two settings with altered pH control. While the parameters remained unchanged (table 3.8) the controller settings were changed in regard to the reference (table 3.9). One process setting should depict the influence of increased CO_2 stress (COP), therefore the maximum CO_2 fraction in the ingas was increased to 15 % compared to 10 % in the reference. Moreover, the controller's response was increased

by changing the proportional factor and the reset time to 12.5 and 7200 s, respectively. The controller settings for the other process parameters remained the same as for the reference. The third process setting (NOB) should investigate the effects of base addition, which was therefore suppressed completely resulting in a slow pH shift downwards. The remaining settings were similar to the reference. All three process settings were performed in biological triplicates.

Table 3.9: Controller settings Fed-Batch for the reference process (REF), the CO_2 stressed process (COP) and the Process with no base addition (NOB)

Process	REF	COP	NOB
Base addition [-]	Yes	Yes	No
Max. fraction CO_2 [%] for pH	10	15	10
Deadband for pH [-]	0.05	0.05	0.05
Proportional factor for pH [-]	10	12.5	10
Reset time for pH [s]	9000	7200	9000
Proportional factor for dissolved oxygen [-]	0.1	0.1	0.1
Reset time for dissolved oxygen [s]	300	300	300
Min. flow ingas for dissolved oxygen [L/h]	3	3	3
Max. flow ingas for dissolved oxygen [L/h]	18	18	18
Min. fraction O_2 for dissolved oxygen [%]	50	50	50
Max. fraction O_2 for dissolved oxygen [%]	100	100	100
Proportional factor for temperature [-]	15	15	15
Reset time for temperature [s]	1800	1800	1800

3.2.3.3 Perfusion Mode

The perfusion cultivation was done in a single bioreactor of the fourfold system used for the fed-batch cultivations. The setup is depicted simplified in figure 3.1. As cell retention device a hollow fiber module CFP-4-E-3X2MA (GE Healthcare, Germany) with a membrane area of 230 cm^2 was connected to the bioreactor. The pore size of the hollow fiber module was 0.45 μm, retaining the cells but no media components. The cells were continuously pumped in a loop between bioreactor and hollow fiber module using a 505s peristaltic pump (Watson Marlow, United Kingdom) with a flow rate of 150 mL/min. Therefore, a tangential flow filtration (TFF) was established to avoid clogging of the membrane surface. The harvest, containing the antibody but no cells, was withdrawn from the hollow fiber module with a 101u peristaltic pump (Watson Marlow, United Kingdom). Furthermore, bleeding of the bioreactor could be installed by taking out cell suspension directly from the bioreactor and replacing the volume with fresh medium. The parameter setpoints for the perfusion can be seen in table 3.10. In contrast to the fed-batch processes the pH setpoint was constantly 6.95 throughout the cultivation and agitation was increased to 250 rpm. The controller settings for the perfusion process were same as for the fed-batch reference process (table 3.9).

Table 3.10: Parameter setpoints Perfusion

Process	Perfusion
Temperature [°C]	36.5
pH [-]	6.95
Dissolved oxygen [%]	60
Agitation [rpm]	250
CO_2 overlay [%]	3

The liquid volume in the bioreactor was held constant at 1.0 L. In the first 24 h the cultivation was performed in batch mode with batch medium. After that, perfusion mode was started using again batch medium. In the following, three different subsequent steady states were reached by changing the flow rates. As depicted in table 3.11 the first perfusion rate was 1.0 L/d, equivalent to 1 reactor volume per day. The bleed rate was kept low at 0.03 L/d to reach the first steady-state (SS1) with growth limita-

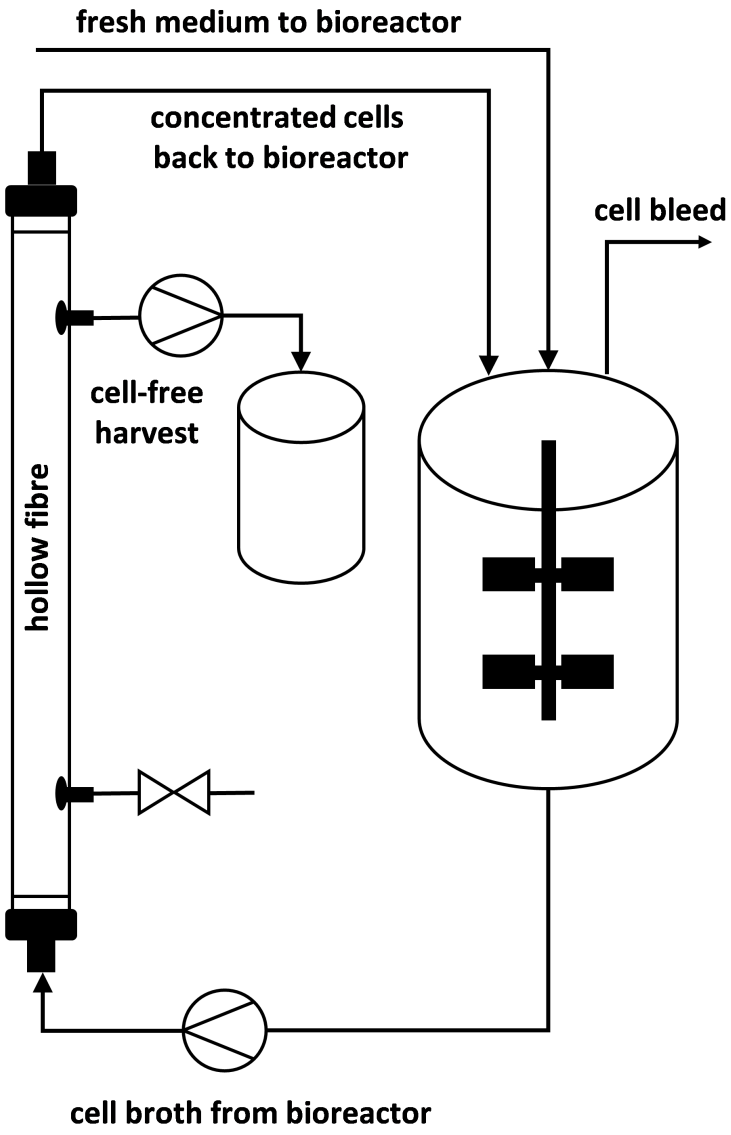

Figure 3.1: Simplified scheme of the perfusion cultivation. The bioreactor was connected to a hollow fiber module and medium was continuously replaced. Cell-free harvest was withdrawn through the pores of the hollow fiber module.

tion due to glucose concentrations below 1 mM and thus an apparent glucose limitation. The according cell density was 15 x 10^6 cells/mL. For the second steady-state (SS2) the perfusion rate was increased to 1.25 L/d but still bleed rates were kept low, again resulting in glucose limitation. The final cell density for SS2 was 25 x 10^6 cells/mL.

For the third steady-state (SS3) both perfusion and bleed rate were increased to 1.50 L/d and 0.25 L/d, respectively. Due to the rise in bleed rate the cell density was artificially constrained at 20 x 10^6 cells/mL and not by glucose limitation. In SS3 medium mixed with glucose stock solution was used to replace the daily bleed to regain glucose concentrations of 35 mM after bleeding. The main difference between SS1 and SS2 on the one side and SS3 on the other side was the glucose limitation in the first two steady-states. Each steady-state was held for at least four days once constant cell densities were reached.

Table 3.11: Perfusion settings and flowrates, modified after Becker, Junghans, Teleki, Bechmann, and Takors (2019b)

Steady-state (SS)	SS1	SS2	SS3
Viable cell density [10^6 cells/mL]	15	25	20
Glucose concentration [mM]	< 1	< 1	> 5
Perfusion rate [L/d]	1.03	1.28	1.50
Bleed rate [L/d]	0.03	0.03	0.25
Harvest rate [L/d]	1.00	1.25	1.25

3.2.3.4 Extracellular Sampling

The sampling for extracellular measurements was done once or twice daily. First, the sample port was flushed with 4 mL of cell suspension from the bioreactor and the suspension was discarded. Afterwards, 4 mL of sample were taken and distributed as follows: Two times 100 μL were pipetted into each 1900 μL 0.01 M potassium hydroxide to shift the carbon equilibrium away from gaseous CO_2 and prevent gassing out. This part was frozen at -20 °C and used for the determination of partial pressure of CO_2 as described in section 3.2.4.7. Further 100 μL were used for the determination of cell density and viability as described in section 3.2.4.1. The remaining sample volume was centrifuged at 800 g and 4 °C for 5 min in a Megafuge 1.0R (Heraeus, Germany). 60 μL of the resulting supernatant were taken for the determination of glucose and lactate concentrations (section 3.2.4.2). The rest of the supernatant was frozen at -70 °C

and thawed later for the quantification of the antibody (section 3.2.4.4) and amino acids (section 3.2.4.3).

3.2.3.5 Intracellular Sampling

Intracellular samples were taken at four distinct time points of the fed-batch processes (early growth phase, middle growth phase, early stationary phase and early decline phase) and every second day for the perfusion process. The first step of the sampling procedure was a fast filtration approach (Matuszczyk, Teleki, Pfizenmaier, & Takors, 2015). Here, cell suspension containing $30x10^6$ cells was taken from the reactor and medium was immediately discarded over a moistened glass fiber filter (Pall, USA), which was retaining the cells, while applying a vacuum of 30 - 60 mbar. This was followed by a washing step with ice cold washing buffer (section 3.1.6) and finally the freezing of the cells on the filter in liquid nitrogen and storage in a -70 °C freezer. For each sample the filtration was repeated three times.
The method by Pfizenmaier et al. (2015) was applied to extract the metabolites using a methanol chloroform extraction as well as evaporation steps. The extracts were then thawed again and used for the quantification of intracellular metabolites (section 3.2.4.5).

3.2.4 Analytics

The following sections describe the analytical methods applied to analyze the metabolic changes due to process conditions.

3.2.4.1 Cell Density and Viability

Determination of total cell density and viability was done using Cedex XS (Roche, Germany) with trypan blue staining. Herefore, the cell suspension was mixed 1:1 with a 0.4 % trypan blue solution (Sigma-Aldrich, USA) after sampling and then measured in triplicates.

3.2.4.2 Glucose and Lactate

For measurement of glucose and lactate concentrations in bioreactor samples, 20 μL of the supernatant was pipetted into LaboTrace reaction vessels with buffer solution. After mixing, the concentrations were determined in triplicates in the LaboTrace analyzer (TraceAnalytics, Germany). If glucose and lactate concentrations were higher than 9 g/L or 2.7 g/L, respectively, dilutions in the buffer solution were increased accordingly.

3.2.4.3 Amino Acids

Extracellular concentrations of amino acids in the supernatant were determined by reversed phase high performance liquid chromatography as described by Pfizenmaier et al. (2015). An Agilent 1200 HPLC (Agilent Technologies, USA) with a fluorescence detector was used for the quantification. Therefore, the wavelengths were set to 230 nm for excitation and 450 nm for emission. Built in were a Zorbax Eclipse Plus C18 guard column and a Zorbax Eclipse Plus C18 column (Agilent Technologies, USA). The gathered chromatograms were analyzed with the software Chemstation (Agilent Technologies, USA) using standards (Sigma-Aldrich, USA) with seven concentration levels for the quantification of each amino acid. Prior to the measurement of samples, the frozen supernatant was thawed, centrifuged and diluted 1:25. Additionally, L-ornithine (Sigma-Aldrich, USA) was used as an internal standard. All measurements were conducted at 40 °C and a flow rate of 1.5 mL/min regarding the mobile phase.

3.2.4.4 Antibody

The antibody titer in the supernatant of the bioreactor samples was determined with enzyme linked immunosorbent assay (ELISA). First, the anti-human IgG F(c) goat antibody (Biomol, Germany) was diluted 1:500 in coating buffer (section 3.1.6). Then the well plates (Greiner, Germany) were coated with the capture antibody and incubated for at least 1 h. After three washing steps with washing buffer (section 3.1.6), the blocking solution (section 3.1.6) containing bovine serum albumin (VWR, Germany) was used to block the non-specific binding sites for 0.5 h. Again, the plate was washed three times. Standards and samples , diluted in dilution buffer (section 3.1.6), were added to the plate in triplicates and incubated for 1 h. Once another threefold washing step was

done, the detection antibody (Biomol, Germany) was diluted 1:90,000 in dilution buffer and added to the wells. After 1 h and five more washing steps, chemiluminescence solution Seramunblau (Seramun Diagnostica, Germany) was added to each well and incubated in the dark for 0.5 h. By adding 0.25 M sulfuric acid the reaction was stopped and a Systec microplate reader (BioTek, USA) was used to measure the absorbance at 450 nm and the reference at 620 nm. The concentration values were then calculated by using the correlation gained from the diluted standards.

3.2.4.5 Intracellular Metabolites

Intracellular adenosine phosphates were quantified from intracellular cell extracts using ion-pair reversed phase high performance liquid chromatography as described by Pfizenmaier et al. (2015). An Agilent 1200 HPLC (Agilent Technologies, USA) with a diode array detector was used for the measurements with a detection wavelength of 260 nm. Built in were a Hypersil BDS C18 guard column and a Supelcosil LC18-T column (Sigma-Aldrich, USA). Elution buffers were prepared as described in section 3.1.6 and used as mobile phase during analysis. The resulting chromatograms were analyzed with the software Chemstation as for the amino acid analysis. Again, seven standard levels for AMP (Fluka, USA), ADP (Gerbu, Germany) and ATP (Gerbu, Germany) were used for calibration and final calculation of sample concentrations. All measurements were conducted at 30 °C and a flow rate of 1.0 mL/min regarding the mobile phase.
The adenylate energy charge (EC) was calculated from the resulting AMP, ADP and ATP concentrations by dividing the sum of ATP and half of ADP concentrations by the sum of all adenosine phosphate concentrations:

$$EC = \frac{c_{ATP} + 0.5 \cdot c_{ADP}}{c_{ATP} + c_{ADP} + c_{AMP}}$$

Intracellular quantifications of metabolites of glycolysis and tricarboxylic acid cycle were done with an Agilent 1200 HPLC system coupled with an Agilent 6410B quadrupole mass spectrometer with an electrospray ion source (Agilent Technologies, USA).
Non-derivatized polar metabolites were quantified as described by Junghans et al. (2019) based on the method described by Teleki, Sánchez-Kopper, and Takors (2015). The apparatus was equipped with a Sequant ZIC-pHILIC column with guard column (Di2chrom, Germany). Metabolites were detected with high selectivity in the multiple reaction

monitoring mode. Absolute quantification was done by isotope dilution using constant addition of $U^{13}C$-labeled algal extracts (Sigma-Aldrich, USA) (Vielhauer, Zakhartsev, Horn, Takors, & Reuss, 2011) as internal standard. Additionally, external calibration was done. The measurements were performed at 40 °C and a flow rate of 0.2 mL/min. Alpha keto acids concentrations were determined with a newly developed method by Junghans et al. (2019). Therefore, derivatization steps were performed to condensate aldehyde and keto groups by phenylhydrazine. The method was adapted from Zimmermann, Sauer, and Zamboni (2014) to cope with LC-MS based quantification. The apparatus was equipped with a ZORBAX SB-C18 column with guard column (Agilent Technologies, USA). Standards were added to quantify metabolites by comparing peak areas. The measurements were performed at 40 °C and a flow rate of 0.3 mL/min. All gathered data was analyzed with the software Masshunter B.05.00 (Agilent Technologies) to calculate final intracellular metabolite concentrations.

3.2.4.6 Osmolality

The osmolality for both cultivation media and buffers were measured using the freezing point depression method with an Osmomat 030 Osmometer (Gonotec, Germany). Before, two point calibration was done by using Nanopure water as zero point and a 300 mOsm/kg or 500 mOsm/kg standard solution as second point. Samples were measured in triplicates.

3.2.4.7 Partial Pressure of CO_2

The inorganic carbon content of the samples, diluted 1:20 in 0.01 M KOH, were determined with a total carbon analyzer (Analytik Jena, Germany) according to Buchholz, Graf, Blombach, and Takors (2014). The samples were thawed and injected into the total inorganic carbon reactor where at first 10% ortho-phosphoric acid was added to shift the equilibrium and gas out the CO_2. In the next step the remaining carbon was determined by combustion at 750 °C turning the carbon compounds to CO_2. The CO_2 from both acidification and combustion was quantified by infrared spectrometry. Standards with defined inorganic carbon content coming from sodium carbonate were used for calibration of the system. All samples were replicated three times. A previously de-

termined Hägg diagramm in combination with measured pH values during cultivation was used for the determination of dissolved CO_2 concentrations.

$$fco_2 = \frac{1}{1 + \frac{10^{\text{-pKS}}}{10^{\text{-pH}}}}$$

The CO_2 fraction f_{CO_2} was calculated at each distinct pH using the acidic dissociation constant pKS. The fraction was then multiplied with the molar concentration of inorganic carbon to yield the dissolved CO_2 concentrations. Finally, the henry coefficient of the medium, also determined in previous experiments, was used to calculate the partial pressure of CO_2.

3.2.5 Cell specific Rates

For all processes the extracellular cell-specific rates were calculated for growth and glucose, lactate, antibody and amino acids production or consumption. For the fed-batch processes cell densities and metabolite concentrations except glucose were fitted with splines using the open access Shape Language Modelling tool in Matlab Version 2013a (Mathworks, USA). All resulting functions were continuously derivable. As described by Wahrheit et al. (2014) no more than four splines were used for each concentration profile to avoid overfitting. Furthermore, only positive values were allowed. Glucose concentrations were not fitted since they were not continuously derivable due to the bolus additions.
For the perfusion process cell specific rates and errors for the above mentioned metabolites were calculated in 24 h intervals from the last three days of each steady-state without spline fitting using mass balance equations:

$$\mu = \frac{B}{V} + \frac{1}{X_V} \cdot \frac{dX_V}{dt}$$

The growth rate μ was calculated using B = bleed rate, V = liquid bioreactor volume, X_V = viable cell density in the bioreactor under the assumption of complete cell retention without cells in the harvest stream.

$$q_{mAb} = \frac{1}{X_V} \cdot \left(\frac{c_{mAb} \cdot P}{V} + \frac{dc_{mAb}}{dt} \right)$$

The cell specific antibody productivity was calculated with c_{mAb} = antibody concentration in the bioreactor, P = perfusion rate under the assumption of the same antibody concentrations in bioreactor and harvest stream.

$$q_{Glc,cons} = \frac{1}{X_V} \cdot \left(\frac{(c_{Glc,m} - c_{Glc}) \cdot P}{V} - \frac{dc_{Glc}}{dt} \right)$$

The cell specific glucose consumption rate was calculated with $c_{Glc,M}$ = glucose concentration in the medium, c_{Glc} = glucose concentration in the bioreactor. For SS3 the glucose consumption rate was determined for the intervals from post-bleeding to pre-bleeding due to the additional glucose feed and the therefore varying glucose bioreactor concentrations.

$$q_{Lac,prod} = \frac{1}{X_V} \cdot \left(\frac{c_{Lac} \cdot P}{V} + \frac{dc_{Lac}}{dt} \right)$$

The cell specific lactate production rate was calculated with c_{Lac} = lactate concentration in the bioreactor.

3.2.6 Flux Balance Analysis

For the quantification of intracellular flux distributions the Cobra Toolbox 2.0 implemented in Matlab Version 2013a was used (Schellenberger et al., 2011). The model was adapted from Sou et al. (2015), using the biomass composition from Selvarasu et al. (2012). It was expanded by exchange reactions for all metabolites as well as reactions for oxidative phosphorylation to calculate ATP formation rates coming from different sources. P/O rations were 2.5 for NADH and 1.5 for $FADH_2$ (see section 2.2.2). The total number of reactions was 213, while 240 metabolites were considered in the compartments cytosol and extracellular. The model was not further compartmentalized into

a mitochondrial part. At the beginning, inequality constraints were imposed by defining reactions either being reversable or non-reversable. The next step was the definition of lower and upper bounds for all measured uptake or production rates. This applied to fluxes of growth, glucose, lactate, antibody and amino acids. For the fed-batch cultivations the boundaries were set as mean value of biological triplicates plus/minus the standard error for each of the three time points. For perfusion, the mean values and errors were calculated from the last three days of each steady-state. For the optimization, the maximization of ATP generating reactions was set as objective to cope with the cellular ATP demand for maintenance and antibody synthesis.
For the determination of flux errors a Monte Carlo sampling method by Thiele et al. (2005) was used. First, 2,500 warmup points were randomly distributed within the solution space and then used to position 2.5 x 10^6 sampling points to eventually calculate the flux errors. Furthermore, the resulting flux distributions were used to calculate ATP formation rates coming from either oxidative phosphorylation (NADH or $FADH_2$), TCA (succinyl-CoA-synthetase) or glycolysis. Carbon balances for incoming and outgoing carbon were derived from flux distributions by calculating each flux on the carbon basis. Moreover, the redox variable R was calculated as described by Nolan & Lee (2011). Herefore, the flux of NADH being generated in glycolysis was divided by the flux of NADH being transformed in oxidative phosphorylation minus the flux of NADH produced in TCA:

$$R = \frac{v_{glycolysis \rightarrow NADH}}{v_{NADH \rightarrow oxPhos} - v_{TCA \rightarrow NADH}}$$

4 Results

This chapter summarizes the results of the applied approaches of process intensification. Both fed-batch and perfusion mode cultivations have been investigated as CHO antibody production processes. The first part deals with the influence of the scale-up sensitive parameters CO_2 and pH on fed-batch cultivations. The second part describes the influence of glucose limitation on cells in steady-state perfusion mode in comparison to non-limited steady-states. In both parts the results are going to be compared regarding changes in cellular phenotype, cell specific rates and production kinetics caused by the different process settings. Furthermore, reasons for these changes are being elucidated by applying flux balance analyses as modelling approach combined with intracellular metabolomics. The focus is put on linking productivity with the intracellular energy availability and the efficiency of cellular carbon metabolism.

4.1 Fed-Batch

In this first part the results of the three different fed-batch settings are described. Results of the following section have been partially published in Becker, Junghans, Teleki, Bechmann, and Takors (2019a) (see appendix A).

4.1.1 Cellular phenotype and product formation under the influence of pH and pCO_2

Three different process settings were carried out in biological triplicates to investigate the influence of the titration agents CO_2 and Na_2CO_3 on the performance of a fed-batch production process: REF (reference process), COP (increased CO_2 stress) and NOB (no base titration). In the industrial reference process (REF) CO_2 addition above the 3 % overlay was needed in the first process period to decrease the pH to setpoint

values of 6.80. Hereafter, the pH controller in the reference process started adding base until the end of the process to keep a constant pH value due to acidification by the cells. In addition to the reference process one process setting aimed at the first phase of the process and had increased CO_2 aeration in the beginning but comparable settings afterwards (COP). The third process setting was similar to the reference in the beginning but base addition was suppressed after that (NOB). A detailed description of the process settings can be found in 3.2.3.2. The different settings resulted in the profiles of pH, pCO_2 and osmolality shown in figure 4.1, which were the basis to distinguish the three process types.

The pH in figure 4.1 A continuously decreased in the first four days for all three process settings towards the setpoint of 6.80. Once the deadband was reached, the pH controller shifted from CO_2 addition to base addition for REF and COP. Accordingly, the pH stayed constant within the deadband in the remaining process time. In contrast, in NOB base addition was suppressed completely and therefore pH kept on decreasing slightly. Final values here were around 6.60.

Partial pressures of CO_2 in figure 4.1 B were around 100 - 120 mbar for REF and NOB during the first four days due to the increased aeration of CO_2 for pH control. After the pH setpoint was reached, pCO_2 fell towards 90 mbar for both the process settings. Meanwhile, COP showed elevated pCO_2 of up to 200 mbar because of the adapted controller settings to investigate CO_2 stress. After 120 h pCO_2 decreased to 90 mbar similar to REF and NOB. In the following, pCO_2 kept on increasing towards the end of the cultivation with final values of approximately 150 mbar for REF and COP. The rise was probably caused by adding Na_2CO_3, hereby increasing the total inorganic carbon content in the system. More base was added for COP, therefore explaining the slightly higher pCO_2. Highest pCO_2 in NOB with final values of around 220 mbar however originated from the lower pH which promoted a shift in carbon equilibrium towards CO_2.

Osmolality in figure 4.1 C was comparable for all three settings until the stationary phase. Mainly through the feed addition the osmolality increased to 360 mOsm/kg. Only after that the effect of base addition got more pronounced. After 238 h the osmolality reached 440 mOsm/kg in REF and COP while it stayed constant in NOB.

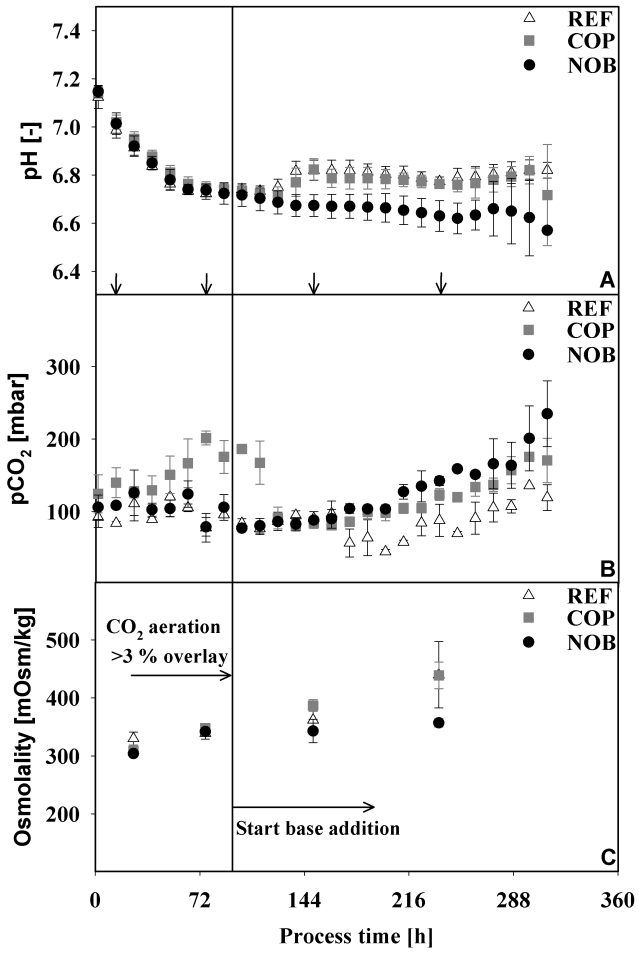

Figure 4.1: Profiles of pH (A), pCO_2 (B) and osmolality (C) over the process time for the three settings REF, COP and NOB. Vertical arrows at the bottom of (A) indicate process times of intracellular sampling. The vertical line in (D) indicates the switch of the pH controller from CO_2 addition to Na_2CO_3 addition in the reference process. Shown errors were determined from biological triplicates. With modifications to appendix A.

To point out differences in the cellular phenotype for the three process settings, the main cell specific rates and their according concentrations were determined. The growth behavior is depicted in figure 4.2. The viable cell density (4.2 A) had comparable profiles despite different process settings. However, the cell density was highest for REF with maximum cell densities of 14.6×10^6 cells/mL. While NOB had slightly lower maximum cell densities of 12.5×10^6 cells/mL, COP showed a significant drop in cell den-

sities with maximum values of only 9.5x10^6 cells/mL. Cell densities began diverging from REF already after 96 h. Moreover, cells in COP entered the decline phase after about 216 h whereas cell densities in REF started declining after 238 h. NOB had a prolonged stationary phase while maintaining maximum cell densities and did not show any severe breakdown in cell densities over the total process time of 312 h.

Kinetics of growth rates (μ) in figure 4.2 B were behaving similarly for all three settings. During early growth phase after 72 h the growth rate was 0.5 to 0.6 1/day for all settings. Nevertheless, rates were highest for REF and lowest for the CO_2 stressed environment in COP in the following, coinciding with the differences in viable cell densities. Cellular growth stopped completely for COP and NOB after 216 h while cells in REF were still growing at very low rates of below 0.1 1/day.

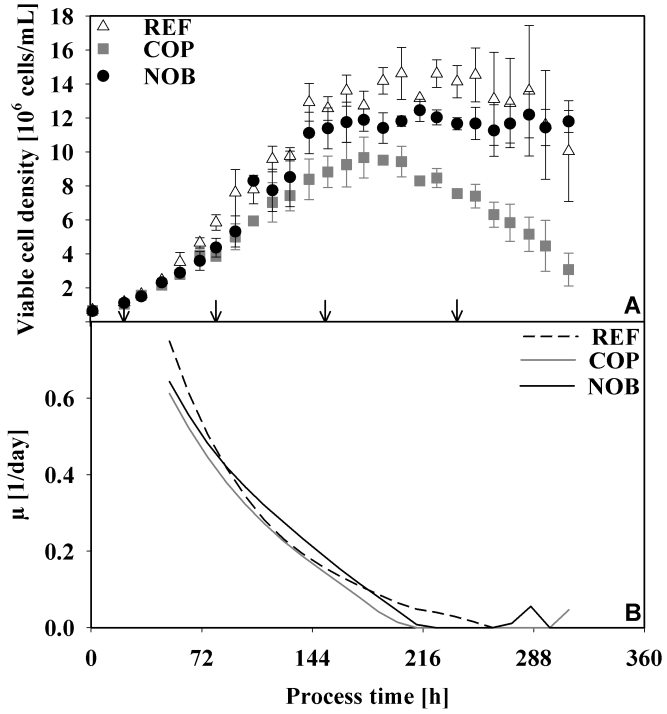

Figure 4.2: Profiles of viable cell density (A) and growth rate (B) over the process time for the three settings REF, COP and NOB. Vertical arrows at the bottom of (A) indicate process times of intracellular sampling. Shown errors were determined from biological triplicates. With modifications to appendix A.

Antibody concentrations in figure 4.3 A were rising identically until 156 h and 0.6 g/L. Only then the profiles started diverging. Whereas REF and NOB both showed further steeply increasing titers, antibody concentrations in COP started to bottom out. Final concentrations in REF were 1.40 g/L while NOB had highest titers of about 1.60 g/L despite the slightly lower cell densities. A substantially reduced titer was found for COP. Here, final titers reached only 0.77 g/L and therefore 50 % of the reference values.

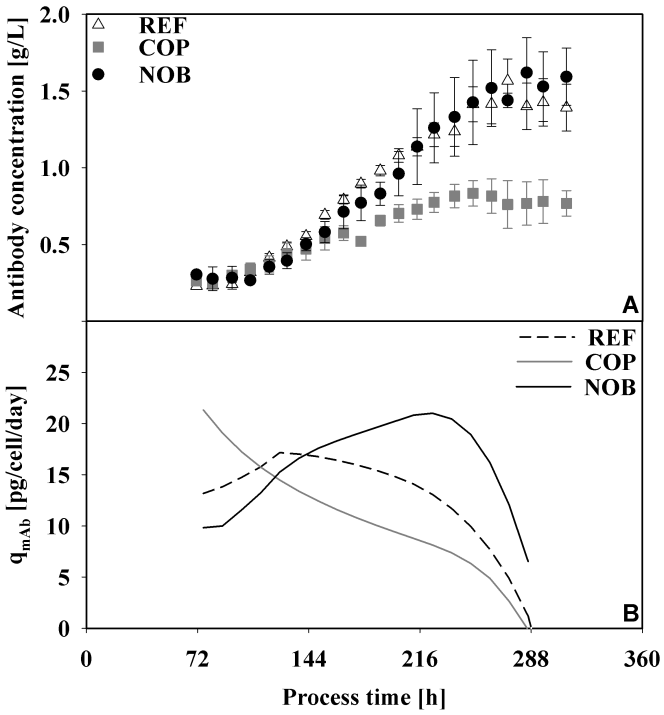

Figure 4.3: Profiles of antibody concentration (A) and cell specific antibody productivity (B) over the process time for the three settings REF, COP and NOB. Shown errors were determined from biological triplicates. With modifications to appendix A.

Striking differences could also be found for the kinetics of antibody productivity (q_{mAb} in figure 4.3 B) for the three settings. REF reached its highest cell specific productivity of 18 pg/cell/day during the growth phase. Hereafter, q_{mAb} declined steadily towards the end of the cultivation. Interestingly, COP reached its peak productivity of 21 pg/cell/day in very early stages of the process when maximum CO_2 stress was present. However, q_{mAb} began diminishing in the following, too, explaining the harsh loss in titer. A completely different profile was determined for NOB. While productiv-

ities were comparable to REF in the early stages, they continued increasing even after q_{mAb} started declining in REF. Consequently, the peak productivity of 21 pg/cell/day was reached in stationary phase 240 h. Since maximum cell densities were present here, final titers were highest in NOB despite the lower cell densities (figure 4.2 A).

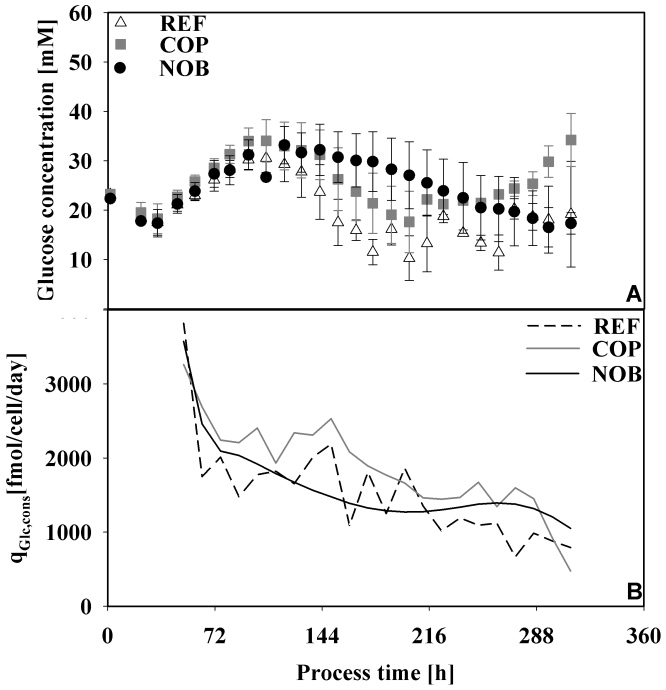

Figure 4.4: Profiles of glucose concentration (A) and cell specific glucose uptake rate (B) over the process time for the three settings REF, COP and NOB. Shown errors were determined from biological triplicates. With modifications to appendix A.

The main substrate of the cells was glucose which was also added by feeding. Glucose concentrations in figure 4.4 A had similar courses for the first 120 h of the cultivation. Due to the feeding concentrations increased to 30 - 35 mM. In the following all three profiles began to fall, although they differed in the extent of glucose uptake. Differences were caused by varying cell densities and glucose uptake rates between the three settings. For REF and COP glucose bolus additions were necessary because glucose concentrations below 11 mM were detected. Only for NOB glucose addition through the constant feed was sufficient. By applying the continuous feed the glucose

concentrations ranged between 11 and 35 mM for all settings during the complete process time, so depletion was avoided.

When comparing the cell specific glucose consumption rate $q_{Glc,\,cons}$ in figure 4.4 B, the profiles were comparable since all showed a steady decrease with the ongoing process. However, cells in COP showed elevated $q_{Glc,\,cons}$ during stationary phase compared to REF and NOB.

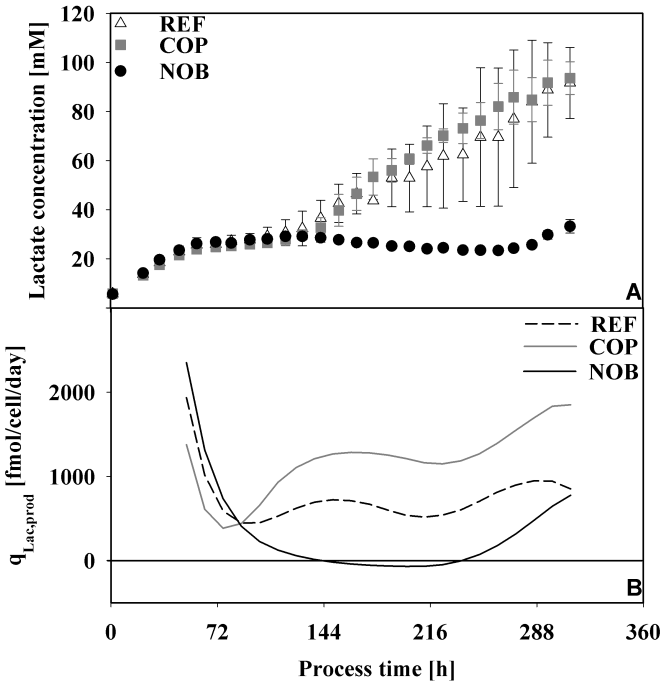

Figure 4.5: Profiles of lactate concentration (A) and cell specific lactate production rate (B) over the process time for the three settings REF, COP and NOB. Negative cell specific lactate production in (B) corresponds to a switch to lactate uptake. Shown errors were determined from biological triplicates. With modifications to appendix A.

The main by-product of the cells resulting out of the carbon metabolism was lactate. The profiles of lactate concentrations (figure 4.5 A) were almost identical for REF and COP although cell densities (figure 4.2 A) were varying. Here, concentrations were constantly increasing to final values above 90 mM. Major differences could be found for NOB where lactate concentrations even started to slightly decrease towards 20 mM from 144 h on. Only in late stationary phase at about 240 h lactate concentrations began

to increase again. Nevertheless, final concentrations of 33 mM were almost 70 % lower than for REF and COP.

The cell specific lactate production rate $q_{Lac,\,prod}$ (figure 4.5 B) was identical in the very early stages of the process where it was declining for all three settings. After 96 h profiles began diverging with cells in both REF and COP producing lactate. However, $q_{Lac,\,prod}$ experienced a more pronounced increase in COP with peak values of almost 2000 fmol/cell/day. The mean lactate production was elevated by about 80 % compared to REF for the process time after 96 h. In contrast, $q_{Lac,\,prod}$ was dropping severely in NOB and cells even began taking up lactate after 144 h, which had been produced before. Only in late process stages from 240 h on the main by-product was produced again.

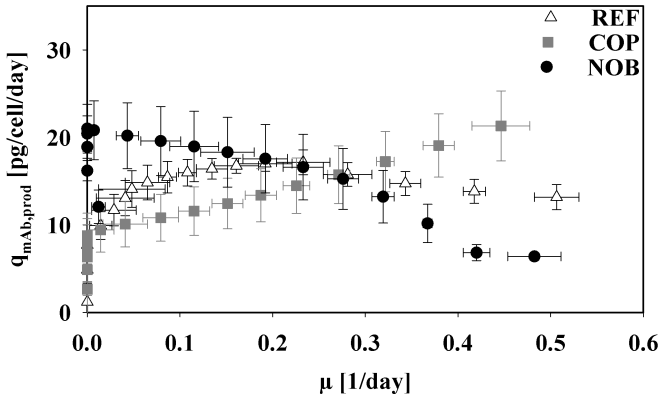

Figure 4.6: Cell specific antibody productivity as a function of growth rate for the three settings REF, COP and NOB. Shown errors were determined from biological triplicates. With modifications to appendix A.

To emphasize the shift in production kinetics observed in figure 4.3 B, q_{mAb} is plotted as a function of μ in figure 4.6. In REF, the cells showed a combination of growth coupled and decoupled antibody production behavior. Remarkably, substantial differences could be observed for COP and NOB. Whereas COP displayed strongly growth coupled production linked to eleveated CO_2 stress, cells in NOB reached peak productivities in stationary phase when μ was heading towards zero.

The resulting effect can clearly be seen when analyzing the volumetric productivity (Q_{mAb}) in figure 4.7. REF reached its highest volumetric productivities of 0.22 g/L/day in early stationary phase after 168 h mainly due to high viable cell densities, since cell

specific productivities were already decreasing at this point (figure 4.3 B). Values of Q_{mAb} in COP mirror the negative long-term effect of increased CO_2 stress on the cells. Here, both cell specific productivity and viable cell density (figure 4.2 A) were lowest. Therefore, the volumetric productivity peaked at 0.11 g/L/day after 144 h. Slightly lower cell densities for NOB were compensated by continuously increased q_{mAb}. As a result Q_{mAb} was highest with 0.26 g/L/day in the stationary phase of the process.

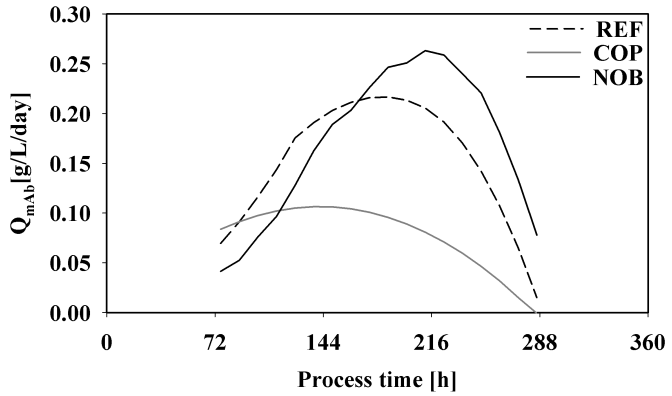

Figure 4.7: Profile of the volumetric productivity of the antibody over the process time for the three settings REF, COP and NOB. With modifications to appendix A.

4.1.2 Intracellular flux distributions and balancing of ATP and carbon

To gain deeper insights into metabolic adaptions to the different process settings, intracellular flux distributions were determined via flux balance analysis. Three distinct states were analyzed: The growth phase after 83 h, the early stationary phase after 154 h and the early decline phase after 238 h. The flux distribution in the growth phase (figure 4.8) reveals no many significant differences between REF, COP and NOB as already observed for the extracellular cell specific rates in section 4.1.1. Early glycolytic flux was around 2000 fmol/cell/day and therefore obviously identical to $q_{Glc,\,cons}$ (figure 4.4 B). Fluxes through pentose pathway were identical as were the growth rates. Byproduct formation in terms of alanine from pyruvate was at about 200 fmol/cell/day for all settings. Flux through TCA was slightly higher for COP along with highest q_{mAb}.

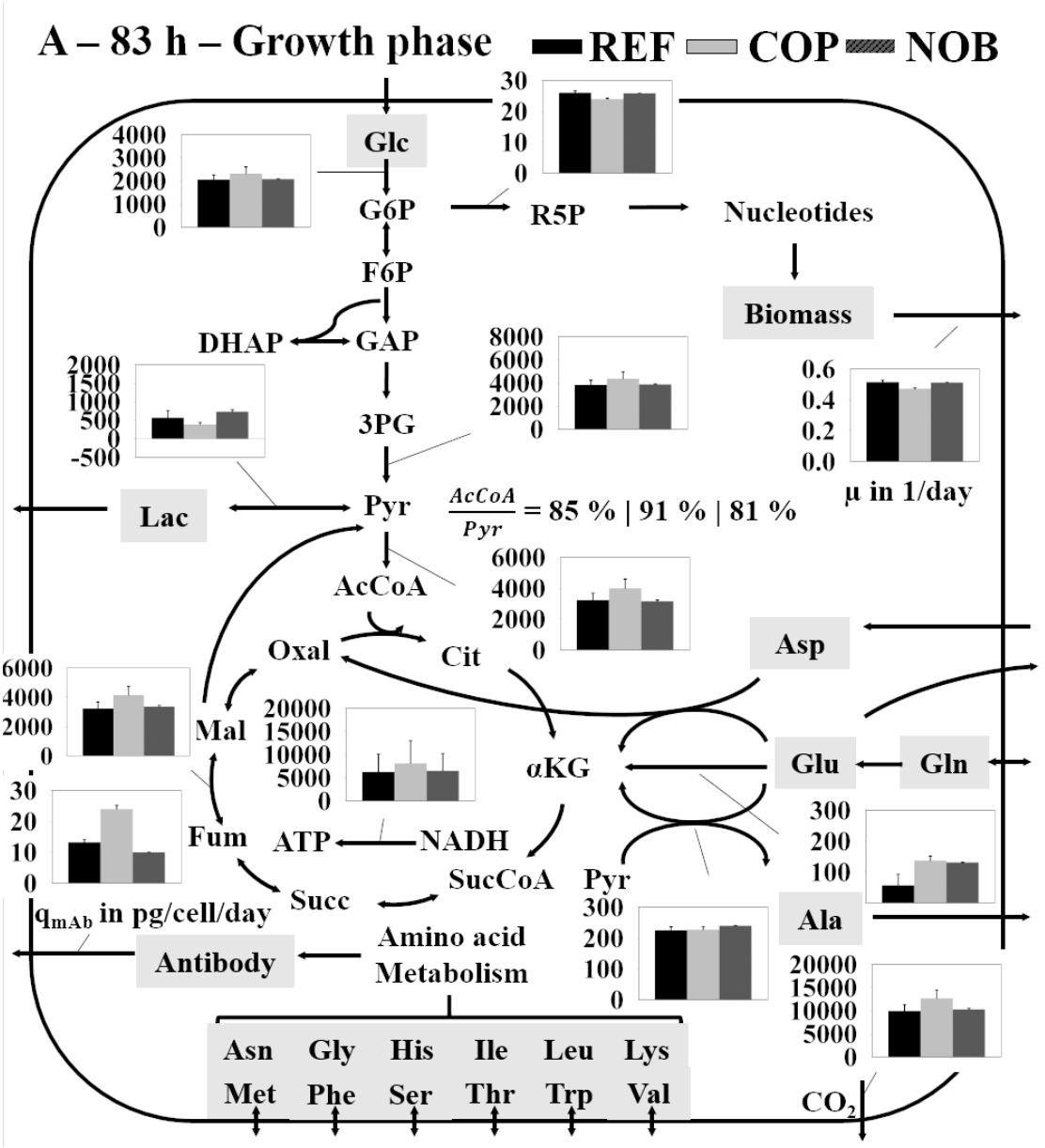

Figure 4.8: Simplified main carbon metabolism representing the results of the flux balance analysis during the growth phase after 83 h for the three settings REF, COP and NOB. Fluxes are given in fmol/cell/day except for growth rate (1/day) and cell specific antibody productivity (pg/cell/day). Errors were determined through Monte Carlo sampling of the solution space for each setting as described in section 3.2.6. With modifications to appendix A.

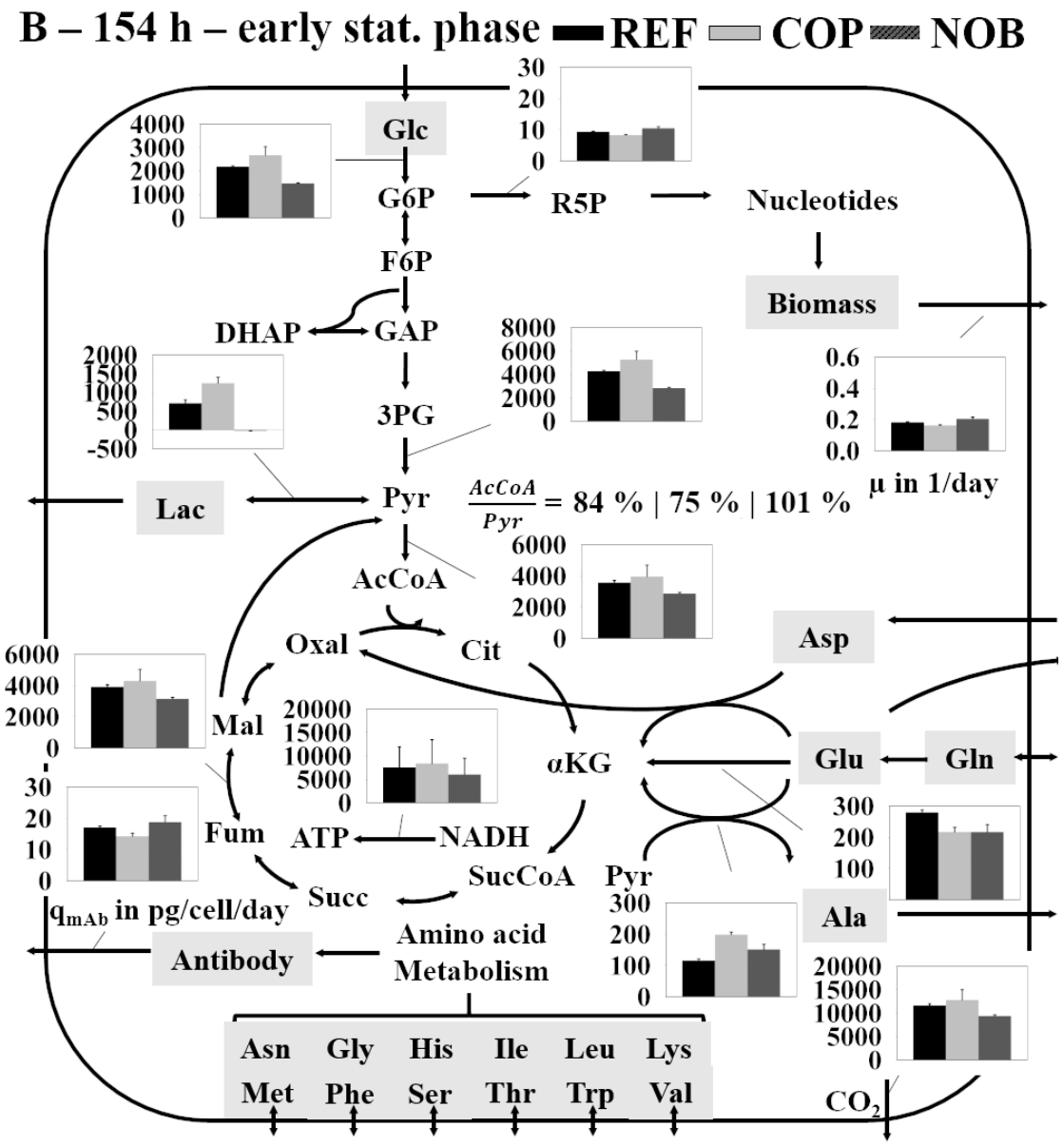

Figure 4.9: Simplified main carbon metabolism representing the results of the flux balance analysis during the early stationary phase after 154 h for the three settings REF, COP and NOB. Fluxes are given in fmol/cell/day except for growth rate (1/day) and cell specific antibody productivity (pg/cell/day). Errors were determined through Monte Carlo sampling of the solution space for each setting as described in section 3.2.6. With modifications to appendix A.

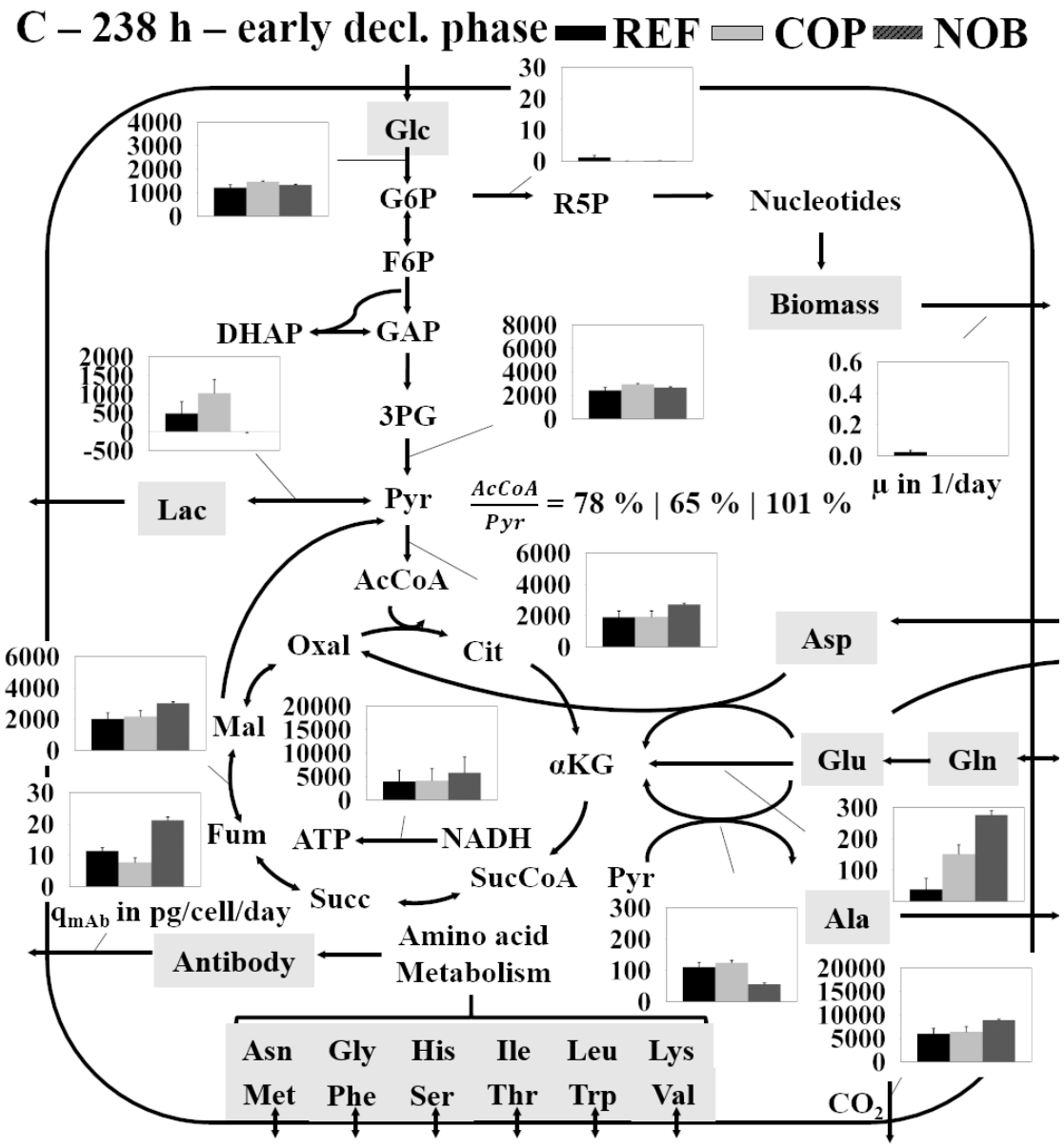

Figure 4.10: Simplified main carbon metabolism representing the results of the flux balance analysis during the early decline phase after 238 h for the three settings REF, COP and NOB. Fluxes are given in fmol/cell/day except for growth rate (1/day) and cell specific antibody productivity (pg/cell/day). Errors were determined through Monte Carlo sampling of the solution space for each setting as described in section 3.2.6. With modifications to appendix A.

In the early stationary phase the flux distributions began diverging (figure 4.9). The glycolytic flux was lowest in NOB according to the lowest $q_{Glc,\,cons}$ (figure 4.4 B). However, since lactate was not produced, all of the pyruvate resulting out of glucose was fueling the TCA. In contrast, only 84 % and 75 % of the pyruvate were entering the TCA in REF and COP, respectively. As a result, fluxes into TCA were only about 20 % lower for NOB although fluxes towards pyruvate had been about 50 % lower. TCA fueling reaction coming from glutamate towards alpha-ketoglutarate was similar at 200 fmol/cell/day for all settings. By-product formation was highest for COP since besides lactate also alanine was produced in identical amounts as in the growth phase. For REF and NOB the alanine flux sank to 100 and 150 fmol/cell/day, respectively.

In the very late stages of the process the glycolytic flux decreased likewise for all settings towards 1000 - 1500 fmol/cell/day (figure 4.10). Along with the growth rates the flux through pentose phosphate pathway decreased sharply. The fraction of pyruvate entering TCA was still at about 100 % for NOB, since neither lactate nor alanine were produced in significant amounts. Furthermore, the flux of glutamate to alpha-ketoglutarate was highest in NOB with almost 300 fmol/cell/day, whereas REF and COP only reached 30 and 150 fmol/cell/day, respectively. Consequently, the flux through TCA was highest for NOB with approximately 3000 fmol/cell/day coinciding with the highest q_{mAb}. REF and COP however did not exceed flux values of 2000 fmol/cell/day in the TCA.

Figure 4.11 shows the cell specific ATP formation rates (q_{ATP}) in the three distinct cultivation phases. During the growth phase (figure 4.11 A) q_{ATP} was highest in COP with almost 40,000 fmol/cell/day, while REF and NOB had formation rates of about 30,000 fmol/cell/day. Interestingly, the elevated q_{ATP} in COP was coinciding with the highest pCO_2 (figure 4.1 B). The fractions of ATP origin were identical for all settings. Oxidative phosphorylation accounted for about 65 % (taking together NADH and $FADH_2$), ATP resulting from succinyl-CoA synthetase in TCA for 10 % and glycolysis directly for 25 %. The yield of mol_{ATP} per carbon mol substrate was also increased in COP with 1.75 compared to 1.58 and 1.55 in REF and NOB, respectively.

During early stationary phase q_{ATP} was similar to the growth phase for all three settings. Changes were not more pronounced than 10 % of the previous value. The ratio of ATP sources remained almost the same. In contrast, cells in all three settings now had almost identical yields of ATP from carbon ranging from 1.88 to 1.96.

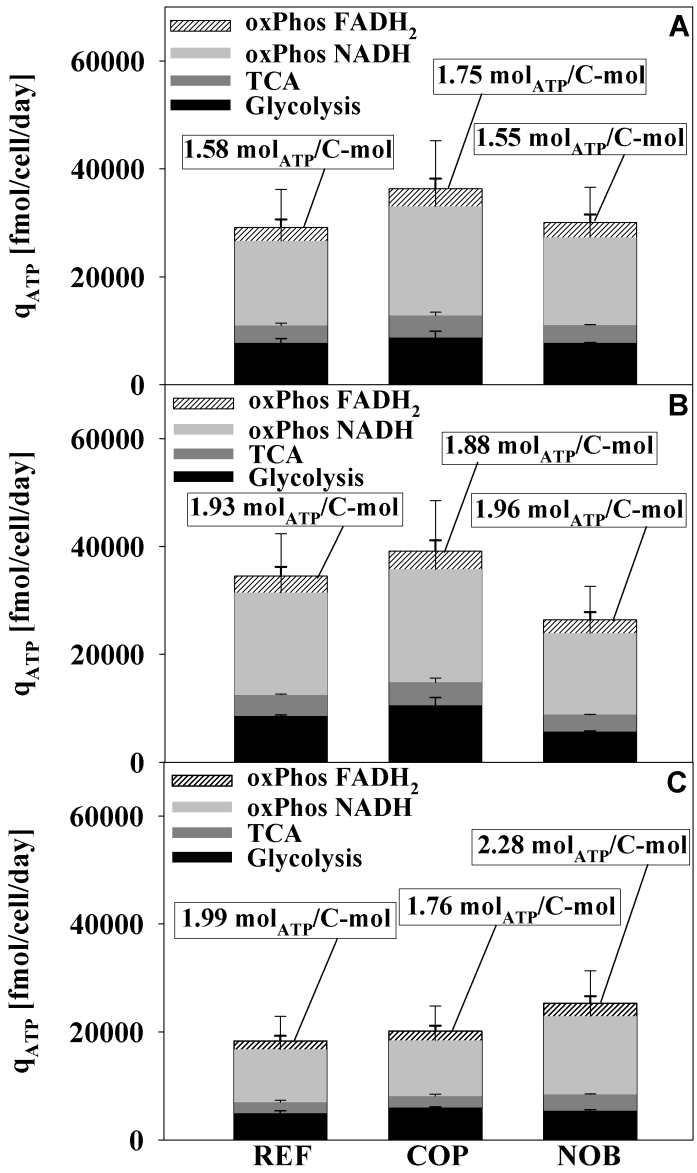

Figure 4.11: Cell specific ATP production rates during growth phase (A), early stationary phase (B) and early decline phase (C) for the three settings REF, COP and NOB. Sources of ATP formation are oxidative phosphorylation either from $FADH_2$ or NADH (from both glycolysis and TCA), succinyl-CoA synthetase in TCA or glycolysis directly. Results were calculated from the flux balance analysis including errors from Monte Carlo sampling of the solution space for each setting as described in 3.2.6. With modifications to appendix A.

In the early decline phase (figure 4.11 C) the ATP formation diverged. While cells in NOB could maintain an almost constant q_{ATP} of 25,000 fmol/cell/day, REF and COP broke down in ATP synthesis. Both processes almost halved their ATP production per cell, therefore ending at 20,000 fmol/cell/day. The fraction of ATP coming from glycolysis decreased to less than 20 % in NOB. Instead, more ATP was coming from oxidative phosphorylation. Additionally, the yield of ATP per carbon mol substrate increased further in NOB to 2.28, whereas it stayed constant in REF and declined to 1.76 in COP.

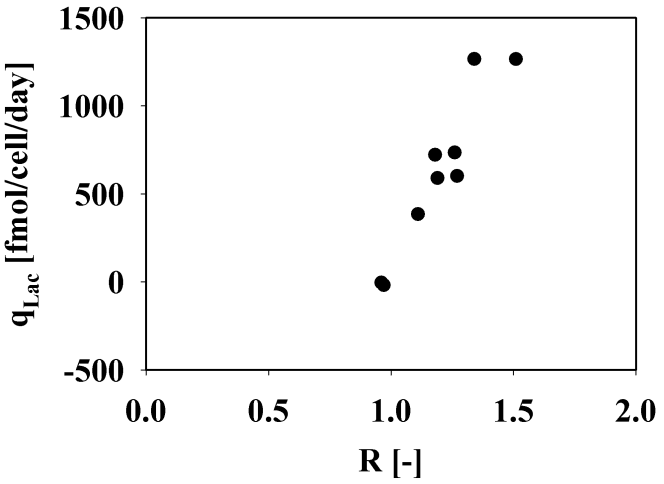

Figure 4.12: Cell specific lactate production rate combined for all three settings REF, COP and NOB as function of the redox variable R. Results were calculated from the flux balance analysis.

Figure 4.12 lumps together the lactate formation of all three process types as function of the redox variable R, which was introduced in section 3.2.6. The lactate formation positively correlates with R. Slight lactate uptake was found in NOB where R was also lowest with values of about 1.0 according to the theoretical definition. Highest R values of 1.3 and 1.5 in COP were coinciding with the highest q_{Lac} of almost 1300 fmol/cell/day.

By contrast, the cell specific antibody productivity was negatively correlating with R (see figure 4.13). Again, values of all three process types are combined. Here, highest q_{mAb} of about 21 pg/cell/day were reached in early stages of COP and late stages of NOB with corresponding R values of 1.1 and 1.0, respectively. Late stages of COP showed lowest q_{mAb} of 7 pg/cell/day and highest R of 1.5.

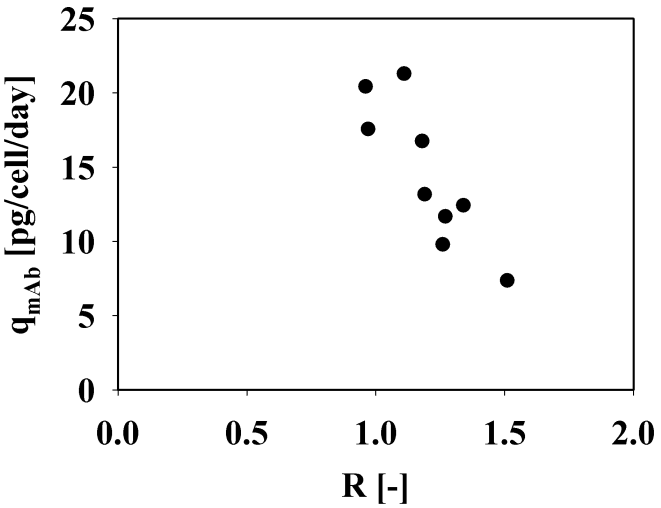

Figure 4.13: Cell specific antibody productivity combined for all three settings REF, COP and NOB as function of the redox variable R. Results were calculated from the flux balance analysis.

Balances for incoming and outgoing carbon during the growth phase are depicted in figure 4.14. For all three settings glucose was accounting for two thirds of the incoming carbon. Asparagine, Glutamine and Leucine were responsible for about 5 - 7 % of the carbon substrate each. The sum of carbon used was similar for all settings and ranging from 18.4 pmol-carbon/cell/day to 20.7 pmol-carbon/cell/day. On the other side, CO_2 was the major product on a carbon basis with approximately 60 %. Biomass accounted for almost 20% and lactate for 10-13 % for REF and NOB and only 6 % for COP.

For REF and COP the fraction of glucose in incoming carbon increased by 10 % in the early stationary phase (figure 4.15). Obviously, the total amount of amino acids reduced accordingly. The flux of carbon stayed constant for REF and COP, whereas it significantly reduced to 13.5 pmol-carbon/cell/day in NOB. The fraction of biomass for the outgoing carbon diminished in all three settings, while the lactate fraction increased to 15-20 % only in REF and COP. NOB was not producing lactate any more. On the other hand, the fraction of CO_2 grew likewise in NOB.

Towards the end of the process, differences between NOB and the other two settings became more obvious. The fraction of glucose as carbon source increased by further 5 % in REF and COP towards 80 %. For NOB, the fraction rose to 70 %, while the remaining

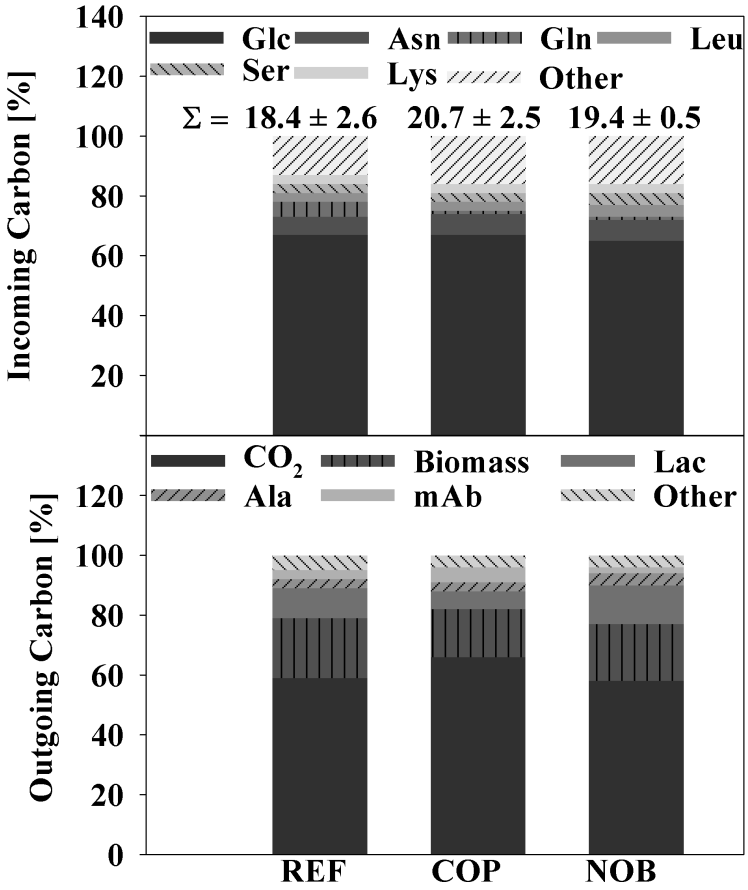

Figure 4.14: Carbon balances showing the main fractions for incoming (A) and outgoing (B) carbon during the growth phase after 83 h for the three settings REF, COP and NOB. Remaining amino acids with minor contributions are lumped into other AA. Carbon balances were calculated from the flux balance analysis.

carbon was split up in minor contributions of different amino acids. The total carbon flux diminished sharply for REF and COP by almost half to 9.2 pmol-carbon/cell/day and 11.4 pmol-carbon/cell/day, respectively. Compared to the stationary phase the flux reduced only slightly to 11.1 pmol-carbon/cell/day for NOB. Differences in outgoing carbon were even more pronounced. While CO_2 was still the major fraction, lactate now accounted for 16 and 27 % in REF and COP. For NOB, still no lactate was formed similar to the state in the stationary phase. Instead, the fraction of CO_2 increased further to 82 %.

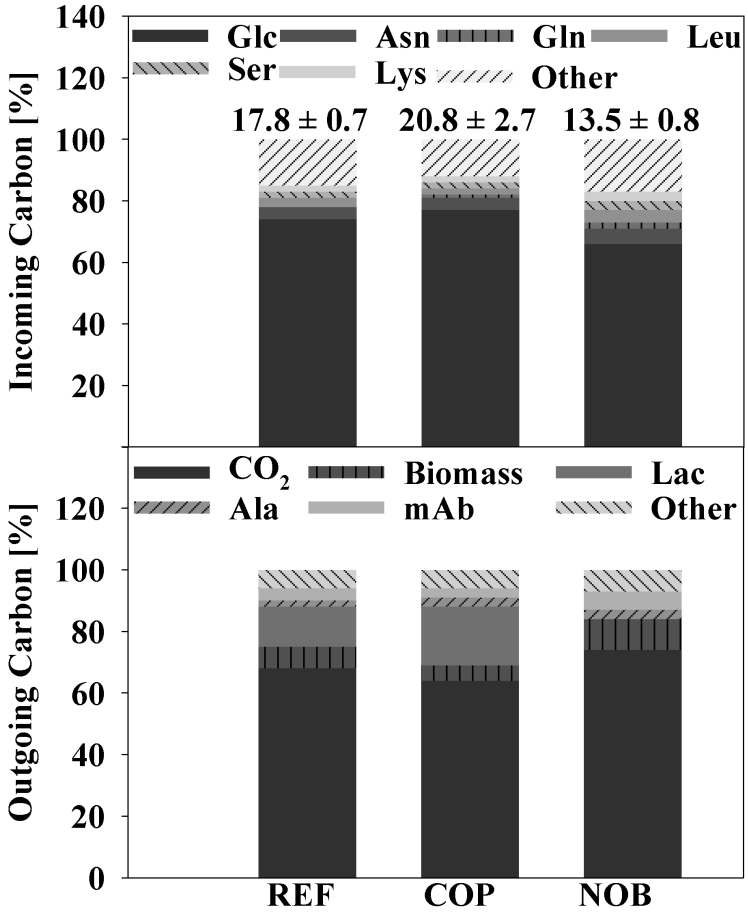

Figure 4.15: Carbon balances showing the main fractions for incoming (A) and outgoing (B) carbon during the early stationary phase after 154 h for the three settings REF, COP and NOB. Remaining amino acids with minor contributions are lumped into other AA. Carbon balances were calculated from the flux balance analysis.

4.1.3 Intracellular pool sizes of glycolysis, TCA and nucleotides in fed-batch phases

Pool sizes of intracellular intermediates of glycolysis, TCA and adenylate nucleotides were determined. The comparison for glycolysis is depicted in figure 4.17.

Similar to glycolysis, no significant differences between the pool sizes of TCA intermediates in the three process settings could be determined (figure 4.17). Pool sizes ranged from 0.01 fmol/cell for cis aconitate to 1.5 fmol/cell for the lumped pool of

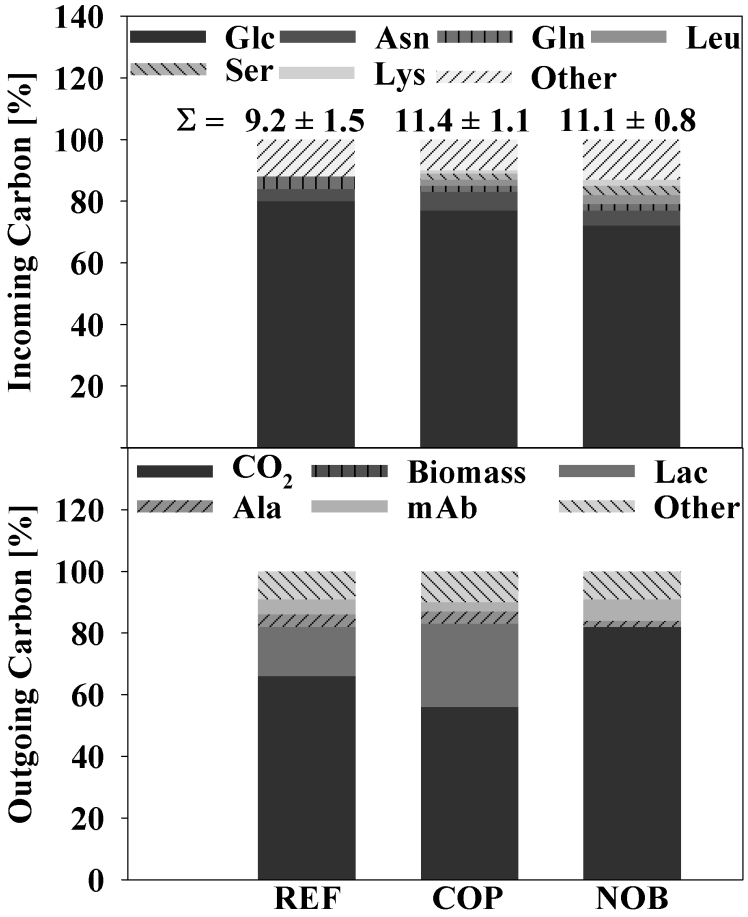

Figure 4.16: Carbon balances showing the main fractions for incoming (A) and outgoing (B) carbon during the early decline phase after 238 h for the three settings REF, COP and NOB. Remaining amino acids with minor contributions are lumped into other AA. Carbon balances were calculated from the flux balance analysis.

citrate/isocitrate. While the concentrations of citrate/isocitrate and cis aconitate stayed almost constant over process time for all settings, the concentrations decreased by about two thirds for malate, fumarate, alpha ketoglutarate and succinate until the end of the process time. For most metabolites no major differences could be found between the three settings, whereas a general declining trend could be observed. Concentrations ranged from 0.05 fmol/cell for DHAP to 2.5 fmol/cell for pyruvate. Only for intracellular pyruvate notable differences were detected. While REF and COP had increased

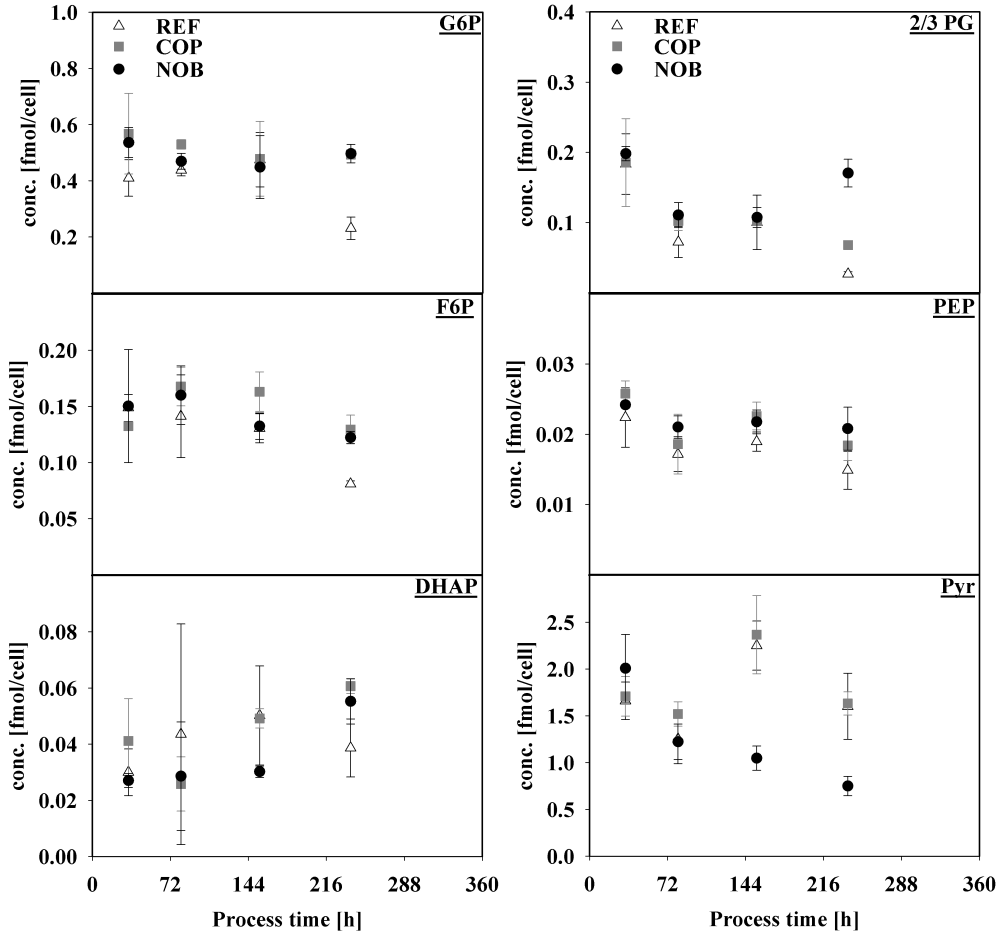

Figure 4.17: Intracellular pool sizes of intermediates of glycolysis for the three settings REF, COP and NOB. Error bars indicate the error of technical triplicates.

pyruvate pool sizes of 2.5 and 1.75 fmol/cell after 153 and 238 h, respectively, pool sizes in NOB were approximately 1.0 fmol/cell. The significantly decreased pyruvate concentrations coincided with lower lactate formation (figure 4.5) and higher yield of pyruvate entering the TCA (figures 4.9 and 4.10). Intracellular concentrations of the nucleotides AMP, ADP and ATP as well as the corresponding adenylate energy charge are shown in figure 4.19. AMP had the lowest intracellular concentrations with about 0.2 fmol/cell. Concentrations were similar during the course of the process, only in the early decline phase after 238 h the concentration in COP was doubled with 0.25 fmol/cell compared to REF and NOB. ADP pool sizes were constant for COP and NOB with approximately

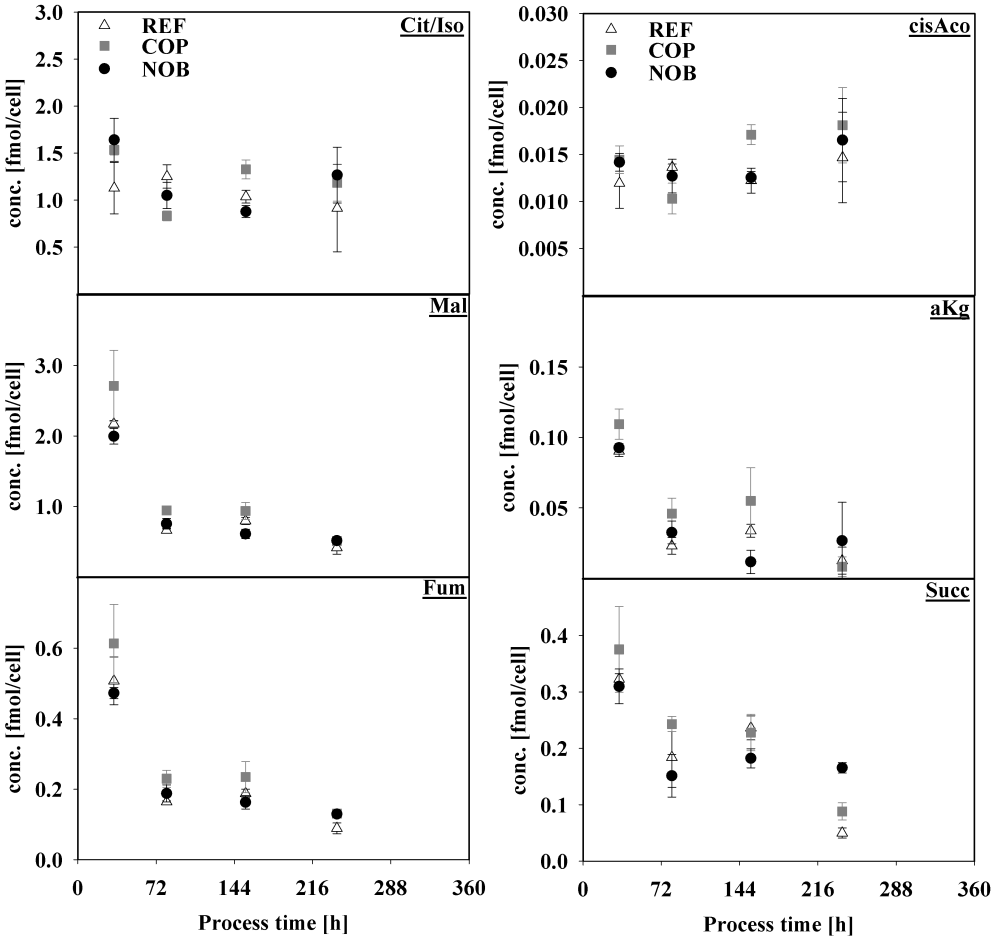

Figure 4.18: Intracellular pool sizes of intermediates of TCA for the three settings REF, COP and NOB. Error bars indicate the error of technical triplicates.

1.0 fmol/cell throughout the process. The same held true for REF, only after 238 h the concentrations were decreased by 50 % like for AMP. Intracellular concentrations of ATP were constant and almost identical at 4.0 fmol/cell for all settings until stationary phase. After 238 h pool sizes diverged significantly. While REF and COP experienced a breakdown in ATP concentrations towards 2.6 and 0.9 fmol/cell/day, NOB revealed rising ATP concentrations up to 5.0 fmol/cell/day. As a result, the adenylate energy charge differed drastically in the early decline phase. Here, the energy charge was kept high at 0.9 for NOB, whereas REF and COP experienced a steep decline to 0.76 and 0.80. The loss of intracellular ATP coincided with the sharp drop of q_{ATP} as shown in figure 4.11.

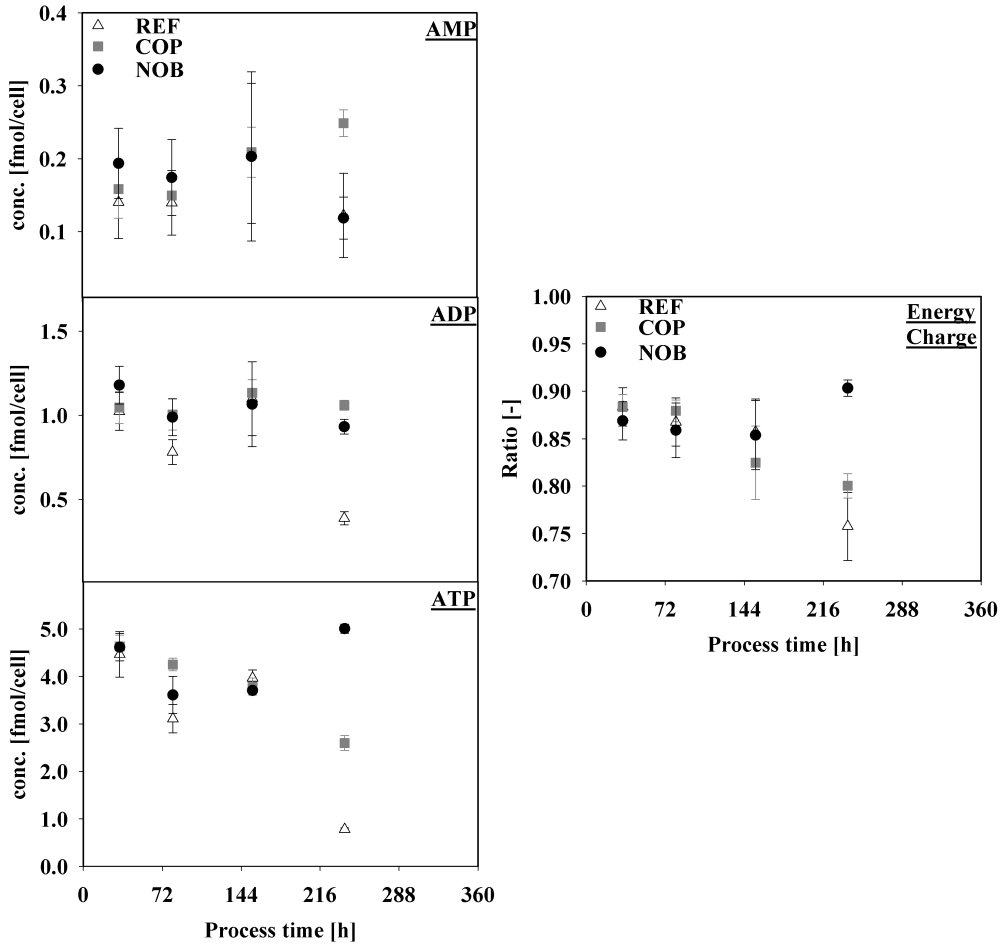

Figure 4.19: Intracellular pool sizes of nucleotides and the corresponding adenylate energy charge for the three settings REF, COP and NOB. Error bars indicate the error of technical triplicates. With modifications to appendix A.

4.2 Perfusion

In the second part of the results the perfusion process is described by comparing the impact of glucose limitation on the cellular metabolism to the non-limited state. Insights into metabolic adaptations especially concerning the energy supply linked to cell specific productivity are of increased interest and are presented in the following. Results of the following section have been partially published in Becker et al. (2019b) (see appendix B).

4.2.1 Growth and metabolic state in reference and glucose-limited steady-states

The settings for the three steady-states during perfusion mode can be found in section 3.2.3.3. The resulting viable cell densities and viabilities over process time are depicted in figure 4.20. The bioreactor was inoculated with a cell density of 0.7x10^6 cells/mL. After the initial batch phase of 24 h the perfusion was started with a perfusion rate of 1.0 L/day equivalent to 1 reactor volume per day. The bleed rate was kept at very low rates of 0.03 L/day. As a result, the cell density increased towards 16x10^6 cells/mL and did not increase any further due to glucose concentrations below 1 mM (compare table 4.1). This first steady-state was held for 96 h until 336 h of process time.

The perfusion rate was then increased to 1.25 L/day, while the bleed rate was kept constant at 0.03 L/day. In the following, the cell density reached the second steady-state, again because of glucose limiting conditions. Here, cell density reached values of 25x10^6 cells/mL. The cell density was kept constant for 120 h until 504 h of process time.

The final steady-state was accomplished by a last rise in perfusion rate to 1.50 L/day. Only here the bleed rate was increased to an average of 0.25 L/day. Through these applied bleedings the cell density in SS3 was artificially decreased to 20x10^6 cells/mL once daily. In between the bleeds the cells were growing, opposite to SS1 and SS2 because glucose concentrations were not limiting anymore (compare table 4.1). The viability remained above 90 % throughout the whole cultivation and did not decrease significantly in any of the steady-states.

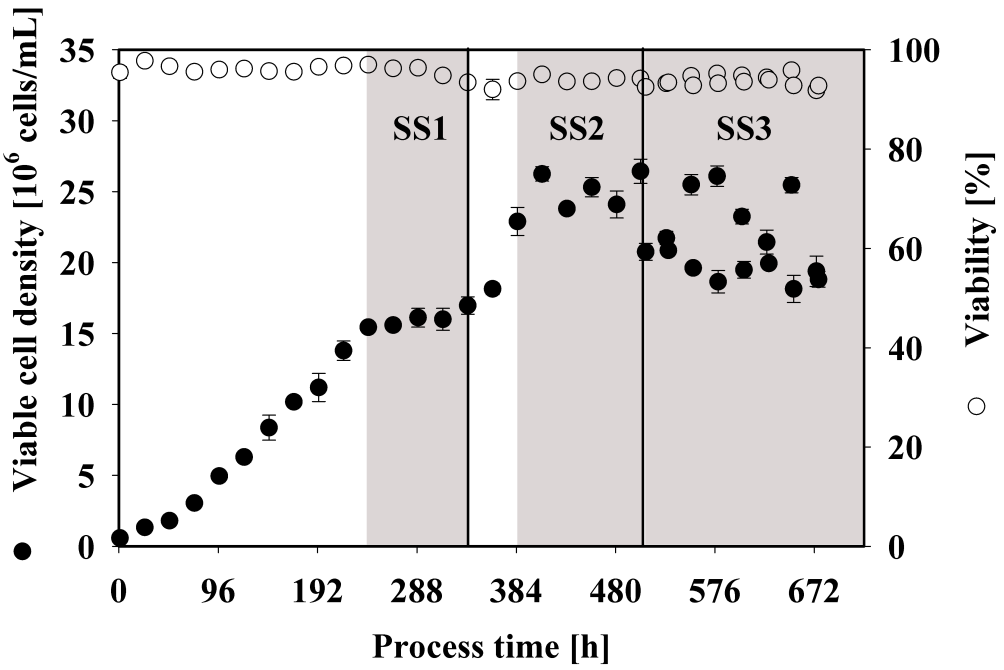

Figure 4.20: Profile of viable cell density over the process time for the three steady-states. Grey zones indicate constant cell densities. For SS3 values before and after cell bleeding are depicted. Shown errors were determined from biological triplicates. With modifications to appendix B.

The according concentrations during the three steady states are listed in table 4.1. Besides viable cell density and antibody titer, the metabolite concentrations of glucose and lactate as well as the measured amino acid are depicted as mean values of the last three days of each steady-state. For SS3, values both before and after daily bleeding are given. Different perfusion rates in each steady-state have to be considered. The antibody titer in the bioreactor was highest in SS2 with 0.28 g/L, but only slightly lower in SS1 with 0.22 g/L. By contrast, in SS3 the titer only reached 0.14 and 0.12 g/L before and after bleeding. As mentioned above, the glucose concentrations were below 1 mmol/L in SS1 and SS2, whereas they exceeded 6 mmol/L throughout SS3. The main by-product lactate stayed at low levels in SS1 and SS2 with 6.5 and 3.3 mmol/L, respectively. Only in SS3 the concentrations climbed to 30 mM before bleeding and 24 mM after bleeding.

All of the measured amino acids stayed in ranges above 40 % of the initial medium concentration. Amino acids produced by the cells were glycine and alanine whereas all other amino acids were consumed. Consequently, concentrations of alanine and glycine

in the bioreactor were highest of all amino acids. Alanine ranged from 3.4 mM in SS2 to 5.7 mM in SS3 and glycine from 4.3 in SS3 to 8.8 in SS1. Lowest concentrated amino acids were histidine and phenylalanine with values from 0.22 to 0.33 mmol/L.

Table 4.1: Viable cell density (VCD), bioreactor antibody and metabolite concentrations of glucose, lactate and amino acids during the three steady states. For SS3 values before and after bleeding are listed. Shown errors were determined from the last three days of each steady-state.

Steady-state (SS)	SS1	SS2	SS3 before bleed	SS3 after bleed
VCD [10^6 cells/mL]	16.4 ±0.4	25.3 ±1.0	22.1 ±2.5	19.0 ±0.7
Antibody [g/L]	0.22 ±0.02	0.28 ±0.02	0.14 ±0.03	0.12 ±0.01
Glucose [mM]	0.96 ±0.33	0.52 ±0.24	6.58 ±0.77	34.29 ±0.59
Lactate [mM]	6.53 ±2.02	3.31 ±0.97	30.31 ±1.47	23.94 ±1.48
Alanine [mM]	5.60 ±0.54	3.41 ±0.91	5.67 ±0.21	5.38 ±0.52
Arginine [mM]	2.36 ±0.23	2.28 ±0.17	2.34 ±0.04	2.38 ±0.16
Asparagine [mM]	0.47 ±0.10	0.44 ±0.01	0.56 ±0.01	0.59 ±0.01
Aspartate [mM]	0.79 ±0.15	0.66 ±0.06	0.49 ±0.01	0.55 ±0.05
Glutamate [mM]	2.24 ±0.78	1.46 ±0.19	0.78 ±0.02	0.86 ±0.13
Glutamine [mM]	1.90 ±1.14	1.06 ±0.15	1.32 ±0.19	1.43 ±0.19
Glycine [mM]	8.76 ±1.57	8.15 ±0.60	4.58 ±0.36	4.28 ±0.65
Histidine [mM]	0.24 ±0.05	0.24 ±0.01	0.22 ±0.01	0.26 ±0.02
Isoleucine [mM]	0.38 ±0.10	0.37 ±0.02	0.36 ±0.01	0.38 ±0.03
Leucine [mM]	0.49 ±0.18	0.46 ±0.01	0.45 ±0.01	0.54 ±0.01
Lysine [mM]	2.24 ±0.26	2.11 ±0.18	2.21 ±0.04	2.28 ±0.14
Methionine [mM]	0.39 ±0.07	0.33 ±0.03	0.38 ±0.01	0.40 ±0.02
Phenylalanine [mM]	0.31 ±0.08	0.26 ±0.03	0.30 ±0.01	0.33 ±0.02
Serine [mM]	0.62 ±0.20	0.39 ±0.03	0.54 ±0.04	0.58 ±0.03
Threonine [mM]	1.66 ±0.63	1.73 ±0.23	3.66 ±0.10	3.88 ±0.39
Tryptophan [mM]	0.31 ±0.04	0.31 ±0.03	0.32 ±0.01	0.33 ±0.02
Valine [mM]	0.36 ±0.12	0.31 ±0.01	0.33 ±0.01	0.38 ±0.01

Process values of pH and partial pressure of CO_2 are given in table 4.2. The pH was similar in SS1 and SS2 with 7.08 and 7.10, respectively. Values above the setpoint of 6.95 are probably due to constant medium exchange and very low lactate formation whereas high lactate formation contributed to a lower pH in SS3. The partial pressure of CO_2 was highest in SS3 with 220 mbar, whereas it reached only 159 and 194 mbar in SS1 and SS2, respectively. Differences were based on varying amounts of Na_2CO_3 titration.

Table 4.2: pH and partial pressure of CO_2 during the three steady states. For SS3 average values were calculated considering values both before and after cell bleeding. Shown errors were determined from the last three days of each steady-state.

Steady-state (SS)	SS1	SS2	SS3
pH	7.08 $\pm$0.04	7.10 $\pm$0.03	6.95 $\pm$0.07
pCO_2	158.7 $\pm$8.7	193.7 $\pm$2.4	220.3 $\pm$25.8

The main cell specific rates are depicted in figure 4.21. For the glucose consumption rate major differences could be detected between the glucose limited SS1 and SS2 on the one hand and SS3 on the other hand. The rate was elevated by about 25 % in SS3 and reached 2000 fmol/cell/day. Moreover, the lactate production increased severely to above 2000 fmol/cell/day. Therefore, more than half of the carbon coming from glucose was transformed to the by-product lactate in SS3. In contrast, cells produced far less lactate in SS1 and SS2. Here, lactate formation was about 75 % smaller, reaching average values of approximately 500 fmol/cell/day.

Glutamine, the second major substrate, was consumed in similar quantities in all three steady-states. Therefore, ammonia production probably did not differ remarkably since glutamine is also the major nitrogen source. The amino acid alanine was the second notable by-product secreted by the cells. The formation rate coming from pyruvate was lowest in SS2 with 200 fmol/cell/day and highest in SS3 with about 400 fmol/cell/day.

Considerable differences could also be found for the growth rate. The cells were growth limited by glucose limited conditions in SS1 and SS2 and only reached growth rates of below 0.1 1/day. By contrast, cells in SS3 reached growth rates of almost 0.3 1/day. Here, the cell density was steadily increasing in between the daily bleeds and cells were not limited in growth by glucose limitation. Striking differences could be

determined for the cell specific antibody productivity. Interestingly, the productivity was highest under glucose limited conditions in SS1 and SS2. Here, the rate was increased by a third compared to SS3. Average productivitities were about 14 pg/cell/day in the first two steady-states while the productivity diminished towards 9 pg/cell/day in SS3.

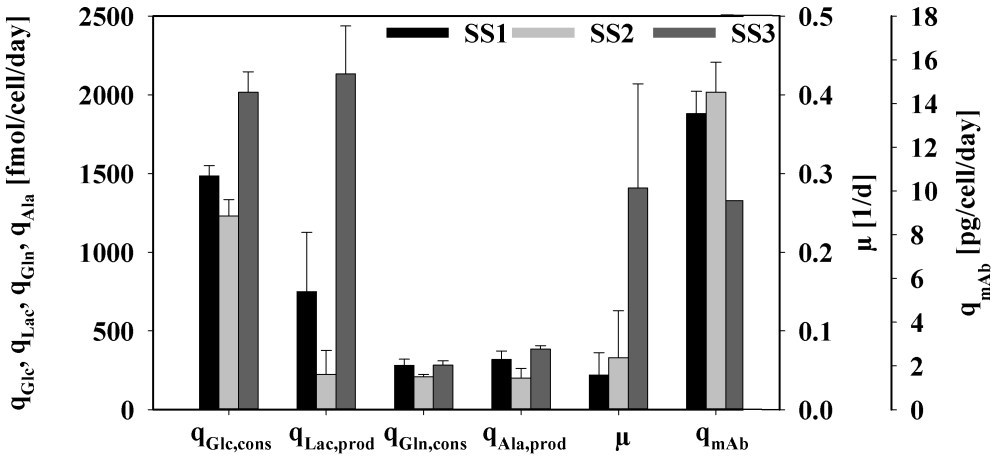

Figure 4.21: Main cell specific rates for the three perfusion steady-states. Shown errors were determined from the last three days of each steady-state. With modifications to appendix B.

4.2.2 Flux balance analysis and cellular energetic and redox state

To gain further insight into metabolic adjustments made by the cells in the distinct steady-states, flux balance analysis was performed as described in section 3.2.6. Results can be seen in figure 4.22. Obviously, the glycolytic flux was highest in SS3 since glucose uptake rate was highest here as well. The flux towards pyruvate from 3PG was increased by about 60 % compared to the first two steady-states. But since lactate was produced in large quantities of 2000 fmol/cell/day in SS3, the yield of pyruvate entering the TCA was severely decreased to 40 %. By contrast, 70 % and 84 % of total pyruvate was fueling the TCA in SS1 and SS2, respectively. As a result, fluxes inside the TCA differed between the glucose limited SS1 and SS2 and the non-limited SS3. Opposite to glycolysis, TCA fluxes were higher in SS1 and SS2, where they reached about 2500 fmol/cell/day. In SS3 fluxes were in the range of 2000 fmol/cell/day. Fluxes into pentose phosphate pathway, providing biomass precursors, were elevated in SS3

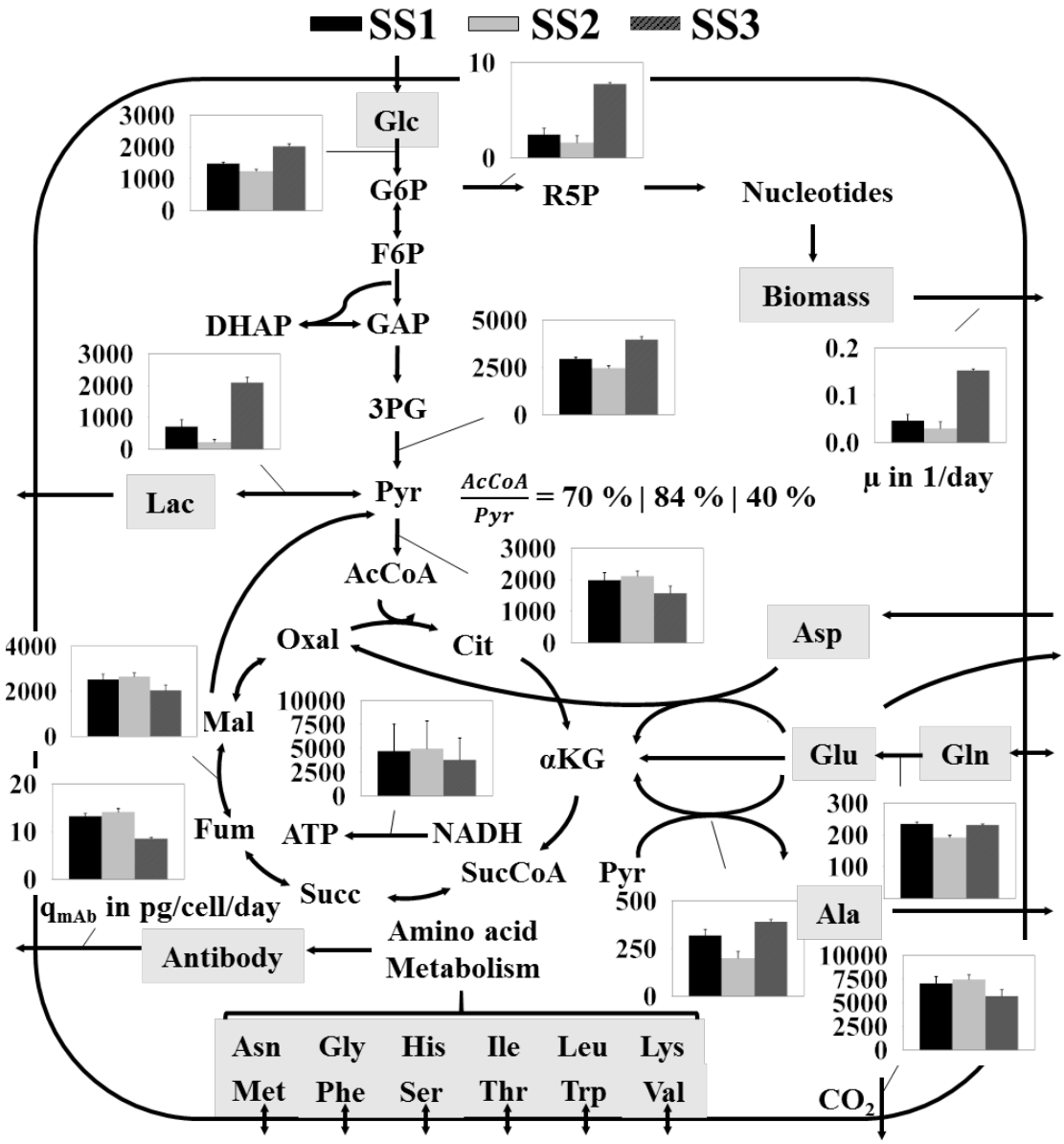

Figure 4.22: Simplified main carbon metabolism representing the results of the flux balance analysis for the three perfusion steady-states SS1, SS2 and SS3. Fluxes are given in fmol/cell/day except for the growth rate (1/day) and the cell specific antibody productivity (pg/cell/day). Errors were determined through Monte Carlo sampling of the solution space for each perfusion steady-state as described in section 3.2.6. With modifications to appendix B.

because of the apparently highest growth rate due to no glucose limitation and the performed bleedings.

To connect the cell specific productivity to the energetic state of the cells in the different steady-states, the cell specific ATP productivity was calculated from the results of flux balance analysis (see figure 4.23). Interestingly, ATP production did not differ much between the glucose limited and the non-limited states. For SS1 and SS2 ATP production summed up to rates of 22,000 fmol/cell/day while in SS3 approximately 21,000 fmol/cell/day were reached. Nevertheless, major differences could be found for the origin of ATP formation. In the first two steady-states the oxidative phosphorylation out of NADH and $FADH_2$ accounted for the most ATP with a fraction of about 65 %.

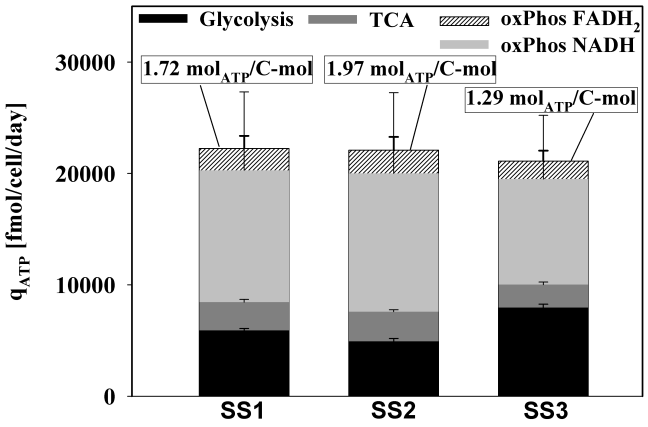

Figure 4.23: Cell specific ATP production rates for the three steady-states. Sources of ATP formation are oxidative phosphorylation either from $FADH_2$ or NADH (from both glycolysis and TCA), succinyl-CoA synthetase in TCA or glycolysis directly. Results were calculated from the flux balance analysis including errors from Monte Carlo sampling of the solution space for each setting as described in 3.2.6. With modifications to appendix B.

In SS3 the fraction of oxidative phosphorylation only summed up to 50 %. In contrast, higher amounts of ATP were derived directly from glycolysis. Here, 40 % of ATP was coming from glycolytic reactions while it only were 25 % in SS1 and SS2. Since GTP production in TCA from succinyl-CoA synthetase was assumed to be ATP equivalent, the fraction of energy coming from TCA directly is considered as well. In contrast to the other contributors, no major differences could be found when comparing the three steady-states. Throughout the process about 10 % of formed ATP were linked to

succinyl-CoA synthetase. Significant differences were determined for the yield of ATP per carbon mol of substrate consumed. While the yield was 1.72 and 1.97 mol ATP per carbon mol in SS1 and SS2, respectively, the yield dropped sharply to 1.29 mol/mol in SS3, indicating a loss in carbon efficiency for the non-limited state.

Resulting from the previous results, the cell specific antibody productivity q_{mAb} and the volumetric productivity Q_{mAb} were linked to the ATP formation rate out of oxidative phosphorylation $q_{ATP,\ oxPhos}$ in figure 4.24. Depicted are the values for each steady-state. A positive correlation between q_{mAb} and $q_{ATP,\ oxPhos}$ was found, meaning that rising ATP formation by oxidative phosphorylation was coinciding with increasing antibody productivities. Both were lowest in SS3, whereas they were elevated under glucose limited conditions in SS1 and even slightly more in SS2, as described before.

Moreover, the volumetric productivity reached its maximum in SS2 with 0.36 g/L/day. This was a combined effect of increased cell specific productivity and high cell densities of $25x10^6$ cells/mL (compare figure 4.20). The volumetric productivities were similar in SS1 and SS3 (0.2 g/L/day) although cell densities differed by $10x10^6$cells/mL. The lower cell density in SS1 was compensated by the increased q_{mAb} pointing out the effect of increased carbon and energetic efficiency under glucose limitation.

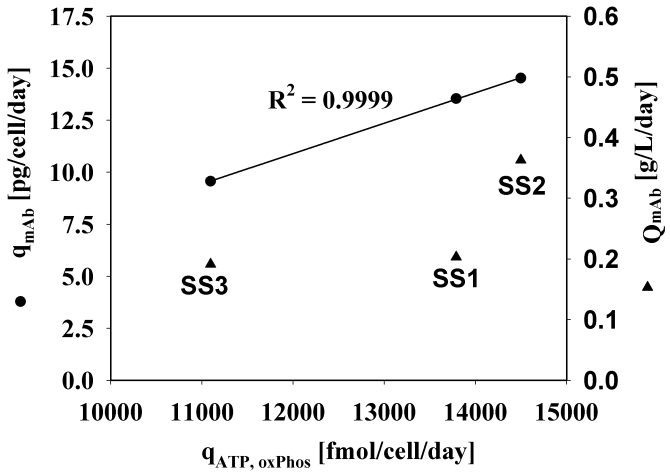

Figure 4.24: Cell specific antibody productivity q_{mAb} and volumetric productivity as a function of ATP formation due to oxidative phosphorylation $q_{ATP,\ oxPhos}$ for the three steady-states. With modifications to appendix B.

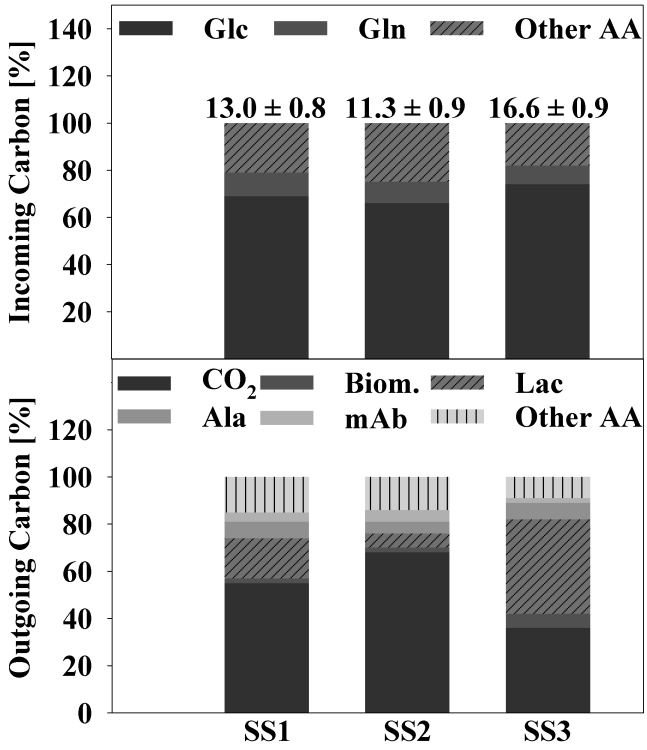

Figure 4.25: Carbon balances showing the main fractions for three steady-states. Remaining amino acids with minor contributions are lumped into other AA. Carbon balances were calculated from the flux balance analysis.

Figure 4.25 displays the carbon balance with fractional contributions of ingoing substrates and outgoing products. Again, the glucose uptake was increased during SS3. Here, total carbon flux summed up to 16.6 pmol-c/cell/day with glucose taking the major part of almost 75 %. In SS1 and SS2, the total fluxes were only 13.0 and 11.3 pmol-c/cell/day. Still, glucose was the biggest carbon source although fractions were nearly 10 % smaller. The difference was mainly compensated by uptake of amino acids other than glutamine. Glutamine itself contributed to about 6 % of total carbon uptake for all three steady states. The outgoing carbon in SS1 and SS2 was mainly CO_2 with 55 – 65 %. The remaining percentage was mostly composed of amino acids (20 %) and a small amount of lactate (5 – 15 %). Major part of the amino acid fraction were taken by alanine and glycine. In SS3 the fraction of lactate was massively increased to 40 %. Additionally, biomass accounted for 6 % of outgoing carbon since cells were constantly

growing. In contrast to SS1 and SS2 only 35 % of carbon were originating from CO_2 due to the smaller flux through TCA and reduced oxidative phosphorylation.

The redox variable R is an indicator for the redox state of the cells and can therefore be connected to lactate formation. Moreover, a positive correlation between the cell specific lactate formation and R was found and depicted in figure 4.26. SS2 had the lowest lactate formation of less than 500 fmol/cell/day. Accordingly, the redox variable was 1.08 and therefore close to 1.0, which corresponds to the theoretical assumption of no lactate formation. In SS1, the lactate formation rate was slightly above 500 fmol/cell/day and R increased to 1.39. Eventually, in SS3 the cell specific lactate formation climbed to above 2000 fmol/cell/day. The redox variable rose to the highest value of 2.37, underlining the strong correlation between lactate formation and redox state with a correlation coefficient of 0.9993.

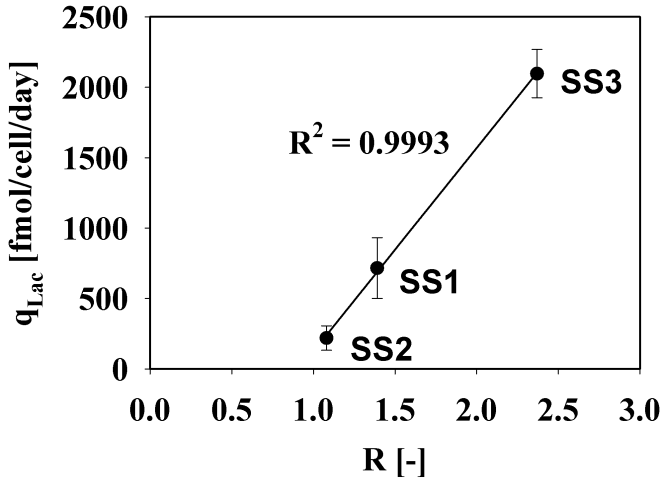

Figure 4.26: Cell specific lactate production rate for the three steady states as function of the redox variable R. Results were calculated from the flux balance analysis. With modifications to appendix B.

Additionally, the correlation between cell specific antibody productivity and the redox variable was investigated. The results are depicted in figure 4.27. Here, a clearly negative correlation was found with a correlation coefficient of 0.9982. The lowest R of 1.08 in SS2 correlated with the highest cell specific productivity of 14.5 pg/cell/day. SS1, also limited in glucose availability, showed similar values with a productivity of 13.5 pg/cell/day and a corresponding R of 1.39. The non-limited SS3 with the signifi-

cantly elevated R of 2.37 had a cell specific antibody productivity of only 9.5 pg/cell/day. Consequently, the redox state of the cells was not only linked to lactate formation, but also to the antibody productivity.

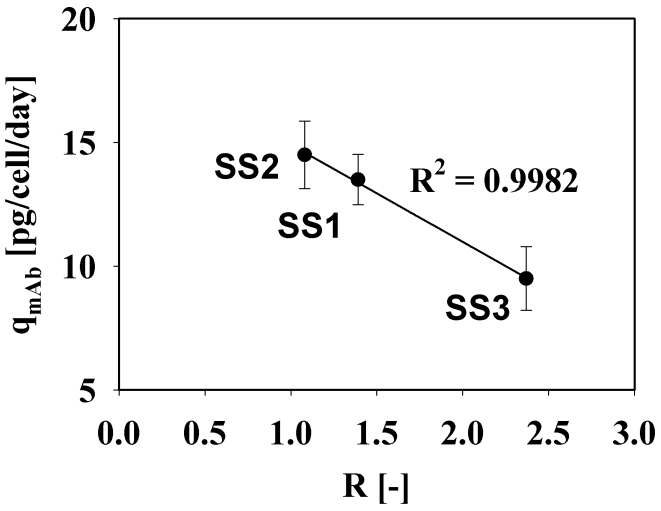

Figure 4.27: Cell antibody lactate production rate for the three steady states as function of the redox variable R. Results were calculated from the flux balance analysis. With modifications to appendix B.

4.2.3 Intracellular pool sizes of glycolysis, TCA and adenylate nucleotides in perfusion steady-states

The concentrations of intracellular metabolites of glycolysis can be seen in figure 4.28. Pools of all glycolytic metabolites followed a similar pattern: concentrations decreased around two thirds after extracellular glucose concentrations fell below 4 mM after 144 h and stayed low until the end of SS1 after 312 h. Here, pyruvate pools were highest with concentrations of 1 fmol/cell, followed by glucose-6-phosphate (g6p) being around 10 times lower and the rest of the metabolites being again 5 – 10 times lower than g6p. After the first increase of the perfusion rate, glycolytic concentrations shortly increased due to increased glucose availability. But eventually, the same values of SS1 were reached in SS2. Only for pyruvate the concentrations increased remarkably to 7.5 fmol/cell and it took 4 – 6 days for them to decrease back to steady-state values.

Interestingly, differences can be seen after the second increase in perfusion rate during the transition to SS3, once extracellular glucose concentrations climbed back above 4 mM. With the exception of DHAP, all concentrations in SS3 reached values above the initial values during growth phase. Along with highest lactate production rates, pyruvate concentrations increased towards 6.5 fmol/cell.

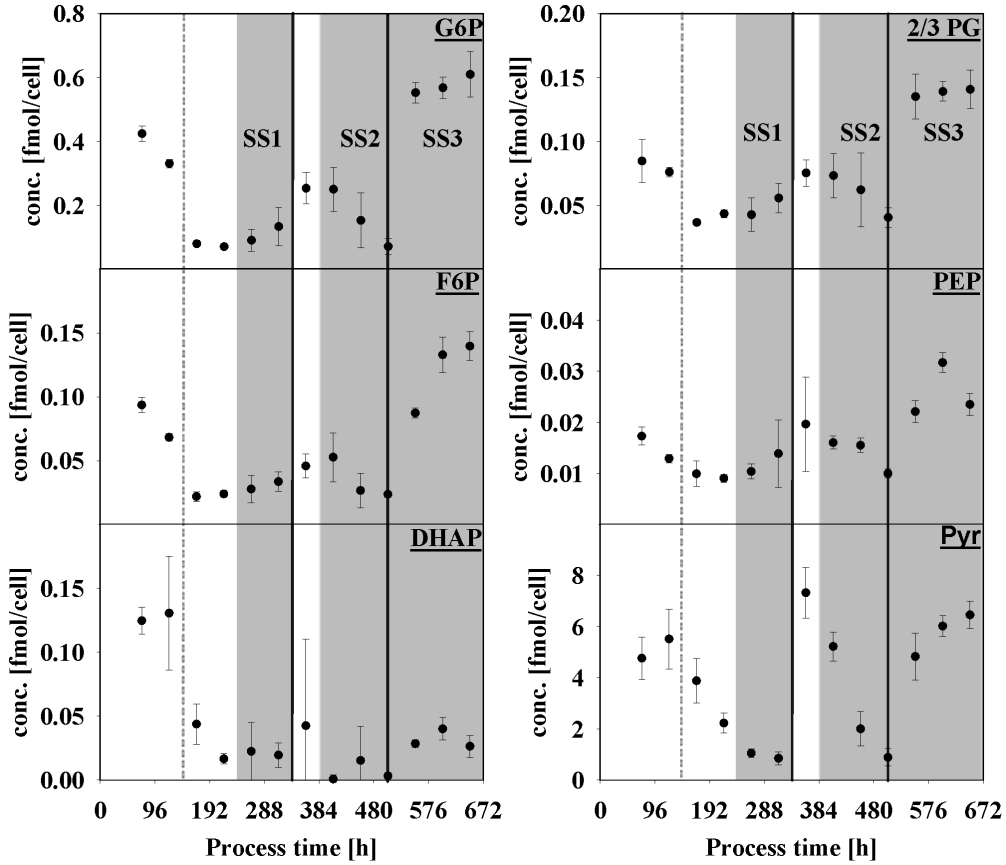

Figure 4.28: Intracellular pool sizes of intermediates of glycolysis for the three steady-states. Error bars indicate the error of technical triplicates.

Intracellular pools of TCA metabolites (figure 4.29), except for malate and fumarate, already showed low levels during growth phase, not being higher than after the occurrence of glucose limitation after 144 h or during SS1. Final concentrations in SS2 were comparable to the concentrations in SS1. Nevertheless, in contrast to glycolysis, 6 – 8 days passed until the steady-state was reached again for all of the TCA metabolites. Except for alpha-ketoglutarate and succinate, all metabolite concentrations increased again

after the second rise in perfusion rate and reached their peak pool size. Citrate and isocitrate lumped together reached final concentrations of 8 fmol/cell. Malate concentrations peaked at 5 fmol/cell while all other concentrations remained below 1 fmol/cell.

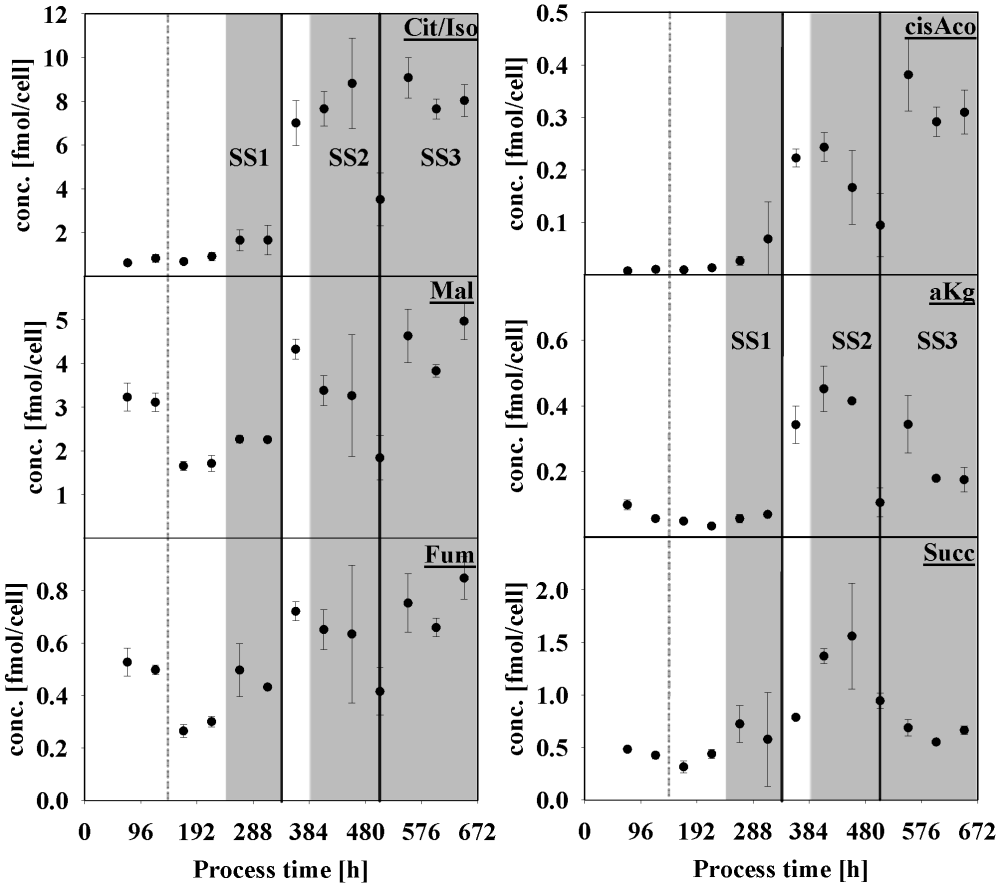

Figure 4.29: Intracellular pool sizes of intermediates of TCA for the three steady-states. Error bars indicate the error of technical triplicates.

Important indicators for energy availability inside the cells are the pool sizes of adenylate nucleotides. Results of the measurements are depicted in figure 4.30. AMP had the lowest total concentrations of the three nucleotides. The concentrations were at 0.2 fmol/cell during the early stages of the process and then steadily increased until they reached 0.8 fmol/cell in SS2. After the transition to SS3 they fell below 0.6 fmol/cell. ADP pool sizes showed a similar behavior, only that concentrations climbed from 1.2 fmol/cell in the beginning to almost 2.0 fmol/cell at the end of SS2. In the following, they declined to values below 1.5 fmol/cell at the end of SS3. The highest concentrations were

detected for ATP. At the end of SS1 and SS2, the pool sizes were between 3.5 and 4.0 fmol/cell, respectively. After a short rise to almost 5 fmol/cell after the switch to SS3, they eventually fell to 3.0 fmol/cell towards the end of the process. The resulting energy charge was highest during the early stages of the process with values of 0.85 to 0.90. Until the end of SS1 the energy charge declined to 0.80. Due to the increasing concentrations of AMP and ADP the energy charge further declined to its lowest value of 0.73 at the end of SS2. The energy charge regenerated to 0.80 only shortly at the beginning of SS3. Finally, it decreased again to 0.76.

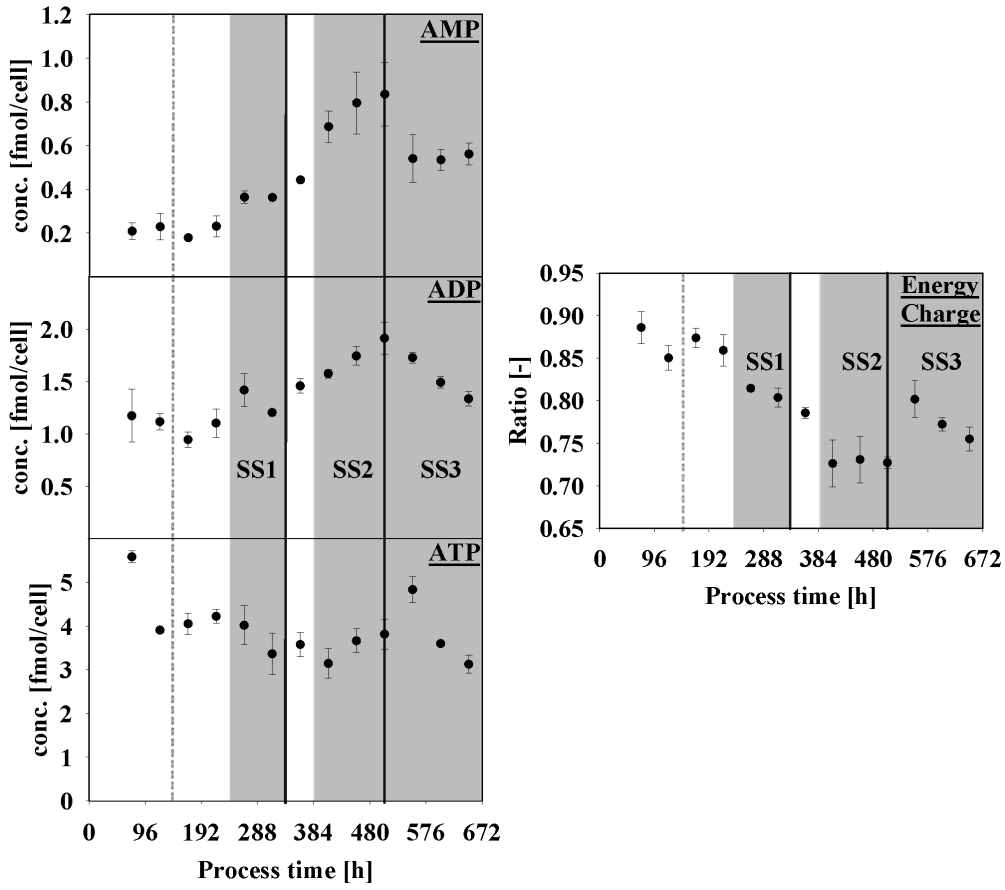

Figure 4.30: Intracellular pool sizes of nucleotides and the corresponding adenylate energy charge for the three steady-states. Error bars indicate the error of technical triplicates. With modifications to appendix B.

5 Discussion

Based on the results in chapter 4, the intensification of biopharmaceutical production processes in both fed-batch and perfusion mode is discussed in the following chapter. While the impact on multiple parameters like growth, substrate consumption and by-product formation is analyzed, the focus in both parts is laid upon the connection of cell specific antibody productivity and carbon metabolism. Especially the resulting ATP generation is of large interest since antibody synthesis is highly energy demanding. Reasons for diminishing productivities in large scale fed-batch cultivations as well as novel perfusion processes have not been fully elucidated yet. Still, the cell specific productivity remains a crucial parameter for economic biopharmaceuticals production.

5.1 Fed-Batch

Both pCO_2 and pH are scale-up sensitive due to the occurrence of inhomogeneities in large scale industrial cultivations. Hence, the effect of early increased pCO_2 stress and decrease in pH on the performed fed-batch cultivations is discussed. The three process types REF (reference process), COP (CO_2 stressed process) and NOB (no base addition) (compare section 4.1.1) are therefore compared. The discussion is split into three parts: the first part focusses on phenotypic changes, the second part on adaptations of the intracellular flux distributions and ATP formation while the third part analyzes changes of measured intracellular metabolite pools.

5.1.1 Early elevated CO_2 and late decreased pH influence growth and induce changes in production kinetics

Significant differences regarding the process parameters could be found for pH, pCO_2 and osmolality (figure 4.1). pCO_2 was increased during early growth phase for COP, pH was lower since early stationary phase for NOB and osmolality was increased for REF as well as for COP in late stages. Therefore, the influence of these process parameters will be considered in the following discussion. Major variations in the concentration courses and metabolic rates were revealed when comparing the three process types.

High osmolalities were reason for reduced growth and viable cell densities as published by Pfizenmaier et al. (2015) and Lin, Takagi, Qu, Gao, and Yoshida (1999). Increased lactate production led to a rise in base addition, which finally resulted in higher osmolalities for REF and COP (figure 4.1). Since in our study significant values of more than 400 mOsm/kg were only reached in the decline phase (figure 4.1), any severe influence of osmolality on the presented processes can be neglected except for the accelerated decline in cell densities towards the end. Viable cell densities (figure 4.2) were reduced by a third and titer (figure 4.3) by half for COP. It was shown before that partial pressures of CO_2 of up to 290 mbar deteriorate the growth rate and average specific productivities (Goudar et al., 2007; Gray et al., 1996; Mostafa & Gu, 2003; Kimura & Miller, 1996; Zanghi, Schmelzer, Mendoza, Knop, & Miller, 1999). Some studies did not find any significant effect on specific productivity but only on growth (DeZengotita, Schmelzer, & Miller, 2002; Takuma, Hirashima, & Piret, 2003). Therefore, the significant reduction of viable cell density in COP can possibly be traced back to the influence of CO_2. As nonpolar molecule CO_2 can easily diffuse through the cellular membrane and influence the intracellular pH of the cells. Thereby, CO_2 can alter glycolytic enzymes and protein glycosylation (Brunner et al., 2017; Zanghi et al., 1999). Moreover, an unfavorably high lactate accumulation is known to have a detrimental effect on growth at values starting at about 60 mM, depending on the used cell line (Lao & Toth, 1997). These values were reached in the early stationary phase for REF and COP (figure 4.5) and might therefore have an additional influence on the earlier decrease of viable cell density in REF and COP.

Average specific productivities were 20 % lower for COP compared to REF. Accordingly, results were similar to the aforementioned literature (Goudar et al., 2007; Gray et al., 1996; Mostafa & Gu, 2003; Kimura & Miller, 1996; Zanghi et al., 1999), which described a deterioration of cell specific productivities with increasing pCO_2. Nevertheless, when taking a look at the time courses, productivities reached their maximum already in early stages when CO_2 stress was present (figure 4.3). Osmotic stress induces a similiar effect, enhancing the cell specific productivity (Pfizenmaier et al., 2016). Analysis of CO_2 stressed cells on a proteomic level by Darja et al. (2016) revealed a GRP78 overexpression, which is a known stress protein. Pieper, Strotbek, Wenger, Olayioye, and Hausser (2017) and Nishimiya, Mano, Miyadai, Yoshida, and Takahashi (2013) linked higher specific productivities to an increased level of GRP78, which would explain the high productivity in the early stage. REF and NOB, with similar conditions in the early stages, showed comparable courses of specific productivity in the beginning until pH values diverged after around 120 h. For REF the pH slightly increased from this time point on because of the starting base addition, while for NOB the pH kept falling slowly. Hence, differences in the remaining process time can be led back to the different pH profiles. Beneficial effects of lower pH on specific productivity can be seen in figure 4.3, where q_{mAb} did not increase any further for REF with higher pH values, while for NOB with falling pH values q_{mAb} kept raising. The average specific productivity increased by almost 20 % due to the decreased pH which is in accordance to literature, where q_{mAb} either increased (Ivarsson et al., 2015; Brunner et al., 2018) or stayed unaffected (Trummer et al., 2006; Zalai et al., 2015; Yoon et al., 2005) when a pH shift downwards was applied. Nevertheless, maximum specific productivities were comparable for all the process types, being in the range of 20 pmol/cell/day. However, the influence of increased pCO_2 and especially decreased pH as a consequence of suppressed base addition showed substantial impact on the kinetics of antibody productivity (figure 4.6). While productivity in REF was neither mainly growth coupled or decoupled, COP showed strongly growth coupled antibody production, whereas the production in NOB was decoupled from growth. Despite decreasing growth rates for all processes, q_{mAb} rose by further 20 % only for NOB until 216 h. Similar to Pfizenmaier et al. (2016), cell specific productivities were elevated while facing minimal growth rates. In contrast, decreasing pH was applied in NOB instead of increasing osmolality as done by Pfizenmaier et al. (2016).

Concluding, the time point of maximum specific productivity is crucial for the final titer. Highly beneficial are maximum specific productivities in the stationary phase where highest cell densities are present. Only then the volumetric output is maximized. This could be shown for NOB due to the rising q_{mAb} towards the stationary phase, whereas COP showed contrary production kinetics (figure 4.6). Consequently, the resulting titers differed significantly (figure 4.3).

The kinetics of glucose consumption did not differ significantly so that no influence of the process setting could be evaluated. However, the absolute amount of glucose uptake was increased for COP. Furthermore, due to the elevated CO_2 stress, the final lactate concentrations were three times higher for COP compared to NOB (figure 4.5) despite almost 50 % lower cell densities. It was shown before that partial pressures of CO_2 of up to 290 mbar elevate lactate production in average (Darja et al., 2016; Brunner et al., 2017, 2018). Moreover, the early CO_2 stimulus seemed to have an influence on the level of lactate production since the course is similar for REF and COP after the process conditions aligned after 120 h. NOB had the same lactate production as REF at first but then switched to lactate consumption. The time point for the divergence coincided with the time point when base was first added to REF and the pH shifted slightly upwards. An increase in average q_{Lac} because of higher pH values was published by Yoon et al. (2005), whereas a downwards shift in pH has been shown to induce a metabolic shift towards lactate consumption before (Liste-Calleja et al., 2015; Zalai et al., 2015). Only for NOB this switch to lactate consumption could be observed while the pH was slightly decreasing. A connection between lower pH and initiation of lactate consumption was reported before by Ivarsson et al. (2015); Liste-Calleja et al. (2015); Zalai et al. (2015) for time averaged rates.

5.1.2 Adjusmtens of intracellular fluxes and energetic state

The specific productivity peaked for all processes when the according lactate production was lowest which might indicate a beneficial metabolic state. Therefore, intracellular flux distributions could give an insight into the cellular adjustments made concerning carbon metabolism and ATP generation.

Less studies have focused on using metabolic flux analysis for analyzing either CO_2 stress (Brunner et al., 2018) or flux balance analysis for pH induced changes in metabolism (Ivarsson et al., 2015) in the recent years. In this work, the glycolytic flux per cell was not necessarily connected to the amount of produced lactate as mentioned before (Brunner et al., 2018; Konakovsky et al., 2016; Zalai et al., 2015). However, Templeton et al. (2013) reported a connection between growth and high glycolytic fluxes on the one side and production and high TCA fluxes on the other side. In general, all three process types showed elevated glycolytic fluxes in the beginning when the growth rate was still increased (figure 4.8). However, when comparing the processes, COP had the highest glycolytic fluxes throughout the process although almost half of the carbon was transformed to lactate. NOB showed first decreasing and then constant low level fluxes through glycolysis. The beginning lactate consumption compensated for decreasing glycolytic fluxes. Consequently, the TCA fluxes were similar to these of REF and COP despite lower carbon uptake (figure 4.9). Ivarsson et al. (2015) showed similar metabolic adaptations for a protein producing CHO batch process. Here, a batch with lowered pH 6.8 also switched to lactate consumption compared to a reference process with a pH of 7.2. Possible impact factors could be glycolytic enzymes with pH dependent activities or cellular measures to regenerate medium pH back to initial values by taking up lactate (S. S. Ozturk et al., 1992).

High specific productivities were coinciding with a high yield of pyruvate fueling the TCA and therefore low lactate production (Templeton et al., 2013; Luo et al., 2012). Excess lactate production is considered as unwanted since glucose is not completely oxidized. Therefore, the metabolism is less efficient regarding energy production compared to fueling carbon directly into the TCA. This is directly correlated to the redox variable R which describes how much NADH is transported into mitochondria. As figure 4.12 shows, the lactate formation in all processes tended to increase with rising R since more NADH remained in the cytosol and was oxidized here (Nolan & Lee, 2011; Brunner et al., 2018). NOB showed the lowest redox variables of all processes. pH reduction might therefore be an approach to reduce the glycolytic NADH generating flux towards lactate production. By contrast, as a consequence of increased CO_2 stress, COP experienced strong glycolytic fluxes. Due to the resulting lactate production and the elevated R, the remaining fraction of NADH being used for oxidative phosphorylation was

obviously lower. Remarkably, the cell specific antibody productivity was negatively correlating to R. Therefore, the antibody productivity was increased the more NADH was fueled into mitochondria towards respiratory ATP generation while lactate formation decreased vice versa.

Since the antibody synthesis is highly energy consuming, the ATP formation plays a crucial role in the determination of cell specific productivity. Moreover, the correlation of productivity with the redox variable points towards a connection with respiratory ATP supply. Interestingly, the total ATP production was highest for COP until early stationary phase where maximum CO_2 stress was present. Afterwards, the ATP formation broke down by almost half. The conditions of elevated CO_2 stress might lead to a higher ATP demand similar to osmotic stress (Pfizenmaier et al., 2015, 2016). CO_2 as a nonpolar molecule can easily diffuse through the cellular membrane which is finally resulting in the decrease in intracellular pH. Therefore, the cellular maintenance demands are increased. DeZengotita et al. (2002) found a decrease in pH_i of around 0.2 for elevated partial pressures of CO_2 (300 mbar), although the medium pH was constant. To keep intracellular pH from falling further, ATP consuming transporters are needed to continuously extrude protons out of the cell (Casey et al., 2010; Roos & Boron, 1981). The ATP is therefore used for maintenance demands and cannot be used for antibody synthesis explaining the rapidly falling specific productivity.

On the contrary, the amount of ATP produced per cell was lower for NOB compared to the REF and COP until the stationary phase. Nevertheless, q_{ATP} stayed almost constant throughout the process while the ratio of ATP per c-mol substrate severely increased towards the end of the process. Accordingly, the fraction of ATP coming from oxidative phosphorylation increased along with the cell specific productivity, analogous to the finding of negatively correlating productivity with R. The applied shift downwards in pH for NOB does not necessarily decrease the intracellular pH as an increased pCO_2 does (Brunner et al., 2017; Wu, Ray, & Shuler, 1993) since the cellular membrane cannot be passed by diffusion as for CO_2. Accordingly, the cells can apply countermeasures without having to spent as much ATP. Concluding, lower total q_{ATP} do not necessarily coincide with decreased q_{mAb} (Ivarsson et al., 2015), given that high respiratory ATP supply promotes antibody productivity.

Carbon balances can provide further insight into the metabolic efficiency since they compare substrates and products on a proportional basis. Although the determination of carbon balances can be complex for mammalian systems due to the bicarbonate buffered system (Bonarius, Houtman, Schmid, de Gooijer, & Tramper, 1999), flux balance analysis was used to avoid the experimental measurement of CO_2 evolution rates. The carbon balances showed lower fractions of glucose for incoming carbon for the high productive states of late NOB. Vice versa, amino acids were compensating the effect. The general declining trend for total carbon uptake over the course of the cultivation (Templeton et al., 2013) was most pronounced for NOB. Here, coinciding with the increasingly productive metabolic state, the switch from lactate production to consumption interrelated with a reduced total carbon uptake by approximately 50 % compared to REF and COP (Templeton et al., 2013). The increased fraction of CO_2 in outgoing carbon for NOB in the early decline phase (figure 4.16) correlates with the still elevated fluxes through TCA. The CO_2 producing fluxes in TCA have been linked to high antibody productivity by Templeton et al. (2013).

5.1.3 Metabolic adaptations of intracellular pool sizes in different fed-batch phases

Intracellular metabolite concentrations of glycolysis and TCA did not show significant deviations in between the three process types (figures 4.17 and 4.18). Although several enzymes of glycolysis are affected by intracellular pH or CO_2/HCO_3 (Brunner et al., 2018), COP showed comparable pool sizes as REF and NOB. Glucose-6-phosphate dehydrogenase, malate dehydrogenase and succinate dehydrogenase are for example inhibited by increased inorganic carbon levels in yeast. Furthermore, an influence of intracellular pH on phosphofructokinase is known, which is the pace determining enzyme in glycolysis (Erecińska, Deas, & Silver, 1995). However, no severe influence could be determined for COP. Only for NOB, pyruvate was substantially decreased from early stationary phase. Pyruvate serves as a key intermediate in metabolism as it is included in several reactions. Pyruvate is especially responsible for the main flux into TCA but also lactate formation. Luo et al. (2012) showed decreased intracellular pyruvate intensities after a switch from lactate production to consumption. Higher levels of intracellular pyruvate could promote overflow metabolism in terms of increased lactate production.

Possible bottlenecks in the catabolic capacity of the TCA could hinder more pyruvate from fueling the TCA. However, the general trend for most TCA pool sizes of all process types was a likewise decline.

Comparing the intracellular nucleotide pool sizes, significant differences were only identified in the late process stages (figure 4.19). Contrary to the other two processes, NOB could maintain both high ATP concentrations and energy charges along with constant q_{mAb}, even towards the decline phase. The intracellular ATP concentrations were the highest of all the processes. Elevated ATP pool sizes have been published for multiple impact factors such as increased osmolality (Pfizenmaier et al., 2015), addition of sodium butyrate (McMurray-Beaulieu, Hisiger, Durand, Perrier, & Jolicoeur, 2009) or varying medium composition (Kochanowski et al., 2008). Likewise, the antibody productivity or glycosylation heterogeneity was improved. Consequently, the intracellular ATP availability plays a crucial role in antibody productivity. Still, the ATP availability is influenced by external factors such as pH or carbonate equilibrium. The lower inorganic carbon concentration due to the suppressed base addition in NOB might lead to lower maintenance demands and therefore higher ATP availability. Moreover, the energy charge was kept high through additional AMP degradation. By contrast, increased AMP levels in COP could be interrelated to the AMP activated protein kinase (AMPK) which is a sensor for the energetic status of the cell. AMPK switches off several metabolic enzymes and anabolic pathways that consume ATP (Hardie, 2011). Accordingly, the synthesis of proteins such as the monoclonal antibody could be downregulated since this is one of the major energy consuming processes for the cells.

5.2 Perfusion

Perfusion processes as emerging production mode are of special interest for multiple reasons. The potential for high cell densities in long term continuous cultivations with possible steady-state conditions is of interest for the production of biopharmaceuticals. Until now, very less studies have focused on the intensification of perfusion processes in terms of specific productivity. Reaching higher cell densities and characterizing different retention techniques has been the focus of research. In the following, the effect of glucose limitation on a perfusion process with different steady-states is evaluated in three sections. The focus is laid upon the impact on cellular carbon metabolism, cell specific productivity and energy availability.

5.2.1 Impact of glucose availability on cell density and main metabolism

As depicted in figure 4.20, all steady-states reached a constant viable cell density for at least four days. Constant operation of perfusion processes with cell densities in the range of 20x10^6 cells/mL using perfusion rates of approximately 1 reactor volume per day has been shown before (Clincke, Molleryd, Zhang, et al., 2013; Karst et al., 2016). The omitting of bleeds as done in SS1 and SS2 has also been described as concentrated fed-batch, but only for non substrate limited cells (Xu, Hoshan, & Chen, 2016; Yang, Minkler, Kshirsagar, Ryll, & Huang, 2016). SS3 was not glucose limited, but had increased bleed rates to keep a constant viable cell density of about 20x106 cells/mL. SS1 and SS2 were both glucose limited but had different perfusion rates to exclude any further detectable limitation of substrates or inhibition by by-products like lactate. As table 4.1 shows, only glucose was below limiting concentrations of about 1 mM in SS1 and SS2. Below this concentration, a stop in growth was observed (Lu, Sun, & Zhang, 2005). Lactate concentrations in neither of the steady-states exceeded inhibiting concentrations of 60 mM (Lao & Toth, 1997), contrary to the fed-batch cultivations. Ammonia inhibition can be ruled out since all steady-states showed similarly low glutamine uptake rates (figure 4.21). Concluding, inhibition by the by-products lactate and ammonia can be excluded. The measured amino acid concentrations stayed above 40 % of the initial medium concentrations. Moreover, concentrations were similar to published

production processes (Selvarasu et al., 2012; Altamirano et al., 2004). Therefore, any limitation of the main substrates besides glucose could be ruled out. Accordingly, the aim of this work to determine the influence of glucose limitation on cellular metabolism and productivity could be analyzed in the following. Possible higher cell densities in perfusion (Clincke, Molleryd, Zhang, et al., 2013; Xu et al., 2016) were not necessary for these investigations, since no cell density dependent metabolic deviations could be found up to cell densities of $2x10^8$ cells/mL (Clincke, Molleryd, Zhang, et al., 2013).

Possible further impact factors on cellular metabolism like pCO_2 and pH were already discussed in the fed-batch part and had to be excluded to focus on glucose limitation. High partial pressures of CO_2 are a known problem in perfusion processes since higher cell densities produce more CO_2 (Gray et al., 1996; Goudar et al., 2007). Additionaly, the increased carbonate addition by base because of the increasing lactate formation is amplifying the problem. However, the latter is partly compensated by the continuous washout of the by-product and the carbon species. Nevertheless, the partial pressure of CO_2 was highest in SS3 (table 4.2), although cell densities were highest in SS2. Detrimental effects of elevated pCO_2 on growth, metabolism or productivity have been reported in the fed-batch part (section 4.1) and various studies (Mostafa & Gu, 2003; Kimura & Miller, 1996; Zhu et al., 2005; DeZengotita et al., 2002). Although a negative impact in SS3 cannot be completely excluded, pCO_2 did not show substantial differences compared to SS2. Likewise, the settings in SS1 and SS2 did show similar cell specific rates (figure 4.21) despite slightly different pCO_2. The pH was approximately 0.1 lower in SS3 due to the higher pCO_2 and lactate concentrations. However, the differences in pH were not as pronounced to deduce impact on cellular metabolism (Trummer et al., 2006).

Accordingly, differences in the main cell specific rates in figure 4.21 can be attributed to the glucose limiting state in SS1 and SS2 compared to the non-limited reference in SS3. The metabolic phenotype was positively influenced by the glucose limitation. Glucose consumption and lactate formation were both decreased by an average of 25 % and 75 %, respectively, in SS1 and SS2, thereby increasing the efficiency of carbon metabolism. By contrast, glutamine uptake and alanine formation remained unchanged compared to SS3. Remarkably, the antibody productivity was significantly increased by

50 %. Potential increase in bioreactor titer due to the retention of product by the hollow fiber as described before (Karst et al., 2016; Clincke, Molleryd, Samani, et al., 2013) was neglected since the measured titer was constant over each steady-state. Fouling of the membrane was probably omitted because of lower cell densities as well as higher pore sizes of 0.45 μm compared to the literature.

Glucose limitation for mammalian cells has been described in few publications concerning both fed-batch (Altamirano et al., 2001; Chee Furng Wong et al., 2005) and continuous or perfusion (Europa, Gambhir, Fu, & Hu, 2000; Takuma et al., 2007) cultivations. In every case, the cells showed less glucose uptake and lactate formation and therefore an improved metabolic phenotype with increased carbon efficiency. However, effects on productivity were not completely consistent since both negative (Altamirano et al., 2001) and insignificant (Europa et al., 2000; Takuma et al., 2007) effects were reported. Additionally, changes in antibody glycosylation have to be considered (Chee Furng Wong et al., 2005), but were not determined in this work. Possible reason for phenotypic changes might be a cell cycle arrest in the G1 phase triggered by the glucose limitation (Dalm, Cuijten, van Grunsven, Tramper, & Martens, 2004). Both glucose limited SS1 and SS2 showed severely decreased growth rates (figure 4.21), eventually leading to constant cell densities. However, viabilities remained constant above 90 % despite diminishing growth rates. Other known approaches leading to cell cycle arrest in the G1 phase are temperature reduction (Furukawa & Ohsuye, 1999; Ahn, Jeon, Jeong, Lee, & Yoon, 2008; Wolf et al., 2018) or osmotic stress (Pfizenmaier et al., 2015, 2016). Temperature reduction showed an improved carbon metabolism with decreased glucose uptake. Additionally, antibody productivity was increased by approximately 50 - 60 %. By contrast, under osmotic stress the productivity rose, but glucose uptake and lacate formation did likewise. Alternatively, partly substituting glucose as primary carbon source with other sugars such as galactose did show lesser lactate formation but no rise in productivity (Altamirano et al., 2004). Consequently, glucose limitation induced beneficial changes in both carbon metabolism and productivity. Moreover, on the economic level medium usage is reduced and less antibody is lost since bleeding rates are substantially decreased.

5.2.2 Adaptations in ATP formation and cellular redox state and effect on productivity

The aforementioned beneficial changes due to glucose limitation were obvious in the cellular phenotype. In the following, adaptations in carbon and energy metabolism are linked to increased productivity using flux balance analysis. One key point in carbon metabolism is the transformation of pyruvate since the influx into TCA is far more efficient regarding ATP yield than the alternatives for pyruvate transformation such as lactate or alanine formation. The efficiency of carbon metabolism was significantly enhanced under glucose limitation (figure 4.22) as the fraction of pyruvate fueling the TCA increased from 40 % in the non-limited SS3 to 70 % and 84 % in SS1 and SS2, respectively. Accordingly, the remaining flux in SS3 was instead mainly turned into by-products (Mulukutla et al., 2012; Dalm et al., 2007). Lactate accounted for approximately 50 % and alanine for about 10 %. Consequently, the fluxes through TCA were highest under glucose limiting conditions in SS1 and SS2. Remarkably, this coincided with the highest productivities similar to the findings of Templeton et al. (2013). They found a direct correlation between CO_2 producing reactions in TCA and cell specific productivity. Furthermore, they reported a strong connection between glycolytic flux and growth on the one side and TCA flux and productivity. This also held true for the three steady states in this work. In SS1 and SS2 fluxes through TCA were elevated along with productivity, whereas glycolytic fluxes and growth rate were increased in SS3. Metabolic changes as seen under glucose limitation were found for the transition from exponential growth phase to stationary phase in fed-batch production processes (Ahn et al., 2008; Mulukutla et al., 2012; Templeton et al., 2013). Likewise, growth slowed down along with glucose uptake and lactate formation. As a result, productivity increased while fluxes through TCA became more pronounced, which indicated a stronger fraction of ATP generation from oxidative phosphorylation. Therefore a beneficial environment for antibody production was observed. Similar results were found for the stationary phase of batch processes after glucose depletion when previously produced lactate was consumed (Martínez et al., 2013). The contrary decrease in growth and rise in productivity was connected by Templeton et al. (2017) when comparing fed-batch and perfusion processes. They argued that the lumped protein production stayed constant whereas the fractions of biomass and antibody diverged. Cells in the stationary

phase of the fed-batch were non-growing and showing a growth decoupled production. Therefore, the fraction of antibody protein was elevated compared to biomass. By contrast, the cells in perfusion mode were constantly growing and showed lower antibody production. Accordingly, applying glucose limitation and therefore halting growth as done in SS1 and SS2 could be beneficial for antibody productivity. Because only the distribution of total protein produced per cell varies, the fraction of biomass protein decreased while the amount of antibody increased. Likewise, alternative approaches for cell cycle arrest like temperature reduction (Furukawa & Ohsuye, 1999; Ahn et al., 2008; Wolf et al., 2018) or osmotic stress (Pfizenmaier et al., 2015, 2016) showed comparable phenotypic effects as discussed in section 5.2.1.

In glucose limitation, an increased flux into TCA could decrease the lactate formation and eventually increase the ATP formation as proposed by Dalm et al. (2007). Although the fraction of pyruvate fueling the TCA was almost doubled under glucose limitation in SS1 and SS2, the total ATP formation rates were similar during all steady states (figure 4.23). Notably, major differences were found for the origin of ATP formation. The respiratory ATP formation from oxidative phosphorylation (both NADH and $FADH_2$) was responsible for two thirds of the total ATP generation in SS1 and SS2. In SS3, oxidative phosphorylation accounted for far less ATP. Specifically, the ATP coming from glycolysis in SS3 equilibrated with the sum of glycolytic and TCA-based ATP in SS1 and SS2. Concluding, the sources of ATP diverged, depending on the state of glucose availability. Remarkably, the efficiency of substrate usage for energy generation was enhanced under glucose limitation. For glucose limited SS1 and SS2, respiratory ATP supply was substantially increased. As a result, the yield of ATP per consumed carbon mol was approximately one third higher in SS1 and SS2 than in SS3. Similar findings were reported by Martínez et al. (2013) for a glucose depleted batch process. The energy efficiency in terms of ATP produced per c-mol consumed was significantly elevated. Concluding, the yield of ATP per c-mol supports the evidence of highly efficient metabolic states under glucose limitation due to increased ATP supply by oxidative phosphorylation.

Moreover, a strong correlation between cell specific antibody productivity and ATP generation from oxidative phosphorylation was revealed (figure 4.24). Templeton et al. (2013) already noted a correlation between CO_2 producing reactions from TCA and

cell specific productivity, therby emphasizing the beneficial effect of increased oxidative metabolism. Accordingly, CO_2 evolution rates were similarly elevated in SS1 and SS2 (figure 4.22) when productivities were highest. However, this finding is specified by the given correlation of productivity with respiratory ATP supply. In the fed-batch processes, cells likely had to face various stress factors such as increased by-product concentrations or elevated partial pressures of CO_2. Consequently, the cells had higher maintenance demands, compensating the higher ATP formation rates (section 5.1.2). Therefore, both cell specific and volumetric productivities were not higher than in perfusion mode. The highest volumetric productivities in perfusion were reached in glucose limited SS2, but only being higher than in SS1 due to the higher cell densities. By increasing the cell densities further, the volumetric productivities could likely be enhanced. Consequently, the latter especially holds true for glucose limited states. The apparent correlation between cell specific productivity and respiratory ATP supply underlines the efficient metabolic state which was established in SS1 and SS2.

Additionally, carbon balances reflected the influence of glucose limitation (figure 4.25). The total flux of carbon was about 25 % lower in SS1 and SS2, mainly due to the glucose limiting conditions which were reducing glucose uptake rates and furthermore promoting the efficient use of substrate for energy generation. A negative correlation of total carbon uptake and antibody productivity was shown similarly for a fed-batch process in transition to stationary phase (Templeton et al., 2013). A general declining trend for total carbon uptake over the course of the cultivation

The interrelation of NAD and NADH plays a crucial role in the carbon efficiency, the ATP generation, and eventually in cell specific productivity. NADH is produced mostly in glycolysis, only in smaller amounts in TCA. The glycolytic NADH is then oxidized to NAD in two major reactions: the unwanted by-product formation of lactate from pyruvate or the oxidative phosphorylation. For the latter the transport of NADH into mitochondria is required. The redox variable R (Nolan & Lee, 2011; Brunner et al., 2018) reflects the ratio of produced glycolytic NADH to NADH which is transported into mitochondria (section 3.2.6). Notably, the redox variable was positively correlating to lactate formation as depicted in figure 4.26 (Nolan & Lee, 2011; Brunner et al., 2018). Therefore, the less NADH was transported into mitochondria, the more remained in the cytosol and was used for lactate formation. Vice versa, the more NADH entered mito-

chondria, the more ATP was generated from oxidative phosphorylation due to a higher NADH availability in mitochondria. The drop in R in SS1 and SS2 was likely due to the decreased NADH availability under glucose limitation. Even lower NADH availability could lead to lactate uptake to maintain redox balance once R decreased below 1.0 (Nolan & Lee, 2011; Brunner et al., 2018; Wilkens, Altamirano, & Gerdtzen, 2011; Zalai et al., 2015). Eventually, the cell specific productivity was negatively correlating with R (figure 4.27) and positively with ATP generation from oxidative phosphorylation (figure 4.24). Concluding, the redox balance decides on the fraction of ATP generation from oxidative phosphorylation. The resulting high ATP availability is crucial for the level of energy-consuming antibody synthesis which could be held high during SS1 and SS2. Glucose limitation therefore led to a beneficial shift in redox balance, ATP generation from oxidative phosphorylation, and eventually antibody synthesis.

5.2.3 Changes in perfusion mode affect intracellular pool sizes of glycolysis, TCA and adenylate nucleotides

To gain a holistic view on cellular metabolism, intracellular pool sizes of metabolites of glycolysis, TCA and nucleotides were quantified. Intracellular concentrations of glycolytic metabolites were strongly dependent on extracellular glucose availability (figure 4.28). Glucose limited concentrations in SS1 and SS2 led to 3 – 5 times smaller concentrations than in SS3. Adaptations times were in the range of 3 days for all metabolites except pyruvate. This is in the range of extracellular metabolic steady-states observed by Karst et al. (2016, 2017) with approximately 3 days since glycolytic metabolites are direct products of incoming glucose. Only for pyruvate it took more than 4 days to stabilize after the increase in perfusion rate at 312 h. Furthermore, a correlation between pyruvate concentrations and lactate formation rates was shown (Luo et al., 2012). Elevated pyruvate levels in the cytoplasma favored lactate formation and probably also influenced the NADH/NAD equilibrium (Dalm et al., 2007). Overflow metabolism was decreased through diminished glucose uptake in SS1 and SS2, leading to lower intracellular glycolytic pool sizes. In contrast, pyruvate concentrations in SS3 were around four times higher than in SS1 and SS2 and correlated with lactate formation, which was similarly increased in SS3.

Time to reach steady-state condition in metabolite pools of TCA (figure 4.29) ranged from 6 – 8 days in SS2. Only then similar pool sizes as in SS1 were found. This is probably due to the complex interplay of different inflowing pathways in contrast to glycolysis. Although glycosylation was not investigated in this study, similar adaption times were reported for steady-states of glycosylation patterns during perfusion (Karst et al., 2016). Metabolite concentrations were increased in SS3, although fluxes were reduced compared to the glucose limited SS1 and SS2 (figure 4.22). Elevated pool sizes in SS3 might point towards a bottleneck resulting in a hampered ATP supply from oxidative phosphorylation. A decrease in intracellular organic acids concentrations in TCA was found before in glucose limited batch processes (Wilkens et al., 2011). A general rise in multiple intermediate concentrations of both glycolysis and TCA was reported by Luo et al. (2012) in fed-batch processes with cells producing lactate compared to lactate consuming cells.

For the adenylate nucleotides in figure 4.30 no significant differences were detected. However, AMP and ADP concentrations were rising until the end of SS2. The ATP pool sizes remained almost constant during the glucose limited SS1 and SS2. The measured values were in comparable ranges of previously analyzed CHO cells (Chong et al., 2010; Pfizenmaier et al., 2015, 2016). Constant intracellular ATP pool sizes were reported before for G1 arrested cells under the condition of high viabilities of more than 80 % (Moore et al., 1997). Arrest in G1 phase was probably a consequence of glucose limitation (compare section 4.2.1) and viabilities above 90 % were given throughout the whole perfusion process. After glucose was present in excess again in SS3, AMP and ADP pool sizes decreased by degradation, probably to regenerate the adenylate energy charge. Under glucose limitation in SS2 the energy charge was lowest with 0.73 because of the constant increase in intracellular AMP and ADP. However, differences to SS3 were only minor since final values here reached approximately 0.76. Energy charges of more than 0.90, as reported for a perfusion process with glucose in excess (Karst et al., 2017), were only found during early growth phase. Consequently, no significant differences were found in both ATP pool sizes and adenylate energy charge. Moreover, values were in physiological ranges in all three steady-states (Chapman & Atkinson, 1973). Therefore, any substantial difference in the impact of energy charge on antibody productivity could be excluded for the used cell line.

5.3 Conclusion

The aim of this thesis was to investigate production processes for biopharmaceuticals. Therefore, fed-batch and perfusion processes using CHO cells to produce monoclonal antibodies were analyzed on a metabolic level. In particular, the cell specific productivity combined with the cell density decides upon the volumetric productivity, eventually defining the economic result of the production processes. The main question arising was if and how the productivity was connected to the carbon metabolism and the resulting ATP supply. Therefore, the cellular phenotype was determined, followed by an analysis of intracellular metabolism via flux balance analysis and intracellular metabolomics for both fed-batch and perfusion.

The fed-batch results focused on the parameters pCO_2 and pH and their influence in distinct phases of the process. The main finding revealed a significant difference of antibody production kinetics between the process settings. On the metabolic level, the productivity was linked to the energy efficiency of the cellular carbon metabolism, which therefore was depending on the prevailing pH and partial pressure of CO_2. The pH shift downwards due to suppressed base addition led to high intracellular ATP availability and constant ATP formation rates until late stationary phase. The cause was a shift from lactate formation to consumption leading to increased NADH transport into mitochondria and eventually a rise in ATP formation from oxidative phosphorylation. As a result, the cell specific productivities were elevated until late process stages. Therefore, antibody production was growth decoupled and volumetric productivities were highest under highest cell density conditions. Contrary, the CO_2 stressed process revealed strongly growth coupled production kinetics probably mainly due to the increased pCO_2 in early process stages. Although the stressed cells showed shortly improved productivities and ATP formation rates, long-term detrimental effects got more pronounced the longer the process continued. Again, increased ATP availability coincided with rising productivities. However, the rapid decline in intracellular ATP was probably the consequence of increased maintenance demands since CO_2 as a non-polar molecule could easily diffuse into the cells and decreased intracellular pH. Finally, the remaining ATP available for antibody synthesis kept on diminishing which proved to be fatal for volumetric productivities. The presented fed-batch results can especially be

useful during scale-up, since both CO_2 and pH are sensitive parameters for the transfer to larger scales. Inhomogeneities occur due to poor mixing conditions and short stress stimuli can already lead to metabolic deviations between different scales and populations. The results might be irreversible long-term negative effects as the CO_2 stressed process showed. The goal should be to reduce the total use of inorganic carbon species concerning both CO_2 and Na_2CO_3 to avoid unwanted concentration fluctuations and ensure reproducible volumetric productivities.

The perfusion process was performed to investigate the influence of glucose limitation during steady-state cultivations. The cells showed substantial metabolic adjustments to the state of glucose limitation compared to the non-limited reference state. Phenotypically, the glucose uptake was decreased due to the lower glucose availability. As a consequence, metabolic efficiency was significantly increased under limited conditions, as lactate formation was severely decreased. Vice-versa, the carbon flux into TCA was elevated same as the flux of NADH into mitochondria. The resulting supply of ATP from respiratory metabolism was substantially higher than under non-limited conditions. Furthermore, a strong correlation between cell specific productivity and ATP generation from oxidative phosphorylation was found. Cells under non-limited conditions produced major amounts of ATP from glycolysis directly and showed lower product formation rates than cells under limitation. The results underline the importance of cellular efficiency and resulting ATP formation for final volumetric productivities. Concluding, the more NADH is fueled into mitochondria instead of being used for lactate formation, the more ATP is provided via oxidative phosphorylation and eventually more antibody is produced. Therefore, glucose limitation is an efficient tool to induce highly efficient metabolic states during perfusion mode. Hereby, volumetric productivities are maximized under high cell density perfusion operation. Additionally, medium cost is saved because cell specific perfusion rates are kept at a minimum, downstreaming is facilitated due to the lower harvest rates and antibody is saved, since bleed rates are minimized to allow for glucose limitation.

In conclusion, cellular productivity in both fed-batch and perfusion processes showed a strong dependence on the origin of ATP supply. Eventually, economic biopharmaceuticals production is simplified by amplifying the fraction of respiratory ATP forma-

tion and hereby enhancing the productivity. The latter can be achieved by avoiding stress through increased levels of inorganic carbon species during large scale fed-batch processes and by applying glucose limitation in high cell density perfusion processes. However, cell line stability and adaptations have to be considered for long-term perfusion processes. Possible future investigations on a transcriptomic or proteomic level might reveal further cellular adaptation measures connected to the increased cellular efficiency.

References

Abu-Absi, S., Xu, S., Graham, H., Dalal, N., Boyer, M., & Dave, K. (2013). Cell culture process operations for recombinant protein production. In *Mammalian cell cultures for biologics manufacturing* (pp. 35–68). Springer.

Aggarwal, S. R. (2014). What's fueling the biotech engine—2012 to 2013. *Nature biotechnology*, *32*(1), 32.

Ahn, W. S., & Antoniewicz, M. R. (2012). Towards dynamic metabolic flux analysis in cho cell cultures. *Biotechnology journal*, *7*(1), 61–74.

Ahn, W. S., Jeon, J. J., Jeong, Y. R., Lee, S. J., & Yoon, S. K. (2008). Effect of culture temperature on erythropoietin production and glycosylation in a perfusion culture of recombinant cho cells. *Biotechnology and Bioengineering*, *101*(6), 1234-44.

Altamirano, C., Illanes, A., Casablancas, A., Gamez, X., Cairó, J. J., & Godia, C. (2001). Analysis of cho cells metabolic redistribution in a glutamate-based defined medium in continuous culture. *Biotechnology Progress*, *17*(6), 1032-1041.

Altamirano, C., Paredes, C., Illanes, A., Cairo, J., & Godia, F. (2004). Strategies for fed-batch cultivation of t-pa producing cho cells: substitution of glucose and glutamine and rational design of culture medium. *Journal of Biotechnology*, *110*(2), 171–179.

Bausch, M., Schultheiss, C., & Sieck, J. B. (2018). Recommendations for comparison of productivity between fed-batch and perfusion processes. *Biotechnology Journal*, e1700721.

Becker, M., Junghans, L., Teleki, A., Bechmann, J., & Takors, R. (2019a). The less the better: How suppressed base addition boosts production of monoclonal antibodies with chinese hamster ovary cells. *Frontiers in bioengineering and biotechnology*, *7*(76).

Becker, M., Junghans, L., Teleki, A., Bechmann, J., & Takors, R. (2019b). Perfusion cultures require optimum respiratory atp supply to maximize cell-specific and

volumetric productivities. *Biotechnology and bioengineering*, *116*(5), 951-960.

Berg, J. M., Tymoczko, J. L., Stryer, L., et al. (2012). *Biochemistry*. New York: WH Freeman,.

Berrios, J., Altamirano, C., Osses, N., & Gonzalez, R. (2011). Continuous cho cell cultures with improved recombinant protein productivity by using mannose as carbon source: Metabolic analysis and scale-up simulation. *Chemical Engineering Science*, *66*(11), 2431–2439.

Bielser, J. M., Wolf, M., Souquet, J., Broly, H., & Morbidelli, M. (2018). Perfusion mammalian cell culture for recombinant protein manufacturing - a critical review. *Biotechnology Advances*, *36*(4), 1328-1340.

Birch, J. R., & Racher, A. J. (2006). Antibody production. *Advanced drug delivery reviews*, *58*(5-6), 671-685.

Bonarius, H. P., Houtman, J. H., Schmid, G., de Gooijer, C. D., & Tramper, J. (1999). Error analysis of metabolic-rate measurements in mammalian-cell culture by carbon and nitrogen balances. *Cytotechnology*, *29*(3), 167–176.

Brunner, M., Doppler, P., Klein, T., Herwig, C., & Fricke, J. (2018). Elevated pco2 affects the lactate metabolic shift in cho cell culture processes. *Engineering in Life Sciences*, *18*(3), 204-214.

Brunner, M., Fricke, J., Kroll, P., & Herwig, C. (2017). Investigation of the interactions of critical scale-up parameters (ph, po 2 and pco 2) on cho batch performance and critical quality attributes. *Bioprocess and biosystems engineering*, *40*(2), 251-263.

Buchholz, J., Graf, M., Blombach, B., & Takors, R. (2014). Improving the carbon balance of fermentations by total carbon analyses. *Biochemical engineering journal*, *90*, 162–169.

Butler, M. (2005). Animal cell cultures: recent achievements and perspectives in the production of biopharmaceuticals. *Applied microbiology and biotechnology*, *68*(3), 283–291.

Carinhas, N., Duarte, T. M., Barreiro, L. C., Carrondo, M. J., Alves, P. M., & Teixeira, A. P. (2013). Metabolic signatures of gs-cho cell clones associated with butyrate treatment and culture phase transition. *Biotechnology and bioengineering*, *110*(12), 3244-3257.

Casey, J. R., Grinstein, S., & Orlowski, J. (2010). Sensors and regulators of intracellular

ph. *Nature reviews Molecular cell biology*, *11*(1), 50.

Chapman, A. G., & Atkinson, D. E. (1973). Stabilization of adenylate energy charge by the adenylate deaminase reaction. *Journal of Biological chemistry*, *248*(23), 8309-8312.

Chee Furng Wong, D., Tin Kam Wong, K., Tang Goh, L., Kiat Heng, C., & Gek Sim Yap, M. (2005). Impact of dynamic online fed-batch strategies on metabolism, productivity and n-glycosylation quality in cho cell cultures. *Biotechnology and Bioengineering*, *89*(2), 164-77.

Chen, K., Liu, Q., Xie, L., Sharp, P. A., & Wang, D. I. (2001). Engineering of a mammalian cell line for reduction of lactate formation and high monoclonal antibody production. *Biotechnology and bioengineering*, *72*(1), 55–61.

Chen, P., & Harcum, S. W. (2006). Effects of elevated ammonium on glycosylation gene expression in cho cells. *Metabolic Engineering*, *8*(2), 123–132.

Chong, W. P., Reddy, S. G., Yusufi, F. N., Lee, D.-Y., Wong, N. S., Heng, C. K., ... Ho, Y. S. (2010). Metabolomics-driven approach for the improvement of chinese hamster ovary cell growth: overexpression of malate dehydrogenase ii. *Journal of biotechnology*, *147*(2), 116–121.

Choo, C.-Y., Tian, Y., Kim, W.-S., Blatter, E., Conary, J., & Brady, C. P. (2007). High-level production of a monoclonal antibody in murine myeloma cells by perfusion culture using a gravity settler. *Biotechnology progress*, *23*(1), 225–231.

Chotteau, V. (2015). Perfusion processes. In *Animal cell culture* (pp. 407–443). Springer.

Clincke, M. F., Molleryd, C., Samani, P. K., Lindskog, E., Faldt, E., Walsh, K., & Chotteau, V. (2013). Very high density of chinese hamster ovary cells in perfusion by alternating tangential flow or tangential flow filtration in wave bioreactor-part ii: Applications for antibody production and cryopreservation. *Biotechnology Progress*, *29*(3), 768-77.

Clincke, M. F., Molleryd, C., Zhang, Y., Lindskog, E., Walsh, K., & Chotteau, V. (2013). Very high density of cho cells in perfusion by atf or tff in wave bioreactor. part i. effect of the cell density on the process. *Biotechnology Progress*, *29*(3), 754-67.

Croughan, M. S., Konstantinov, K. B., & Cooney, C. (2015). The future of industrial bioprocessing: Batch or continuous? *Biotechnology and bioengineering*, *112*(4), 648-651.

Dalm, M. C., Cuijten, S. M., van Grunsven, W. M., Tramper, J., & Martens, D. E. (2004). Effect of feed and bleed rate on hybridoma cells in an acoustic perfusion bioreactor: part i. cell density, viability, and cell-cycle distribution. *Biotechnology and Bioengineering*, *88*(5), 547-57.

Dalm, M. C., Lamers, P. P., Cuijten, S. M., Tjeerdsma, A., Van Grunsven, W. M., Tramper, J., & Martens, D. E. (2007). Effect of feed and bleed rate on hybridoma cells in an acoustic perfusion bioreactor: metabolic analysis. *Biotechnology progress*, *23*(3), 560-569.

Darja, O., Stanislav, M., Saša, S., Andrej, F., Lea, B., & Branka, J. (2016). Responses of cho cell lines to increased pco2 at normal (37 c) and reduced (33 c) culture temperatures. *Journal of biotechnology*, *219*, 98-109.

DeZengotita, V. M., Schmelzer, A. E., & Miller, W. M. (2002). Characterization of hybridoma cell responses to elevated pco2 and osmolality: intracellular ph, cell size, apoptosis, and metabolism. *Biotechnology and bioengineering*, *77*(4), 369-380.

Dickson, A. J. (2014). Enhancement of production of protein biopharmaceuticals by mammalian cell cultures: the metabolomics perspective. *Current opinion in biotechnology*, *30*, 73-79.

Ecker, D. M., Jones, S. D., & Levine, H. L. (2015). The therapeutic monoclonal antibody market. In *Mabs* (Vol. 7, pp. 9–14).

Elsayed, E., Medronho, R., Wagner, R., & Deckwer, W.-D. (2006). Use of hydrocyclones for mammalian cell retention: separation efficiency and cell viability (part 1). *Engineering in Life Sciences*, *6*(4), 347–354.

Erecińska, M., Deas, J., & Silver, I. (1995). The effect of ph on glycolysis and phosphofructokinase activity in cultured cells and synaptosomes. *Journal of neurochemistry*, *65*(6), 2765–2772.

Europa, A. F., Gambhir, A., Fu, P., & Hu, W. (2000). Multiple steady states with distinct cellular metabolism in continuous culture of mammalian cells. *Biotechnology and bioengineering*, *67*(1), 25-34.

Feist, A. M., & Palsson, B. Ø. (2008). The growing scope of applications of genome-scale metabolic reconstructions using escherichia coli. *Nature biotechnology*, *26*(6), 659.

Feist, A. M., & Palsson, B. O. (2010). The biomass objective function. *Current opinion*

in microbiology, *13*(3), 344–349.

Furukawa, K., & Ohsuye, K. (1999). Enhancement of productivity of recombinant -amidating enzyme by low temperature culture. *Cytotechnology*, *31*(1-2), 85-94.

Gaughan, C. L. (2016). The present state of the art in expression, production and characterization of monoclonal antibodies. *Molecular diversity*, *20*(1), 255-270.

Glacken, M. W. (1988). Catabolic control of mammalian cell culture. *Bio/technology*, *6*(9), 1041.

Gorenflo, V. M., Smith, L., Dedinsky, B., Persson, B., & Piret, J. M. (2002). Scale-up and optimization of an acoustic filter for 200 l/day perfusion of a cho cell culture. *Biotechnology and bioengineering*, *80*(4), 438–444.

Goudar, C. T., Matanguihan, R., Long, E., Cruz, C., Zhang, C., Piret, J. M., & Konstantinov, K. B. (2007). Decreased pco2 accumulation by eliminating bicarbonate addition to high cell-density cultures. *Biotechnology and bioengineering*, *96*(6), 1107-1117.

Gray, D. R., Chen, S., Howarth, W., Inlow, D., & Maiorella, B. L. (1996). Co 2 in large-scale and high-density cho cell perfusion culture. *Cytotechnology*, *22*(1-3), 65-78.

Han, Y. K., Koo, T. Y., & Lee, G. M. (2009). Enhanced interferon-β production by cho cells through elevated osmolality and reduced culture temperature. *Biotechnology progress*, *25*(5), 1440–1447.

Hardie, D. G. (2011). Amp-activated protein kinase—an energy sensor that regulates all aspects of cell function. *Genes & development*, *25*(18), 1895–1908.

Hassell, T., Gleave, S., & Butler, M. (1991). Growth inhibition in animal cell culture. *Applied biochemistry and biotechnology*, *30*(1), 29–41.

Hinkle, P. C. (2005). P/o ratios of mitochondrial oxidative phosphorylation. *Biochimica et Biophysica Acta (BBA)-Bioenergetics*, *1706*(1-2), 1–11.

Huang, Y.-M., Hu, W., Rustandi, E., Chang, K., Yusuf-Makagiansar, H., & Ryll, T. (2010). Maximizing productivity of cho cell-based fed-batch culture using chemically defined media conditions and typical manufacturing equipment. *Biotechnology progress*, *26*(5), 1400–1410.

Huang, Z., Lee, D., & Yoon, S. (2017). Quantitative intracellular flux modeling and applications in biotherapeutic development and production using cho cell cultures. *Biotechnology and bioengineering*, *114*(12), 2717-2728.

Ivarsson, M., Noh, H., Morbidelli, M., & Soos, M. (2015). Insights into ph-induced metabolic switch by flux balance analysis. *Biotechnology progress*, *31*(2), 347-357.

Jiang, Z., & Sharfstein, S. T. (2008). Sodium butyrate stimulates monoclonal antibody over-expression in cho cells by improving gene accessibility. *Biotechnology and bioengineering*, *100*(1), 189–194.

Junghans, L., Teleki, A., Wijaya, A. W., Becker, M., Schweikert, M., & Takors, R. (2019). From nutritional wealth to autophagy: In vivo metabolic dynamics in the cytosol, mitochondrion and shuttles of igg producing cho cells. *Metabolic Engineering*, *54*, 145-159.

Kantardjieff, A., & Zhou, W. (2013). Mammalian cell cultures for biologics manufacturing. In *Mammalian cell cultures for biologics manufacturing* (pp. 1–9). Springer.

Karst, D. J., Serra, E., Villiger, T. K., Soos, M., & Morbidelli, M. (2016). Characterization and comparison of atf and tff in stirred bioreactors for continuous mammalian cell culture processes. *Biochemical Engineering Journal*, *110*, 17-26.

Karst, D. J., Steinhoff, R. F., Kopp, M. R., Serra, E., Soos, M., Zenobi, R., & Morbidelli, M. (2017). Intracellular cho cell metabolite profiling reveals steady-state dependent metabolic fingerprints in perfusion culture. *Biotechnology Progress*, *33*(4), 879-890.

Kaufmann, H., Mazur, X., Fussenegger, M., & Bailey, J. E. (1999). Influence of low temperature on productivity, proteome and protein phosphorylation of cho cells. *Biotechnology and bioengineering*, *63*(5), 573–582.

Kelly, W., Scully, J., Zhang, D., Feng, G., Lavengood, M., Condon, J., ... Bhatia, R. (2014). Understanding and modeling alternating tangential flow filtration for perfusion cell culture. *Biotechnology progress*, *30*(6), 1291–1300.

Kim, B. J., Oh, D. J., & Chang, H. N. (2008). Limited use of centritech lab ii centrifuge in perfusion culture of rcho cells for the production of recombinant antibody. *Biotechnology progress*, *24*(1), 166–174.

Kim, J. Y., Kim, Y.-G., & Lee, G. M. (2012). Cho cells in biotechnology for production of recombinant proteins: current state and further potential. *Applied microbiology and biotechnology*, *93*(3), 917–930.

Kim, N. S., & Lee, G. M. (2002). Response of recombinant chinese hamster ovary cells

to hyperosmotic pressure: effect of bcl-2 overexpression. *Journal of biotechnology*, *95*(3), 237–248.

Kimura, R., & Miller, W. M. (1996). Effects of elevated pco2 and/or osmolality on the growth and recombinant tpa production of cho cells. *Biotechnology and bioengineering*, *52*(1), 152-160.

Kochanowski, N., Blanchard, F., Cacan, R., Chirat, F., Guedon, E., Marc, A., & Goergen, J.-L. (2008). Influence of intracellular nucleotide and nucleotide sugar contents on recombinant interferon-γ glycosylation during batch and fed-batch cultures of cho cells. *Biotechnology and bioengineering*, *100*(4), 721–733.

Komolpis, K., Udomchokmongkol, C., Phutong, S., & Palaga, T. (2010). Comparative production of a monoclonal antibody specific for enrofloxacin in a stirred-tank bioreactor. *Journal of Industrial and Engineering Chemistry*, *16*(4), 567–571.

Konakovsky, V., Clemens, C., Müller, M. M., Bechmann, J., Berger, M., Schlatter, S., & Herwig, C. (2016). Metabolic control in mammalian fed-batch cell cultures for reduced lactic acid accumulation and improved process robustness. *Bioengineering*, *3*(1), 5.

Kunert, R., & Reinhart, D. (2016). Advances in recombinant antibody manufacturing. *Applied microbiology and biotechnology*, *100*(8), 3451-3461.

Langheinrich, C., & Nienow, A. W. (1999). Control of ph in large-scale, free suspension animal cell bioreactors: Alkali addition and ph excursions. *Biotechnology and bioengineering*, *66*(3), 171-179.

Lao, M., & Toth, D. (1997). Effects of ammonium and lactate on growth and metabolism of a recombinant chinese hamster ovary cell culture. *Biotechnology progress*, *13*(5), 688-691.

Li, F., Vijayasankaran, N., Shen, A., Kiss, R., & Amanullah, A. (2010). Cell culture processes for monoclonal antibody production. In *Mabs* (Vol. 2, pp. 466–479).

Lin, J., Takagi, M., Qu, Y., Gao, P., & Yoshida, T. (1999). Metabolic flux change in hybridoma cells under high osmotic pressure. *Journal of bioscience and bioengineering*, *87*(2), 255–257.

Liste-Calleja, L., Lecina, M., Lopez-Repullo, J., Albiol, J., Solà, C., & Cairó, J. J. (2015). Lactate and glucose concomitant consumption as a self-regulated ph detoxification mechanism in hek293 cell cultures. *Applied microbiology and biotechnology*, *99*(23), 9951-9960.

Ljunggren, J., & Häggström, L. (1992). Glutamine limited fed-batch culture reduces the overflow metabolism of amino acids in myeloma cells. *Cytotechnology*, *8*(1), 45–56.

Lu, S., Sun, X., & Zhang, Y. (2005). Insight into metabolism of cho cells at low glucose concentration on the basis of the determination of intracellular metabolites. *Process Biochemistry*, *40*(5), 1917-1921.

Luo, J., Vijayasankaran, N., Autsen, J., Santuray, R., Hudson, T., Amanullah, A., & Li, F. (2012). Comparative metabolite analysis to understand lactate metabolism shift in chinese hamster ovary cell culture process. *Biotechnology and bioengineering*, *109*(1), 146-156.

Martínez, V. S., Dietmair, S., Quek, L., Hodson, M. P., Gray, P., & Nielsen, L. K. (2013). Flux balance analysis of cho cells before and after a metabolic switch from lactate production to consumption. *Biotechnology and bioengineering*, *110*(2), 660-666.

Matuszczyk, J., Teleki, A., Pfizenmaier, J., & Takors, R. (2015). Compartment-specific metabolomics for cho reveals that atp pools in mitochondria are much lower than in cytosol. *Biotechnology journal*, *10*(10), 1639-1650.

McMurray-Beaulieu, V., Hisiger, S., Durand, C., Perrier, M., & Jolicoeur, M. (2009). Na-butyrate sustains energetic states of metabolism and t-pa productivity of cho cells. *Journal of bioscience and bioengineering*, *108*(2), 160–167.

Moore, A., Mercer, J., Dutina, G., Donahue, C. J., Bauer, K. D., Mather, J. P., ... Ryll, T. (1997). Effects of temperature shift on cell cycle, apoptosis and nucleotide pools in cho cell batch cultues. *Cytotechnology*, *23*(1-3), 47–54.

Morrison, C., & Lähteenmäki, R. (2017). Public biotech in 2016—the numbers. *Nature biotechnology*, *35*(7), 623.

Mortimer, C. E., & Müller, U. (2001). *Das basiswissen der chemie.* Georg Thieme Verlag Stuttgart, New-York.

Mostafa, S. S., & Gu, X. S. (2003). Strategies for improved dco2 removal in large-scale fed-batch cultures. *Biotechnology progress*, *19*(1), 45-51.

Mullard, A. (2012). Can next-generation antibodies offset biosimilar competition? *Nature Reviews Drug Discovery*, *11*, 426-428.

Mulukutla, B. C., Gramer, M., & Hu, W.-S. (2012). On metabolic shift to lactate consumption in fed-batch culture of mammalian cells. *Metabolic engineering*, *14*(2), 138-149.

Niklas, J., & Heinzle, E. (2011). Metabolic flux analysis in systems biology of mammalian cells. In *Genomics and systems biology of mammalian cell culture* (pp. 109–132). Springer.

Nishimiya, D., Mano, T., Miyadai, K., Yoshida, H., & Takahashi, T. (2013). Overexpression of chop alone and in combination with chaperones is effective in improving antibody production in mammalian cells. *Applied microbiology and biotechnology*, *97*(6), 2531-2539.

Nolan, R. P., & Lee, K. (2011). Dynamic model of cho cell metabolism. *Metabolic Engineering*, *13*(1), 108-24.

Orth, J. D., Thiele, I., & Palsson, B. Ø. (2010). What is flux balance analysis? *Nature biotechnology*, *28*(3), 245.

Osman, J. J., Birch, J., & Varley, J. (2001). The response of gs-ns0 myeloma cells to ph shifts and ph perturbations. *Biotechnology and bioengineering*, *75*(1), 63-73.

Ozturk, S., & Hu, W.-S. (2005). *Cell culture technology for pharmaceutical and cell-based therapies*. CRC press.

Ozturk, S. S., Riley, M. R., & Palsson, B. O. (1992). Effects of ammonia and lactate on hybridoma growth, metabolism, and antibody production. *Biotechnology and bioengineering*, *39*(4), 418–431.

Pfizenmaier, J., Junghans, L., Teleki, A., & Takors, R. (2016). Hyperosmotic stimulus study discloses benefits in atp supply and reveals mirna/mrna targets to improve recombinant protein production of cho cells. *Biotechnology journal*, *11*(8), 1037-1047.

Pfizenmaier, J., Matuszczyk, J., & Takors, R. (2015). Changes in intracellular atp-content of cho cells as response to hyperosmolality. *Biotechnology progress*, *31*(5), 1212-1216.

Pieper, L. A., Strotbek, M., Wenger, T., Olayioye, M. A., & Hausser, A. (2017). Atf6-based fine-tuning of the unfolded protein response enhances therapeutic antibody productivity of chinese hamster ovary cells. *Biotechnology and bioengineering*, *114*(6), 1310-1318.

Pinto, R. C., Medronho, R. A., & Castilho, L. R. (2008). Separation of cho cells using hydrocyclones. *Cytotechnology*, *56*(1), 57–67.

Pohlscheidt, M., Jacobs, M., Wolf, S., Thiele, J., Jockwer, A., Gabelsberger, J., ... Burg, J. (2013). Optimizing capacity utilization by large scale 3000 l perfusion

in seed train bioreactors. *Biotechnology progress*, *29*(1), 222–229.

Pörtner, R. (2009). Characteristics of mammalian cells and requirements for cultivation. In *Cell and tissue reaction engineering* (pp. 13–53). Springer.

Puck, T. T., Cieciura, S. J., & Robinson, A. (1958). Genetics of somatic mammalian cells: Iii. long-term cultivation of euploid cells from human and animal subjects. *Journal of Experimental Medicine*, *108*(6), 945–956.

Reinhart, D., Kaisermayer, C., Damjanovic, L., & Kunert, R. (2013). Benchmarking of commercially available cho cell culture media for antibody production. In *Bmc proceedings* (Vol. 7, p. P13).

Roos, A., & Boron, W. F. (1981). Intracellular ph. *Physiological reviews*, *61*(2), 296-434.

Russell, J. B. (2007). The energy spilling reactions of bacteria and other organisms. *Journal of molecular microbiology and biotechnology*, *13*(1-3), 1-11.

Ryll, T., Dutina, G., Reyes, A., Gunson, J., Krummen, L., & Etcheverry, T. (2000). Performance of small-scale cho perfusion cultures using an acoustic cell filtration device for cell retention: Characterization of separation efficiency and impact of perfusion on product quality. *Biotechnology and bioengineering*, *69*(4), 440–449.

Schellenberger, J., Que, R., Fleming, R. M., Thiele, I., Orth, J. D., Feist, A. M., ... others (2011). Quantitative prediction of cellular metabolism with constraint-based models: the cobra toolbox v2. 0. *Nature protocols*, *6*(9), 1290-1307.

Schneider, M., Marison, I. W., & von Stockar, U. (1996). The importance of ammonia in mammalian cell culture. *Journal of biotechnology*, *46*(3), 161–185.

Selvarasu, S., Ho, Y. S., Chong, W. P., Wong, N. S., Yusufi, F. N., Lee, Y. Y., ... Lee, D. (2012). Combined in silico modeling and metabolomics analysis to characterize fed-batch cho cell culture. *Biotechnology and bioengineering*, *109*(6), 1415-1429.

Seth, G., Hossler, P., Yee, J. C., & Hu, W.-S. (2006). Engineering cells for cell culture bioprocessing–physiological fundamentals. In *Cell culture engineering* (pp. 119–164). Springer.

Shen, D., Kiehl, T. R., Khattak, S. F., Li, Z. J., He, A., Kayne, P. S., ... Sharfstein, S. T. (2010). Transcriptomic responses to sodium chloride-induced osmotic stress: A study of industrial fed-batch cho cell cultures. *Biotechnology progress*, *26*(4), 1104–1115.

Shen, Y., & Yanagimachi, K. (2011). Cfd-aided cell settler design optimization and scale-up: Effect of geometric design and operational variables on separation performance. *Biotechnology progress*, *27*(5), 1282–1296.

Shirgaonkar, I. Z., Lanthier, S., & Kamen, A. (2004). Acoustic cell filter: a proven cell retention technology for perfusion of animal cell cultures. *Biotechnology advances*, *22*(6), 433–444.

Shukla, A. A., & Thömmes, J. (2010). Recent advances in large-scale production of monoclonal antibodies and related proteins. *Trends in biotechnology*, *28*(5), 253-261.

Sieblist, C., Hägeholz, O., Aehle, M., Jenzsch, M., Pohlscheidt, M., & Lübbert, A. (2011). Insights into large-scale cell-culture reactors: Ii. gas-phase mixing and co2 stripping. *Biotechnology journal*, *6*(12), 1547-1556.

Sou, S. N., Sellick, C., Lee, K., Mason, A., Kyriakopoulos, S., Polizzi, K. M., & Kontoravdi, C. (2015). How does mild hypothermia affect monoclonal antibody glycosylation? *Biotechnology and bioengineering*, *112*(6), 1165–1176.

Steinebach, F., Ulmer, N., Wolf, M., Decker, L., Schneider, V., Walchli, R., ... Morbidelli, M. (2017). Design and operation of a continuous integrated monoclonal antibody production process. *Biotechnology Progress*, *33*(5), 1303-1313.

Stephanopoulos, G., Aristidou, A. A., & Nielsen, J. (1998). *Metabolic engineering: principles and methodologies*. Elsevier.

Takuma, S., Hirashima, C., & Piret, J. M. (2003). Effects of glucose and co 2 concentrations on cho cell physiology. In *Animal cell technology: Basic & applied aspects* (p. 99-103). Springer.

Takuma, S., Hirashima, C., & Piret, J. M. (2007). Dependence on glucose limitation of the pco2 influences on cho cell growth, metabolism and igg production. *Biotechnology and Bioengineering*, *97*(6), 1479-88.

Teleki, A., Sánchez-Kopper, A., & Takors, R. (2015). Alkaline conditions in hydrophilic interaction liquid chromatography for intracellular metabolite quantification using tandem mass spectrometry. *Analytical biochemistry*, *475*, 4-13.

Templeton, N., Dean, J., Reddy, P., & Young, J. D. (2013). Peak antibody production is associated with increased oxidative metabolism in an industrially relevant fed-batch cho cell culture. *Biotechnology and bioengineering*, *110*(7), 2013-2024.

Templeton, N., Xu, S., Roush, D. J., & Chen, H. (2017). (13)c metabolic flux analysis

identifies limitations to increasing specific productivity in fed-batch and perfusion. *Metabolic Engineering*, *44*, 126-133.

Thiele, I., Price, N. D., Vo, T. D., & Palsson, B. . (2005). Candidate metabolic network states in human mitochondria impact of diabetes, ischemia, and diet. *Journal of Biological Chemistry*, *280*(12), 11683-11695.

Trummer, E., Fauland, K., Seidinger, S., Schriebl, K., Lattenmayer, C., Kunert, R., ... Katinger, H. (2006). Process parameter shifting: Part i. effect of dot, ph, and temperature on the performance of epo-fc expressing cho cells cultivated in controlled batch bioreactors. *Biotechnology and bioengineering*, *94*(6), 1033-1044.

Urlaub, G., Käs, E., Carothers, A. M., & Chasin, L. A. (1983). Deletion of the diploid dihydrofolate reductase locus from cultured mammalian cells. *Cell*, *33*(2), 405–412.

Urlaub, G., Mitchell, P. J., Kas, E., Chasin, L. A., Funanage, V. L., Myoda, T. T., & Hamlin, J. (1986). Effect of gamma rays at the dihydrofolate reductase locus: deletions and inversions. *Somatic cell and molecular genetics*, *12*(6), 555–566.

Vallez-Chetreanu, F., Ferreira, L. F., Rabe, R., von Stockar, U., & Marison, I. (2007). An on-line method for the reduction of fouling of spin-filters for animal cell perfusion cultures. *Journal of biotechnology*, *130*(3), 265–273.

Vielhauer, O., Zakhartsev, M., Horn, T., Takors, R., & Reuss, M. (2011). Simplified absolute metabolite quantification by gas chromatography–isotope dilution mass spectrometry on the basis of commercially available source material. *Journal of Chromatography B*, *879*(32), 3859-3870.

Voisard, D., Meuwly, F., Ruffieux, P. A., Baer, G., & Kadouri, A. (2003). Potential of cell retention techniques for large-scale high-density perfusion culture of suspended mammalian cells. *Biotechnology and Bioengineering*, *82*(7), 751-765.

Wahrheit, J., Nicolae, A., & Heinzle, E. (2014). Dynamics of growth and metabolism controlled by glutamine availability in chinese hamster ovary cells. *Applied microbiology and biotechnology*, *98*(4), 1771-1783.

Walsh, G. (2014). Biopharmaceutical benchmarks 2014. *Nature biotechnology*, *32*(10), 992-1000.

Warburg, O. (1956). On the origin of cancer cells. *Science*, *123*(3191), 309–314.

Warikoo, V., Godawat, R., Brower, K., Jain, S., Cummings, D., Simons, E., ... Wright,

B. (2012). Integrated continuous production of recombinant therapeutic proteins. *Biotechnology and bioengineering*, *109*(12), 3018-3029.

Wen, Z.-Y., Teng, X.-W., & Chen, F. (2000). A novel perfusion system for animal cell cultures by two step sequential sedimentation. *Journal of biotechnology*, *79*(1), 1–11.

Wilkens, C. A., Altamirano, C., & Gerdtzen, Z. P. (2011). Comparative metabolic analysis of lactate for cho cells in glucose and galactose. *Biotechnology and Bioprocess Engineering*, *16*(4), 714.

Wlaschin, K. F., & Hu, W.-S. (2006). Fedbatch culture and dynamic nutrient feeding. In *Cell culture engineering* (pp. 43–74). Springer.

Wolf, M. K. F., Closet, A., Bzowska, M., Bielser, J. M., Souquet, J., Broly, H., & Morbidelli, M. (2018). Improved performance in mammalian cell perfusion cultures by growth inhibition. *Biotechnology Journal*, e1700722.

Wu, P., Ray, N., & Shuler, M. (1993). A computer model for intracellular ph regulation in chinese hamster ovary cells. *Biotechnology progress*, *9*(4), 374-384.

Wurm, F. M. (2004). Production of recombinant protein therapeutics in cultivated mammalian cells. *Nature biotechnology*, *22*(11), 1393-1398.

Xie, L., & Wang, D. I. (1994). Applications of improved stoichiometric model in medium design and fed-batch cultivation of animal cells in bioreactor. *Cytotechnology*, *15*(1-3), 17–29.

Xing, Z., Kenty, B. M., Li, Z. J., & Lee, S. S. (2009). Scale-up analysis for a cho cell culture process in large-scale bioreactors. *Biotechnology and bioengineering*, *103*(4), 733-746.

Xu, S., Hoshan, L., & Chen, H. (2016). Improving lactate metabolism in an intensified cho culture process: productivity and product quality considerations. *Bioprocess and Biosystems Engineering*, *39*(11), 1689-702.

Xu, S., Jiang, R., Mueller, R., Hoesli, N., Kretz, T., Bowers, J., & Chen, H. (2018). Probing lactate metabolism variations in large-scale bioreactors. *Biotechnology progress*, *34*(3), 756-766.

Yang, W. C., Minkler, D. F., Kshirsagar, R., Ryll, T., & Huang, Y.-M. (2016). Concentrated fed-batch cell culture increases manufacturing capacity without additional volumetric capacity. *Journal of biotechnology*, *217*, 1–11.

Yoon, S. K., Choi, S. L., Song, J. Y., & Lee, G. M. (2005). Effect of culture ph on

erythropoietin production by chinese hamster ovary cells grown in suspension at 32.5 and 37.0 c. *Biotechnology and bioengineering*, *89*(3), 345-356.

Zalai, D., Koczka, K., Párta, L., Wechselberger, P., Klein, T., & Herwig, C. (2015). Combining mechanistic and data-driven approaches to gain process knowledge on the control of the metabolic shift to lactate uptake in a fed-batch cho process. *Biotechnology progress*, *31*(6), 1657-1668.

Zanghi, J. A., Schmelzer, A. E., Mendoza, T. P., Knop, R. H., & Miller, W. M. (1999). Bicarbonate concentration and osmolality are key determinants in the inhibition of cho cell polysialylation under elevated pco2 or ph. *Biotechnology and bioengineering*, *65*(2), 182-191.

Zboray, K., Sommeregger, W., Bogner, E., Gili, A., Sterovsky, T., Fauland, K., ... others (2015). Heterologous protein production using euchromatin-containing expression vectors in mammalian cells. *Nucleic acids research*, *43*(16), e102–e102.

Zhang, L., Shen, H., & Zhang, Y. (2004). Fed-batch culture of hybridoma cells in serum-free medium using an optimized feeding strategy. *Journal of Chemical Technology & Biotechnology*, *79*(2), 171–181.

Zhang, X., Wen, Y., & Yang, S. (2011). Modes of culture/animal cells. In *Comprehensive biotechnology* (pp. 285–302). Elsevier.

Zhu, M. M., Goyal, A., Rank, D. L., Gupta, S. K., Boom, T. V., & Lee, S. S. (2005). Effects of elevated pco2 and osmolality on growth of cho cells and production of antibody-fusion protein b1: a case study. *Biotechnology progress*, *21*(1), 70–77.

Zimmermann, M., Sauer, U., & Zamboni, N. (2014). Quantification and mass isotopomer profiling of -keto acids in central carbon metabolism. *Analytical chemistry*, *86*(6), 3232-3237.

A Manuscript I

The following manuscript was published in Frontiers in Bioengineering and Biotechnology, 7, 76 in 2019 and reproduced with permission of the authors (copyright holders).

Becker, M., Junghans, L., Teleki, A., Bechmann, J., Takors, R. (2019a). The less the better: How suppressed base addition boosts production of monoclonal antibodies with chinese hamster ovary cells. *Frontiers in bioengineering and biotechnology, 7, 76*.

frontiers in Bioengineering and Biotechnology

ORIGINAL RESEARCH
published: 11 April 2019
doi: 10.3389/fbioe.2019.00076

The Less the Better: How Suppressed Base Addition Boosts Production of Monoclonal Antibodies With Chinese Hamster Ovary Cells

Max Becker[1], *Lisa Junghans*[1], *Attila Teleki*[1], *Jan Bechmann*[2] *and Ralf Takors*[1]*

[1] *Institute of Biochemical Engineering, University of Stuttgart, Stuttgart, Germany,* [2] *Boehringer Ingelheim Pharma GmbH & Co. KG, Biberach an der Riss, Germany*

Biopharmaceutical production processes strive for the optimization of economic efficiency. Among others, the maximization of volumetric productivity is a key criterion. Typical parameters such as partial pressure of CO_2 (pCO_2) and pH are known to influence the performance although reasons are not yet fully elucidated. In this study the effects of pCO_2 and pH shifts on the phenotypic performance were linked to metabolic and energetic changes. Short peak performance of q_{mAb} (23 pg/cell/day) was achieved by early pCO_2 shifts up to 200 mbar but followed by declining intracellular ATP levels to 2.5 fmol/cell and 80% increase of q_{Lac}. On the contrary, steadily rising q_{mAb} could be installed by slight pH down-shifts ensuring constant cell specific ATP production (q_{ATP}) of 27 pmol/cell/day and high intracellular ATP levels of about 4 fmol/cell. As a result, maximum productivity was achieved combining highest q_{mAb} (20 pg/cell/day) with maximum cell density and no lactate formation. Our results indicate that the energy availability in form of intracellular ATP is crucial for maintaining antibody synthesis and reacts sensitive to pCO_2 and pH-process parameters typically responsible for inhomogeneities after scaling up.

Keywords: CHO, fed-batch, CO_2, pH, flux analysis, metabolomics, productivity, lactate

OPEN ACCESS

Edited by:
Roland Wohlgemuth, Lodz University of Technology, Poland

Reviewed by:
Debendra K. Sahoo, Institute of Microbial Technology (CSIR), India
Michael Butler, National Institute for Bioprocessing Research and Training (NIBRT), Ireland

***Correspondence:**
Ralf Takors
takors@ibvt.uni-stuttgart.de

Specialty section:
This article was submitted to Bioprocess Engineering, a section of the journal Frontiers in Bioengineering and Biotechnology

Received: *11 July 2018*
Accepted: *25 March 2019*
Published: *11 April 2019*

Citation:
Becker M, Junghans L, Teleki A, Bechmann J and Takors R (2019) The Less the Better: How Suppressed Base Addition Boosts Production of Monoclonal Antibodies With Chinese Hamster Ovary Cells. Front. Bioeng. Biotechnol. 7:76. doi: 10.3389/fbioe.2019.00076

INTRODUCTION

The global sales for biopharmaceuticals are constantly on the rise which is the major driving force for the optimization of industrial production processes (Walsh, 2014; Morrison and Lähteenmäki, 2017). Additionally, the growing number of expiring patent protections and the subsequent emergence of biosimilar producing companies and processes has increased the urge for optimized processes even further (Mullard, 2012; Gaughan, 2016). Especially the major biopharmaceutical product group of monoclonal antibodies and their main production host Chinese hamster ovary (CHO) cells are in the focus of research (Ecker et al., 2015). As a result, product titers have increased substantially over the past years (Kunert and Reinhart, 2016) and process intensification toward continuous processes (Hammerschmidt et al., 2014) as well as an increased use of single-use bioreactors (Löffelholz et al., 2013) has taken place. But since fed-batch cultivation remains the predominant large-scale process in industry, a large number of studies focusing on fed-batch processes have been published over the past decades. An improved understanding of media and feeding was therefore already achieved (Birch and Racher, 2006; Shukla and Thömmes, 2010). Despite the gathered knowledge many uncertainties remain, particularly during scale-up into industry relevant scales. Challenges occurring during scale-up can be inhomogeneities due to local

accumulation of feed or base or merely poor mixing (Xu et al., 2018). Especially addition of titration agents like CO_2 or Na_2CO_3 can lead to gradients and therefore inhibition of cellular growth and productivity (Xing et al., 2009; Sieblist et al., 2011). The result of these inhomogeneities can be gradients in pCO_2 or pH influencing the cellular metabolism and hence the productivity of the process (Langheinrich and Nienow, 1999; Osman et al., 2001; Xing et al., 2009). In contrast, a shift to lactate consumption by the cells is considered as beneficial and can even occur when glucose is present in excess, but is not yet fully understood (Mulukutla et al., 2012). Since high lactate concentrations lower the pH and can downregulate certain enzymes it is favorable to avoid an accumulation of lactate (Leite et al., 2011). Effect of these parameters on intracellular metabolic fluxes and the energy household was seldom published although these factors are known to be crucial for the outcome of the process (Russell, 2007; Dickson, 2014; Huang et al., 2017).

In this study, the influence of the parameters pH and pCO_2 on a fed-batch production process was investigated. Regarding pCO_2, a stimulus effect in early stages and its impact on the further cellular state was studied. Secondly, a slow pH shift downwards should give an insight into metabolic adjustments made due to sinking pH, whereas other negative side effects of base addition like rising osmolality were suppressed. On the basis of extracellular rates, intracellular metabolomics and flux balance analysis the process parameters could be linked to specific metabolic states and their corresponding production kinetics. The found connections can be used for process parameter adjustments to lead cells into a more efficient state or to identify inhibiting influences of gradients occurring after scale-up.

MATERIALS AND METHODS

Cell Line, Seed Train, and Bioreactor Cultivation

The CHO cell line 2-09 producing the monoclonal antibody type IgG1 was provided by the industrial partner Boehringer Ingelheim and cultivated in chemically defined basal and feed media. After thawing the cryo culture, the cells were expanded in a seed train consisting of a sequence of six shake flasks (Corning, USA) ranging from 125 to 1,000 mL before seeding the bioreactor. The humidified incubator (Infors HT, Switzerland) was set to 37°C, 5% CO_2 and 120 RPM. Bioreactor cultivations in fed-batch mode were performed in a 4-fold parallel bioreactor system DS1500ODSS (DASGIP, Germany) with a starting volume of 1.0 L and an initial cell density of 0.7×10^6 cells/mL. The feed was added continuously starting at 24 h of process time. In case of glucose concentrations falling below 2 g/L a concentrated glucose solution was added as a bolus to re-install glucose levels of 4 g/L. Setpoints of dissolved oxygen and temperature were always fixed at 60% and 36.5°C, respectively. The pH setpoint of 6.95 in the first 48 h and 6.80 in the remaining process time was controlled using CO_2 as acid and 1 M Na_2CO_3 as base. The deadband range of the pH controller was 0.05. Increased addition of CO_2 was mainly necessary in the early stages of the cultivation due to the initial medium pH of 7.2 and because cell densities were still low. During the course of cultivation, lactate formation increased and amino acid consumption reduced which was reflected by changing pH control shifting to a minimum of 3% CO_2 overlay and Na_2CO_3 addition. In addition to the reference process (REF) two different settings were performed in which the influence of the two titrating agents should be investigated in regard to pH and pCO_2. The lower threshold for CO_2 gassing was set to 3% of the inlet gassing for all processes, while the upper boundary was set to 15% for the process testing the influence of CO_2 (COP) and 10% for the other processes. Additionally, for COP the proportional factor of the controller was increased and reset time decreased to ensure a higher pCO_2. For the third process type the use of base was eliminated completely resulting in a slow pH

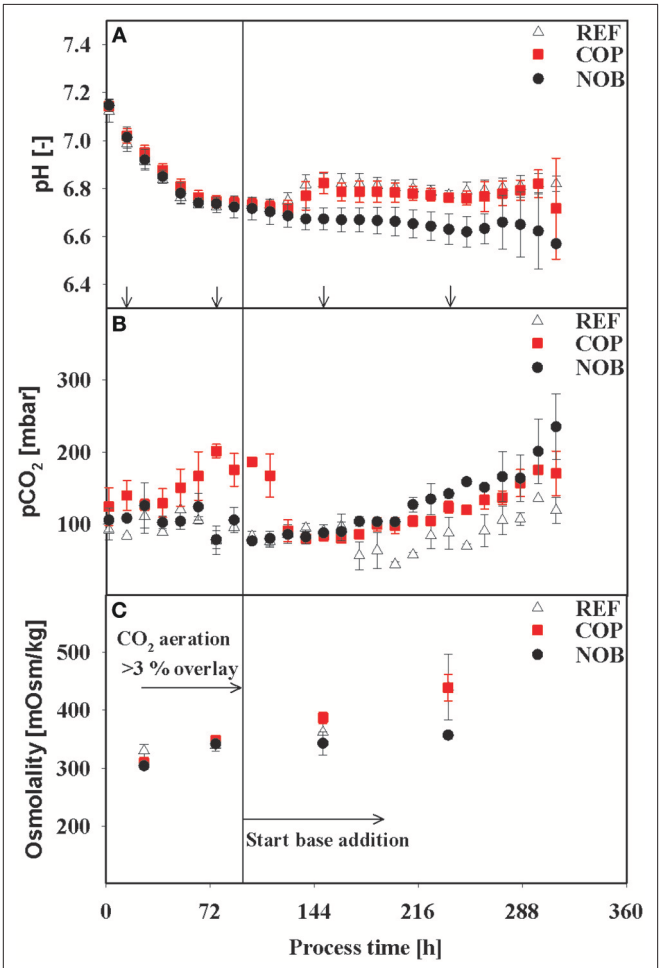

FIGURE 1 | Courses of the process parameters pH **(A)**, pCO_2 **(B)**, and Osmolality **(C)** for the three process settings. Osmolality was measured for each time point of intracellular sampling and flux balance analysis (no FBA performed for first time point). Arrows in **(A)** indicate the time points for intracellular samples, last three points also indicate time points of flux balance analysis. The vertical line in **(C)** marks the switch from CO_2 aeration higher than the 3% overlay to base addition in the reference process. Errors were derived out of bioreactor cultivations in triplicates.

Abbreviations: REF, reference process; COP, CO_2 stressed process; NOB, no base titration process.

shift downwards (NOB). Each of the three setting was performed in triplicates.

Sampling and Sample Preparation

Sampling for cell density and extracellular measurements was done twice a day whilst intracellular metabolomics samples were taken four times in total in different cultivation phases. For extracellular sampling the sample port was flushed with 4 mL of cell suspension before taking 4 mL sample volume. To prevent CO_2 gassing out 100 µL were separated twice and each diluted immediately 1:20 in 1,900 µL 0.01 M KOH. They were frozen at −20°C and used for the quantification of total inorganic carbon using Multi N/C 2100s (Analytik Jena, Germany) as described in Buchholz et al. (2014) after thawing. Additional 100 µL of the original sample were used to determine the cell density with a Cedex XS cell counter (Roche, Germany). The remaining sample volume was centrifuged at 800 g and 4°C for 5 min. Sixty microliter of the supernatant were used to determine triplicates of glucose and lactate concentrations using a Labotrace automatic analyzer (TraceAnalytics, Germany). The remaining supernatant was frozen at −70°C and used for antibody titer and amino acid measurements after thawing. The determination of intracellular metabolite concentrations followed the fast filtration protocol of Matuszczyk et al. (2015) with slight changes. Each experimental setting was replicated three times (bioreactor cultivations in triplicates) and each sample analyzed in triplicates. Samples were taken after 33 h (early growth phase, phase 1), 82 h (middle growth phase, phase 2), 154 h (early stationary phase, phase 3), and 238 h (early decline phase, phase 4) of process time. Before intracellular sampling cell densities were determined to ensure sampling of 30×10^6 cells. The fast filtration protocol of Matuszczyk et al. (2015) was performed by using glass fiber filter A/D with a pore size of 3 µm (Pall, USA) applying 30 mbar vacuum. Then the cells were quenched with ice cold washing buffer adjusted to the pH and osmolality at each process time which was determined in previous experiments. The filters were shifted into sample cups and then frozen in liquid nitrogen and stored at −70°C. Metabolite extraction followed the procedure of Pfizenmaier et al. (2015) applying chloroform and methanol. The feed rates were reduced to compensate the volume drain for sampling.

Extracellular Analytics

Osmolality was analyzed via freezing point depression with an Osmomat 030 (Gonotec, Germany). Antibody titers were determined by enzyme-linked immunosorbent assay (ELISA) as described by Pfizenmaier et al. (2015). Reversed phase HPLC for the detection of amino acids used Agilent 1200 (Agilent, USA)

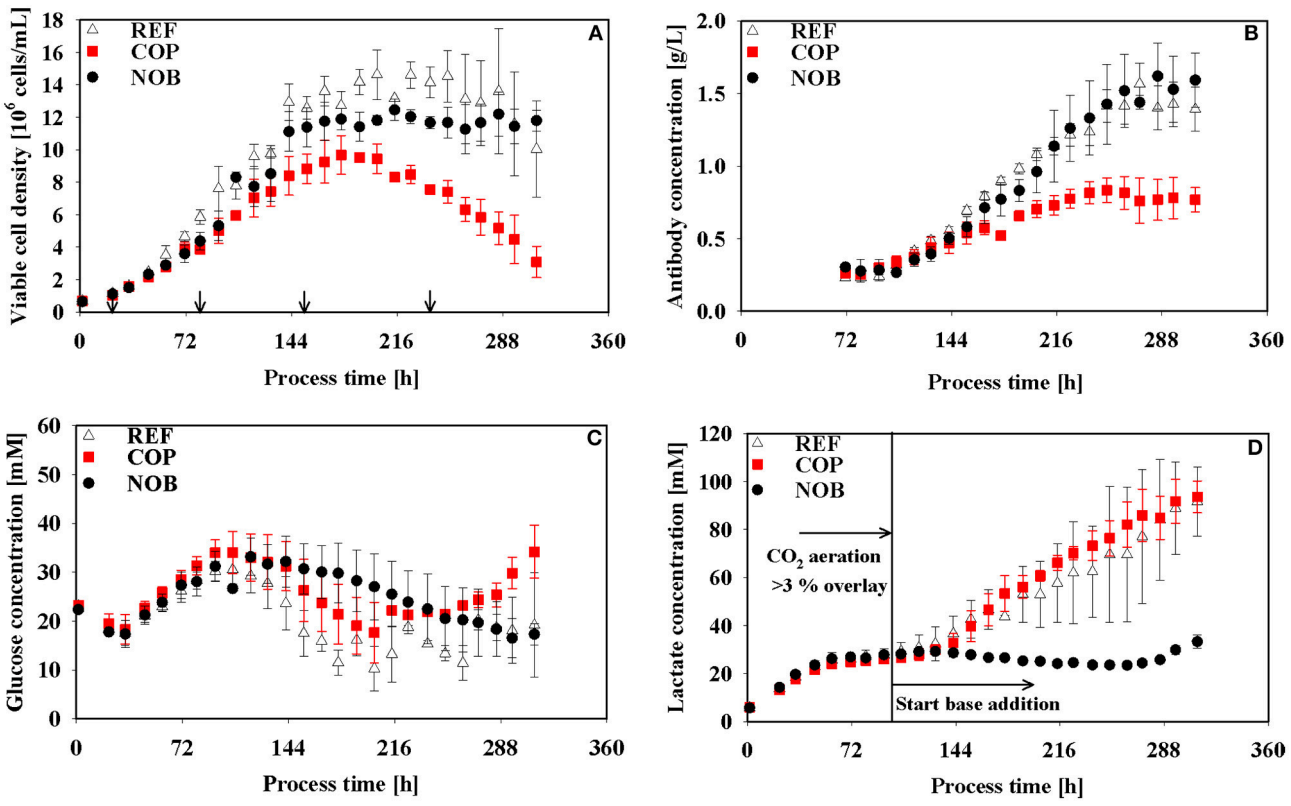

FIGURE 2 | Viable cell density **(A)**, antibody titer **(B)**, glucose **(C)**, and lactate **(D)** concentrations over process time for the three different process settings. Arrows in **(A)** indicate the time points for intracellular samples, last three points also indicate time points of flux balance analysis. The vertical line in **(D)** marks the switch from CO_2 aeration higher than the 3% overlay to base addition in the reference process. Error bars indicate the error of bioreactor cultivations in triplicates.

according to Buchholz et al. (2013). L-Ornithine was used as an internal standard.

Intracellular Analytics

Concentrations of intracellular adenosine phosphates (AXP) were determined following the HPLC protocol of Pfizenmaier et al. (2016). Intermediates of glycolysis and tricarboxylic acid (TCA) cycle were quantified using Agilent 1200 HPLC combined with Agilent 6410B triple quadrupole mass spectrometer (Agilent, USA). The liquid chromatography isotope dilution mass spectrometry (LC-IDMS) method (Teleki et al., 2015) using 13C labeled algae (Vielhauer et al., 2011) as internal standard was used to quantify intracellular pools of the non-labeled metabolites. Intracellular alpha-keto acids concentrations

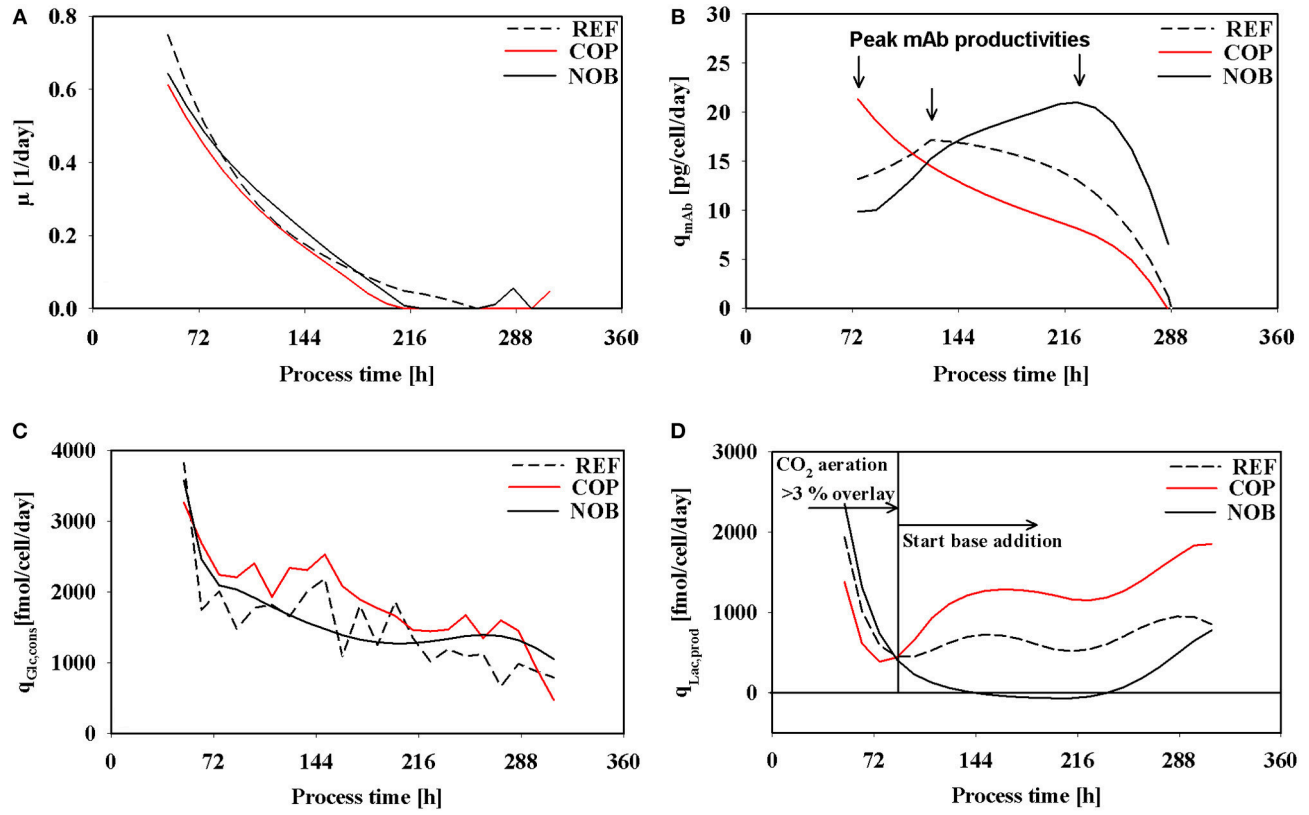

FIGURE 3 | Specific rates of growth **(A)**, antibody production **(B)**, glucose consumption **(C),** and lactate production **(D)** over process time for the three different process settings. The vertical line in **(D)** marks the switch from CO_2 aeration higher than the 3% overlay to base addition in the reference process as described in **Figure 1**. Negative values in **(D)** indicate a switch from lactate production to lactate consumption.

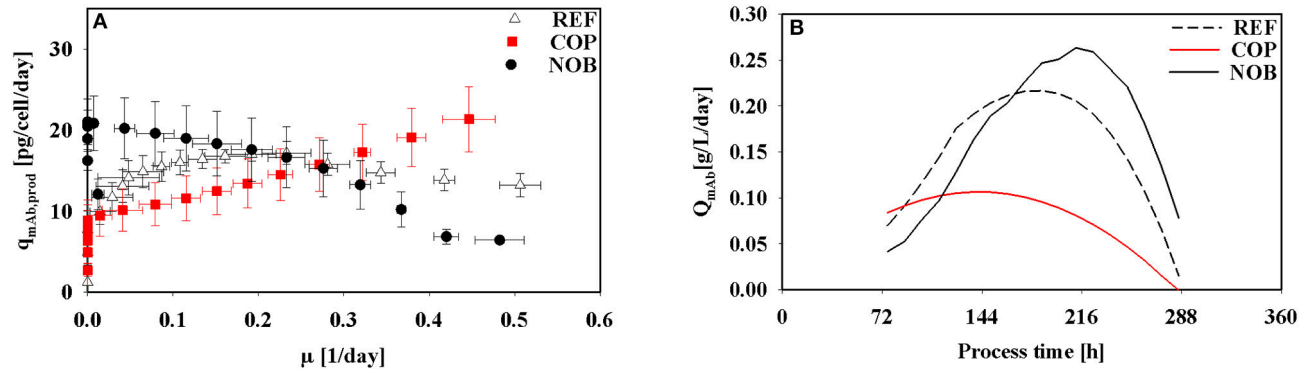

FIGURE 4 | Kinetics of antibody production in dependence of growth rate **(A)** and volumetric productivity of the antibody over process time **(B)** for the three different process settings.

were quantified with an adapted method (Zimmermann et al., 2014) with derivatization steps due to the high reactivity of the compounds.

Calculation of Specific Rates

For the calculation of the extracellular cell-specific rates the measured concentrations of metabolites as well as the cell densities were interpolated with steadily derivable functions using the Shape Language Modeling (SLM) tool in MATLAB Version 2013a (The Mathworks, USA). To avoid overfitting not more than four splines were used and only positive values were allowed similar to Wahrheit et al. (2014). Glucose concentrations were not fitted for the processes with necessary bolus additions since they showed intrinsic step functions.

Flux Balance Analysis

Flux Balance Analysis made use of the models of Sou et al. (2015) and Carinhas et al. (2013) using the biomass composition of Selvarasu et al. (2012). For the use within the Cobra Toolbox in MATLAB the inclusion of exchange reactions for all metabolites between the two compartments cytosol and extracellular region was done. This was necessary to account for the systems biology markup language (SBML) model structure, which is required by the toolbox. To consider not only directly ATP producing pathways, reactions for oxidative phosphorylation were added. A P/O ratio of 2.5 for NADH and 1.5 for $FADH_2$ was assumed, so that ATP production could be calculated out of the total produced NADH and $FADH_2$. The number of intracellular reactions was 99. The additional number of exchange reactions was 114. The total number of metabolites in both compartments was 240. The objective function was chosen to be the maximization of ATP yielding reactions. Input parameters were the measured extracellular cell-specific rates for growth, antibody production, glucose, lactate, and amino acids. Constraints for the optimization were selected according to the error of these rates for the bioreactor cultivations in triplicates of each setting. Therefore, the upper and lower bounds were set as plus-minus the error of the rates at the time point of analysis. Flux Balance Analysis was done at the same time points as the intracellular sampling but neglecting the first time point at 33 h in the early growth phase since calculated rates were too erroneous due to low cell densities. The resulting flux error was calculated with a Monte Carlo sampling method (Thiele et al., 2005) included in the Cobra Toolbox. The solution space was sampled with 2.5×10^6 randomly distributed points using 2,500 starting points for each analyzed time point.

RESULTS

Influence of Process Parameters on Cell Density, Substrate, and Product Profiles

Bioreactor cultivations in triplicates of the setups REF (reference process), COP (increased CO_2 impact), and NOB (no base titration) were performed as described above. **Figure 1** gives an overview of the key parameters of the different process phases.

As expected, all cultivations were controlled at pH 6.8 after initial adaptation and diverged only after approximately 120 h when base addition was suppressed in setup NOB. The latter showed minimum pH of 6.60 whereas REF and COP remained stable within the controller's deadband of 0.05 of the respective process phase. The partial pressure of CO_2 was elevated up to 200 mbar during the growth phase (83 h) of COP whilst values of REF and NOB ranged from 75 to 120 mbar. Until 120 h pCO_2 values of all processes conformed to about 90 mbar, showed similar tendency for 48 h and diverged again >158 h with COP and NOB showing maximum pCO_2 values at the very end of 170 and 220 mbar, respectively. Osmolality showed minor differences throughout the process, only in stationary phase the process without base addition (NOB) revealed significantly lower osmolalities of 357 mOsm/kg compared to the average values of REF and COP (440 mOsm/kg). REF and NOB showed similar courses of viable cell densities as depicted in **Figure 2A**. Maximum cell density was slightly higher for the reference process with 15×10^6 cells/mL compared to 13×10^6 cells/mL. In contrast, maximum cell density in COP reached only about 9×10^6 cells/mL and cell densities fell earlier than for the other two processes. Highest final titer of 1.6 g/L was achieved in NOB which was slightly higher than in REF with 1.4 g/L and doubled the value of COP (**Figure 2B**). Frequent glucose addition was necessary for REF and COP reflecting sugar needs that exceeded the feed supply (**Figure 2C**). Strikingly, lactate concentrations (**Figure 2D**) steadily increased in REF and COP but remained stable on the low level of around 25 mmol/L > 72 h in NOB.

Growth and Product Formation Kinetics

Cell specific rates of growth, antibody production, glucose consumption, and lactate production are depicted in **Figure 3**. All growth rates (**Figure 3A**) indicate the same declining trend irrespective of the setting although maximum cell densities of COP were the lowest (**Figure 2A**). In REF growth continued until 264 h whereas in COP and NOB growth stopped after 216 h. The altered process settings resulted in different kinetics of productivity of the monoclonal antibody as can be seen in **Figure 3B**. REF and NOB depicted similarly increasing productivities until 120 h when productivity peaked at 18 pg/cell/day in REF. Notably, cell specific productivities declined in REF whereas in NOB they rose steadily to the maximum of 20 pg/cell/day (240 h). On contrast, q_{mAb} values in COP steadily declined from the initial value of 23 pg/cell/day when pCO_2 was still elevated (**Figure 1**). Time courses of glucose uptake rates (**Figure 3C**) showed similar declining trends in all settings. However, COP revealed highest demands. A striking observation is shown in **Figure 3D**: Specific lactate production rates showed high similarities during the first 72 h but differed significantly after base addition. Whereas, lactate formation almost persisted in REF, COP showed strong rise and NOB even intermediary stop. As a result the lactate production rate was about 70% higher in COP compared to REF. In NOB, cells even switched from lactate production to consumption between 144 and 240 h (compare **Supplementary Figures S1–S3** for carbon balances).

Interestingly, kinetics of cell specific antibody formation q_{mAb} as a function of μ (**Figure 4A**) revealed properties depending on the process setting. In REF highest productivities were observed in the operational window of moderate growth (0.2 1/d). On contrast, COP showed highest productivities linked to highest

growth rates (0.4 1/d). Highest productivities in NOB were achieved at low growth rates approaching the stationary phase when maximum cell densities were present.

The volumetric productivity for all process types is depicted in **Figure 4B**. REF and NOB showed a rising trend toward the stationary phase due to increasing cell densities (**Figure 2A**). But since for REF the specific productivity (**Figure 3B**) started decreasing after 120 h its volumetric productivity peaked at 0.2 g/L/day after 192 h and therefore 36 h earlier than in NOB with a maximum value of 0.25 g/L/day. COP reached its peak value of 0.1 g/L/day after 144 h because of the lowest cell densities along with decreasing cell specific productivities from 72 h on.

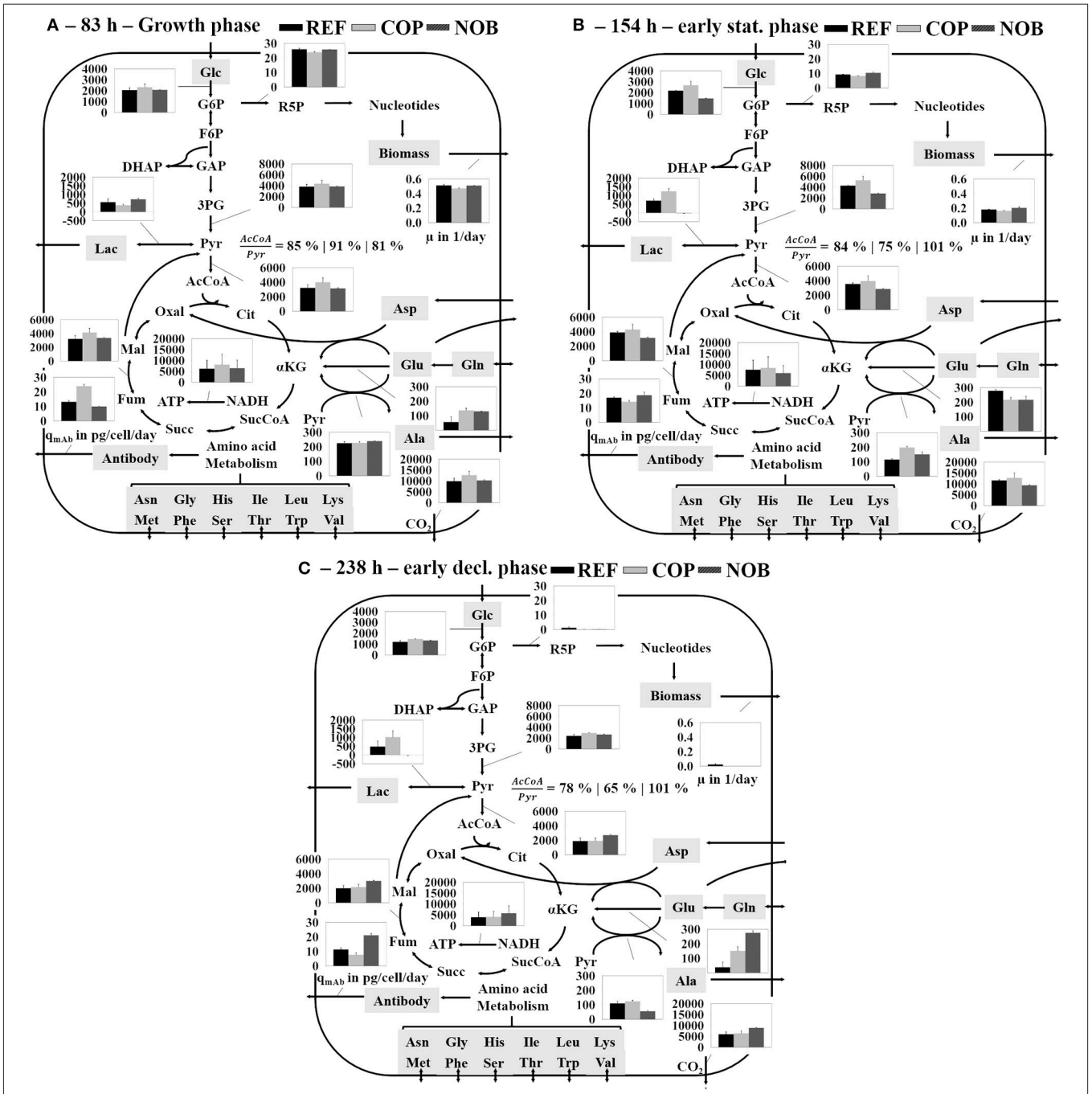

FIGURE 5 | Simplified overview of the results of the flux balance analysis depicting the main carbon metabolism during growth phase **(A)**, early stationary phase **(B),** and early decline phase **(C)** for all three process settings. The three bars of each flux belong to the according process shown in the top right. Fluxes are given in fmol/cell/day unless otherwise stated. Errors were determined through Monte Carlo sampling of the solution space of each the bioreactor cultivations in triplicates.

Flux Balance Analysis and Intracellular Metabolite Levels

Flux balance analysis was performed for all settings for growth phase (83 h, phase 2), early stationary phase (154 h, phase 3) and early decline phase (238 h, phase 4; see **Figure 5**). In accordance to the extracellular rates shown in **Figure 3** the glycolytic flux patterns of phase 2 (**Figure 5A**) were comparable for all three settings with only marginally increased fluxes in COP. Accordingly, the flux into TCA was slightly higher in COP as well as the drain into TCA from the pyruvate knot. The remaining pyruvate was converted to lactate (around 500 fmol/cell/day) and alanine (200 fmol/cell/day) for all three processes. At the beginning of the stationary phase (**Figure 5B**) fluxes through glycolysis and TCA remained constant in REF. The 20% increased conversion rate from 3PG to pyruvate in COP was solely used for the production of lactate. Accordingly, lactate dehydrogenase flux doubled to 1,200 fmol/cell/day, but flux into TCA persisted. In NOB, the glycolytic flux decreased by a third and lactate production stopped which resulted in constant TCA flux activity compared to the growth phase. Energy production via oxidative phosphorylation remained at the same level for all three processes. During phase 4 (**Figure 5C**) the flux through glycolysis was cut in half in REF and in COP whilst fluxes remained constant in NOB. Activity of pentose phosphate pathway apparently broke down in all processes. Interestingly, only NOB could preserve TCA fluxes even in phase 4. REF and COP revealed declines. In essence, this was the result of no lactate formation and reduced alanine formation from pyruvate.

Figure 6 depicts that highest cell specific ATP production rates were found in phase 2 of COP. q_{ATP} increased by 10% in REF and in COP in the stationary phase (phase 3) whereas it decreased by 10% for NOB (**Figure 6B**). The ATP production yield $Y_{ATP,C}$ was estimated as ATP generated per c-mol substrate consumed. The criterion turned out to be similar for all three processes with values ranging from 1.88 to 1.96 molATP/c-mol. Both, REF and COP showed halving of ATP formation in phase 4 (**Figure 6C**) when NOB could maintain the previous level of ∼25,000 fmol/cell/day. The development was accompanied by severely increasing $Y_{ATP,C}$ to 2.28 molATP/c-mol. Throughout the cultivation the ratio between the sources of ATP generation remained similar. The oxidative phosphorylation of total NADH and $FADH_2$ contributed about 65% to the energy produced. ATP out of

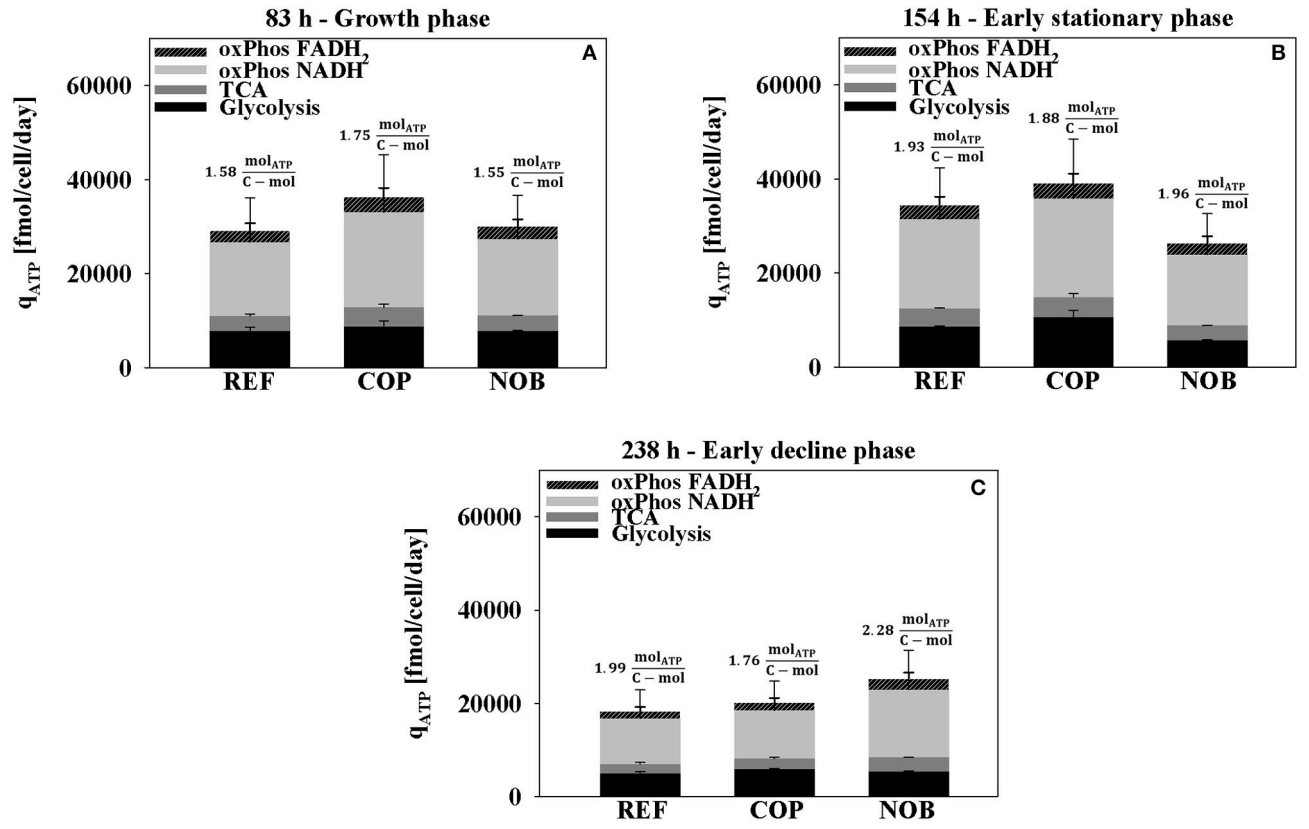

FIGURE 6 | ATP production rate during growth phase **(A)**, early stationary phase **(B),** and early decline phase **(C)** for the three process settings divided into the origin of ATP formation. Values for oxidative phosphorylation include NADH or $FADH_2$ produced in both glycolysis and TCA. ATP directly from TCA originates from succinyl-CoA synthetase. Results were obtained from the flux balance analysis. Errors were determined through Monte Carlo sampling of the solution space of each the bioreactor cultivations in triplicates.

succinyl-CoA synthetase in the TCA accounted for 10% and ATP out of glycolysis for 25%.

Results of intracellular measurements of nucleotides as well as the resulting adenylate energy charge (AEC) are depicted in **Figure 7**. Major differences between the settings could be found in phase 4 when AEC was highest for NOB with a value of 0.90 whilst the other processes revealed an ever declining trend resulting in AECs of 0.76 and 0.80.

Intracellular metabolite concentrations of Glycolysis and TCA did not show large deviations in between the three process types (data not shown). Only intracellular pyruvate concentrations in **Figure 8** showed a steady decline for NOB whereas the other two processes reached maximum pool concentrations of 2.20 fmol/cell in phase 3 and even showed doubled pool sizes at the end of the processes compared to NOB.

DISCUSSION

Impact of pH and Elevated CO_2 Levels on Growth and By-Product Formation

As depicted in **Figure 1**, pH, pCO_2, and osmolality courses differed between the three settings. NOB revealed low pH reflecting eliminated base addition after entering the stationary phase. COP had elevated pCO_2 levels during growth phase. Interestingly, only NOB disclosed stop of lactate production after base feeding had been prevented. The link between low pH and initiation of lactate consumption was already reported by Ivarsson et al. (2015), Liste-Calleja et al. (2015), and Zalai et al. (2015). Typically step-wise pH down shifts were investigated. Furthermore, high pH settings were found to increase q_{Lac} (Yoon et al., 2005).

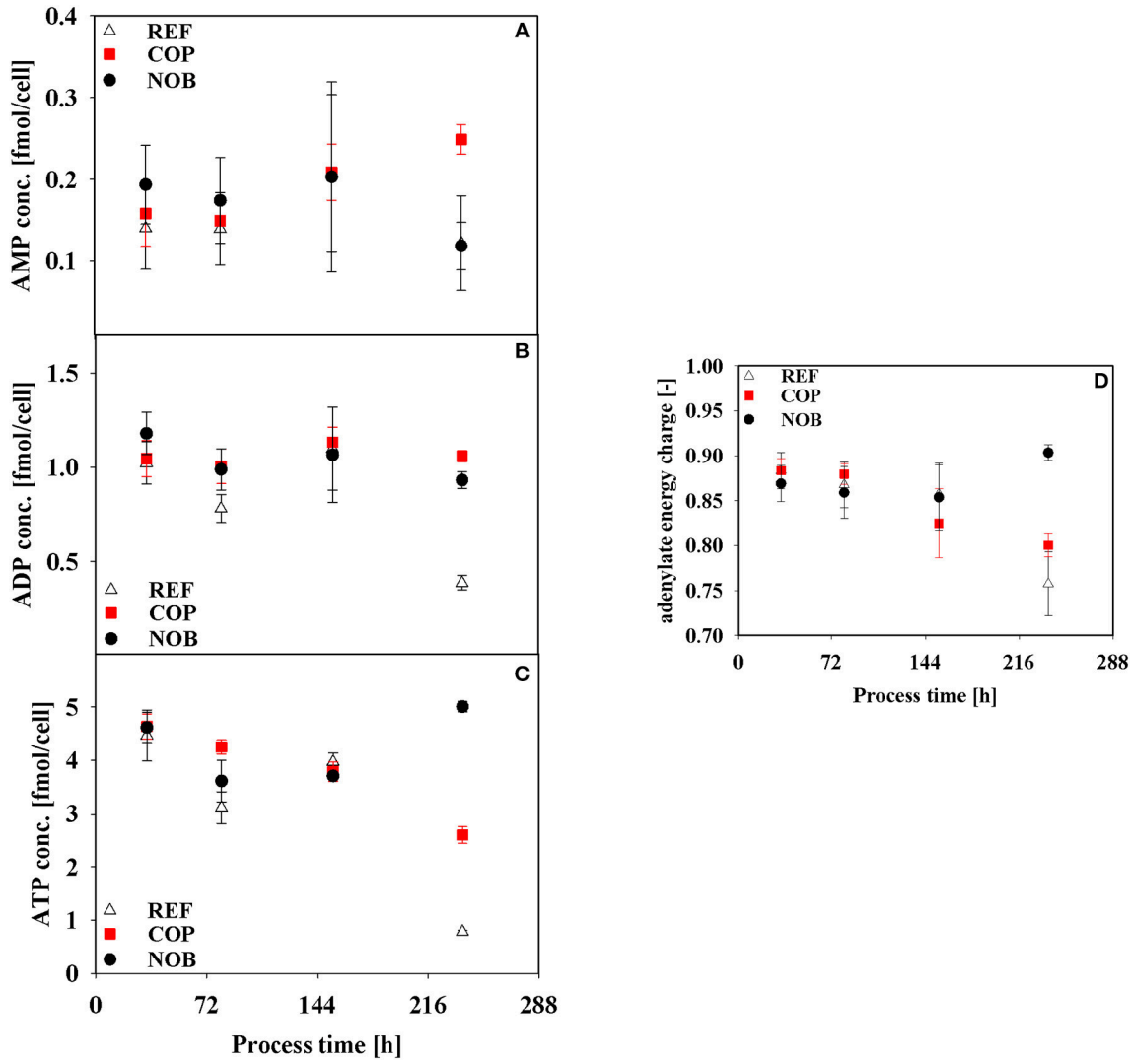

FIGURE 7 | Intracellular concentrations of AMP **(A)**, ADP **(B)**, ATP **(C)**, and adenylate energy charge **(D)** during the three different processes. Error bars indicate the error of measurement of samples in triplicates.

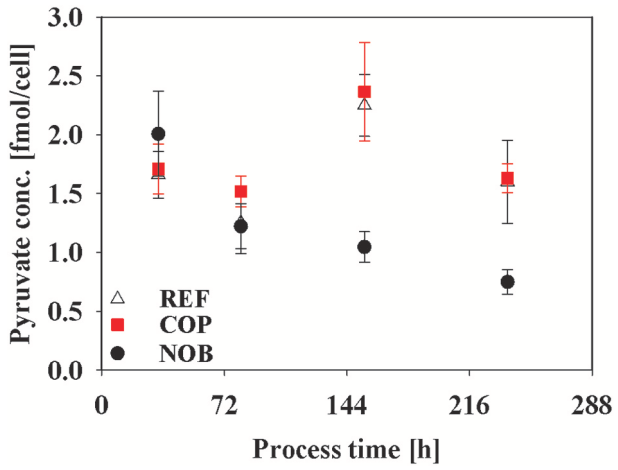

FIGURE 8 | Intracellular concentration of pyruvate during the three different processes. Error bars indicate the error of measurement of samples in triplicates.

Lao and Toth (1997) published cell line specific threshold values of 60 mM lactate indicating the start of detrimental effects on growth rates. This level was reached in the early stationary phase of REF and COP (**Figure 2D**) consequently leading to the decrease of viable cell density earlier in REF and COP than in NOB. Moreover, increased lactate production caused equal rise of base addition reflected by elevated osmolalities in REF and COP compared to NOB (**Figures 1**, **2D**). High osmolalities were known to cause reduction of growth and viable cell densities (Lin et al., 1999) and an increase in lactate formation (Xu et al., 2018). Furthermore, Pfizenmaier et al. (2015) outlined that cells were increasingly arrested in G1 phase under hyperosmotic conditions finally improving cell specific productivities of recombinant mAb production. However, considering osmolalities >400 mOsm/kg as hyperosmotic (Pfizenmaier et al., 2015) such stress conditions were only reached in the decline phase >238 h (**Figure 1**) which rules out any further impact before.

The Interaction of pH and Elevated CO_2 Levels With mAb Production

The impact of elevated pCO_2 pressures on cell specific productivities is not fully elucidated yet. Partial CO_2 pressures of 290 mbar were found to deteriorate average specific productivities (Gray et al., 1996; Kimura and Miller, 1996; Zanghi et al., 1999; Mostafa and Gu, 2003; Goudar et al., 2007) and to rise lactate production (Darja et al., 2016; Brunner et al., 2017, 2018). On contrast, some studies did not find any significant effect on cell specific productivities but only on growth (DeZengotita et al., 2002; Takuma et al., 2003). All studies have in common that high pCO_2 values were installed throughout the complete process thereby preventing time-resolved analysis of interactions between pCO_2 levels, process dynamics and cell specific productivities. By trend, elevated pCO_2 values were found to reduce q_{mAb}. However, particularities of individual cell lines and product formation kinetics need to be analyzed for each individual case.

Exploiting the experimental settings for REF, COP, and NOB, the impact of different pCO_2 and pH levels on q_{mAb} courses can be deciphered for the process periods revealing two outstanding observations:

- *Cell specific productivities were high despite high pCO_2 values*: COP showed maximum q_{mAb} in early stages when CO_2 stress was present (**Figure 3B**) and growth rates were similar in all experimental settings. The observation is in agreement with proteomic studies of Darja et al. (2016) linking elevated pCO_2 with the amplification of the stress protein GRP78 which in turn was correlated with increased productivities in CHO protein producers by Pieper et al. (2017) and Nishimiya et al. (2013).
- *NOB production kinetics are uncoupled from growth:* In COP, q_{mAb} kinetics were tightly coupled to cellular growth (**Figure 4A**). REF showed similar trends, however without the initial benefits of (i). In both settings cell specific productivities and growth rates steadily decreased after about 120 h until the end. Strikingly, NOB kinetics were significantly different. Although growth rates reduced parallel to REF and COP, cell specific productivities did not. On contrast, q_{mAb} kept raising until 216 h increasing values by almost 20% (**Figure 2D**). The dynamics coincided with slightly falling pH in NOB. The observation is in accordance with other studies outlining either beneficial (Ivarsson et al., 2015; Brunner et al., 2018) or no significant (Yoon et al., 2005; Trummer et al., 2006; Zalai et al., 2015) impact of pH downshifts on cell specific productivity. The finding also conforms to studies of Pfizenmaier et al. (2016) outlining that cell specific productivities can be increased under non-growing conditions, presumably because of elevated supply of ATP. In NOB, the effects led to maximum specific productivities of 20 pmol/cell/day which were slightly higher than in REF. However, most desirable is a high productivity coinciding with high viable cell densities to reach the highest volumetric output. This could be achieved for NOB due to specific productivity being maintained at a high level (**Figure 4B**). COP on the contrary peaked in specific productivity during growth phase where cell densities were still low and therefore the titer was severely decreased. Interesting enough, maximum cell specific productivities in REF, COP, and NOB coincided with minimum lactate formation. Therefore, intracellular flux distributions should be used to decipher the metabolic adjustments made due to changing process conditions.

Metabolic and Energetic Adjustments Due to Shifted pH and Elevated pCO_2

Only recently more studies investigated the influence of process parameters on a more detailed level via metabolic flux analysis for pCO_2 effects (Brunner et al., 2018) and flux balance analysis for pH effects (Ivarsson et al., 2015). However, the connection between changes of production kinetics and energetic state over distinct process phases has not been unraveled yet.

The levels of glucose uptake and lactate production could only be correlated for the early stationary phase comparing the three process types and not throughout the process as described before (Zalai et al., 2015; Konakovsky et al., 2016; Brunner et al., 2018). Nevertheless, COP showed the highest glycolytic fluxes throughout the process (**Figure 5**). Lower fluxes in NOB were compensated through slight lactate uptake so that TCA fluxes were similar to these of the other processes. This effect was shown by Ivarsson et al. (2015) during a batch process with pH 6.8 compared to a reference process with a pH of 7.2. Possible factors inducing lactate uptake were hypothesized to be pH dependent glycolytic enzymes or a cellular measure to increase extracellular pH again (Ozturk et al., 1992). Higher levels of intracellular pyruvate promoted overflow metabolism for REF and COP in terms of increased lactate production (**Figure 8**). Lower pH in NOB coincided with decreased pyruvate levels and simultaneous lactate uptake >144 h. Luo et al. (2012) showed similar results for relative intensities of intracellular pyruvate when comparing different cell lines.

The analysis of intracellular fluxes revealed furthermore that a high efficiency at the pyruvate branch toward TCA and therefore low lactate production were coinciding with high specific productivities (Luo et al., 2012; Templeton et al., 2013). The CO_2 stressed environment in the early stages of COP revealed a remarkable energy producing state with low lactate production. The elevated ATP production was ongoing until early stationary phase at 154 h although pCO_2 went back to reference values around 24 h before. However, intracellular ATP concentrations and productivity had already begun diminishing while lactate formation was increasing. Therefore stress conditions of elevated pCO_2 might lead to a higher ATP usage due to the decrease in intracellular pH and therefore higher maintenance demands (Ozturk et al., 1992). DeZengotita et al. (2002) showed that increased partial pressures of CO_2 led to a reduction in pH_i of around 0.2 since CO_2 as a non-polar molecule can easily diffuse through the cellular membrane. To keep intracellular pH from falling further, ATP consuming transporters are known which continuously extrude protons out of the cell (Roos and Boron, 1981; Casey et al., 2010). The more CO_2 enters the cells, the less ATP can be used for energy demanding protein synthesis which would explain the rapidly falling specific productivities.

On the contrary the amount of ATP produced per cell stayed on a constant lower level for NOB. A smaller q_{ATP} was shown in a batch with lowered pH of 6.8 along with higher average specific productivities compared to a reference with pH 7.2 (Ivarsson et al., 2015) and for cells after the switch to lactate consumption in a batch with depleted glucose (Martínez et al., 2013). Contrary to the other two processes NOB could maintain a high intracellular AEC and stable intracellular ATP concentrations along with constant q_{ATP} and increasing q_{mAb}, even toward the decline phase. Pfizenmaier et al. (2015) also showed an increased productivity along with higher intracellular ATP concentrations under non-growing conditions for cells under osmotic stress. The same could be observed for NOB with a shift toward non-growth coupled product formation. The shift downwards in pH might be not as severe as the applied CO_2 stress in COP. Hence the cells can apply countermeasures toward a physiological pH_i (Wu et al., 1993; Brunner et al., 2017) without having to spend as much ATP.

Our results indicate that there is a strong connection between the process parameters CO_2 and pH on the one side and the production kinetics and the cellular energetic efficiency on the other side. The NOB approach ensures steady production conditions which may be of particular importance when the process should be scaled up in industrial settings. CO_2 and pH can be crucial parameters creating non-wanted population inhomogeneities. Following the NOB setting the problem should be reduced which in turn should increase the chances of successful scale-up.

A short CO_2 stimulus—for example due to an unoptimized controller or poor mixing (Xu et al., 2018)—in the early stages of a process can have long-term detrimental effects even when pCO_2 is back to reference values. Although specific productivity was shortly increased under stress conditions during early growth phase, the altered kinetics of productivity and lactate production combined with decreasing ATP levels revealed a fatal development for the process. A slow pH shift downwards on the other side turned out to be advantageous for the ongoing process. Substrate uptake was kept low and lactate was partly consumed. A shift toward non-growth coupled production was observed until highest cell densities were reached. Constantly high adenylate energy charges throughout the process together with persistent ATP production rates proved to be beneficial for maintaining high productivities.

AUTHOR CONTRIBUTIONS

MB performed the cultivations, extracellular analytics and modeling, designed the study, and prepared the manuscript. MB, LJ, and AT performed the intracellular metabolomics. JB performed critical revision of the data. RT designed the study and prepared the manuscript.

ACKNOWLEDGMENTS

The authors gratefully acknowledge the funding by the Ministerium für Wissenschaft, Forschung und Kunst Baden-Württemberg (MWK, Grant 32-7546.31/1/4).

SUPPLEMENTARY MATERIAL

The Supplementary Material for this article can be found online at: https://www.frontiersin.org/articles/10.3389/fbioe.2019.00076/full#supplementary-material

REFERENCES

Birch, J. R., and Racher, A. J. (2006). Antibody production. *Adv. Drug Deliv. Rev.* 58, 671–685. doi: 10.1016/j.addr.2005.12.006

Brunner, M., Doppler, P., Klein, T., Herwig, C., and Fricke, J. (2018). Elevated pCO_2 affects the lactate metabolic shift in CHO cell culture processes. *Eng. Life Sci.* 18, 204–214. doi: 10.1002/elsc.201700131

Brunner, M., Fricke, J., Kroll, P., and Herwig, C. (2017). Investigation of the interactions of critical scale-up parameters (pH, pO_2 and pCO_2) on CHO batch performance and critical quality attributes. *Bioprocess Biosyst. Eng.* 40, 251–263. doi: 10.1007/s00449-016-1693-7

Buchholz, J., Graf, M., Blombach, B., and Takors, R. (2014). Improving the carbon balance of fermentations by total carbon analyses. *Biochem. Eng. J.* 90, 162–169. doi: 10.1016/j.bej.2014.06.007

Buchholz, J., Schwentner, A., Brunnenkan, B., Gabris, C., Grimm, S., Gerstmeir, R., et al. (2013). Platform engineering of *Corynebacterium glutamicum* with reduced pyruvate dehydrogenase complex activity for improved production of L-lysine, L-valine, and 2-ketoisovalerate. *Appl. Environ. Microbiol.* 79, 5566–5575. doi: 10.1128/AEM.01741-13

Carinhas, N., Duarte, T. M., Barreiro, L. C., Carrondo, M. J., Alves, P. M., and Teixeira, A. P. (2013). Metabolic signatures of GS-CHO cell clones associated with butyrate treatment and culture phase transition. *Biotechnol. Bioeng.* 110, 3244–3257. doi: 10.1002/bit.24983

Casey, J. R., Grinstein, S., and Orlowski, J. (2010). Sensors and regulators of intracellular pH. *Nat. Rev. Mol. Cell Biol.* 11, 50–61. doi: 10.1038/nrm2820

Darja, O., Stanislav, M., Saša, S., Andrej, F., Lea, B., and Branka, J. (2016). Responses of CHO cell lines to increased pCO_2 at normal (37 C) and reduced (33 C) culture temperatures. *J. Biotechnol.* 219, 98–109. doi: 10.1016/j.jbiotec.2015.12.013

DeZengotita, V. M., Schmelzer, A. E., and Miller, W. M. (2002). Characterization of hybridoma cell responses to elevated pCO_2 and osmolality: intracellular pH, cell size, apoptosis, and metabolism. *Biotechnol. Bioeng.* 77, 369–380. doi: 10.1002/bit.10176

Dickson, A. J. (2014). Enhancement of production of protein biopharmaceuticals by mammalian cell cultures: the metabolomics perspective. *Curr. Opin. Biotechnol.* 30, 73–79. doi: 10.1016/j.copbio.2014.06.004

Ecker, D. M., Jones, S. D., and Levine, H. L. (2015). The therapeutic monoclonal antibody market. *MAbs* 7, 9–14. doi: 10.4161/19420862.2015.989042

Gaughan, C. L. (2016). The present state of the art in expression, production and characterization of monoclonal antibodies. *Mol. Divers.* 20, 255–270. doi: 10.1007/s11030-015-9625-z

Goudar, C. T., Matanguihan, R., Long, E., Cruz, C., Zhang, C., Piret, J. M., et al. (2007). Decreased pCO_2 accumulation by eliminating bicarbonate addition to high cell-density cultures. *Biotechnol. Bioeng.* 96, 1107–1117. doi: 10.1002/bit.21116

Gray, D. R., Chen, S., Howarth, W., Inlow, D., and Maiorella, B. L. (1996). CO_2 in large-scale and high-density CHO cell perfusion culture. *Cytotechnology* 22, 65–78. doi: 10.1007/BF00353925

Hammerschmidt, N., Tscheliessnig, A., Sommer, R., Helk, B., and Jungbauer, A. (2014). Economics of recombinant antibody production processes at various scales: industry-standard compared to continuous precipitation. *Biotechnol. J.* 9, 766–775. doi: 10.1002/biot.201300480

Huang, Z., Lee, D. Y., and Yoon, S. (2017). Quantitative intracellular flux modeling and applications in biotherapeutic development and production using CHO cell cultures. *Biotechnol. Bioeng.* 114, 2717–2728. doi: 10.1002/bit.26384

Ivarsson, M., Noh, H., Morbidelli, M., and Soos, M. (2015). Insights into pH-induced metabolic switch by flux balance analysis. *Biotechnol. Prog.* 31, 347–357. doi: 10.1002/btpr.2043

Kimura, R., and Miller, W. M. (1996). Effects of elevated pCO_2 and/or osmolality on the growth and recombinant tPA production of CHO cells. *Biotechnol. Bioeng.* 52, 152–160.

Konakovsky, V., Clemens, C., Müller, M. M., Bechmann, J., Berger, M., Schlatter, S., et al. (2016). Metabolic control in mammalian fed-batch cell cultures for reduced lactic acid accumulation and improved process robustness. *Bioengineering* 3:5. doi: 10.3390/bioengineering3010005

Kunert, R., and Reinhart, D. (2016). Advances in recombinant antibody manufacturing. *Appl. Microbiol. Biotechnol.* 100, 3451–3461. doi: 10.1007/s00253-016-7388-9

Langheinrich, C., and Nienow, A. W. (1999). Control of pH in large-scale, free suspension animal cell bioreactors: alkali addition and pH excursions. *Biotechnol. Bioeng.* 66, 171–179.

Lao, M. S., and Toth, D. (1997). Effects of ammonium and lactate on growth and metabolism of a recombinant Chinese hamster ovary cell culture. *Biotechnol. Prog.* 13, 688–691. doi: 10.1021/bp9602360

Leite, T. C., Coelho, R. G., Silva, D., Coelho, W. S., Marinho-Carvalho, M. M., and Sola-Penna, M. (2011). Lactate downregulates the glycolytic enzymes hexokinase and phosphofructokinase in diverse tissues from mice. *FEBS Lett.* 585, 92–98. doi: 10.1016/j.febslet.2010.11.009

Lin, J., Takagi, M., Qu, Y., Gao, P., and Yoshida, T. (1999). Metabolic flux change in hybridoma cells under high osmotic pressure. *J. Biosci. Bioeng.* 87, 255–257. doi: 10.1016/S1389-1723(99)89025-2

Liste-Calleja, L., Lecina, M., Lopez-Repullo, J., Albiol, J., Solà, C., and Cairó, J. J. (2015). Lactate and glucose concomitant consumption as a self-regulated pH detoxification mechanism in HEK293 cell cultures. *Appl. Microbiol. Biotechnol.* 99, 9951–9960. doi: 10.1007/s00253-015-6855-z

Löffelholz, C., Husemann, U., Greller, G., Meusel, W., Kauling, J., Ay, P., et al. (2013). Bioengineering parameters for single-use bioreactors: overview and evaluation of suitable methods. *Chem. Ing. Tech.* 85, 40–56. doi: 10.1002/cite.201200125

Luo, J., Vijayasankaran, N., Autsen, J., Santuray, R., Hudson, T., Amanullah, A., et al. (2012). Comparative metabolite analysis to understand lactate metabolism shift in Chinese hamster ovary cell culture process. *Biotechnol. Bioeng.* 109, 146–156. doi: 10.1002/bit.23291

Martínez, V. S., Dietmair, S., Quek, L. E., Hodson, M. P., Gray, P., and Nielsen, L. K. (2013). Flux balance analysis of CHO cells before and after a metabolic switch from lactate production to consumption. *Biotechnol. Bioeng.* 110, 660–666. doi: 10.1002/bit.24728

Matuszczyk, J. C., Teleki, A., Pfizenmaier, J., and Takors, R. (2015). Compartment-specific metabolomics for CHO reveals that ATP pools in mitochondria are much lower than in cytosol. *Biotechnol. J.* 10, 1639–1650. doi: 10.1002/biot.201500060

Morrison, C., and Lähteenmäki, R. (2017). Public biotech in 2016—the numbers. *Nat. Biotechnol.* 35, 623–629. doi: 10.1038/nbt.3917

Mostafa, S. S., and Gu, X. S. (2003). Strategies for improved dCO_2 removal in large-scale fed-batch cultures. *Biotechnol. Prog.* 19, 45–51. doi: 10.1021/bp0256263

Mullard, A. (2012). Can next-generation antibodies offset biosimilar competition? *Nat. Rev. Drug Discov.* 11, 426–428. doi: 10.1038/nrd3749

Mulukutla, B. C., Gramer, M., and Hu, W.-S. (2012). On metabolic shift to lactate consumption in fed-batch culture of mammalian cells. *Metab. Eng.* 14, 138–149. doi: 10.1016/j.ymben.2011.12.006

Nishimiya, D., Mano, T., Miyadai, K., Yoshida, H., and Takahashi, T. (2013). Overexpression of CHOP alone and in combination with chaperones is effective in improving antibody production in mammalian cells. *Appl. Microbiol. Biotechnol.* 97, 2531–2539. doi: 10.1007/s00253-012-4365-9

Osman, J. J., Birch, J., and Varley, J. (2001). The response of GS-NS0 myeloma cells to pH shifts and pH perturbations. *Biotechnol. Bioeng.* 75, 63–73. doi: 10.1002/bit.1165

Ozturk, S. S., Riley, M. R., and Palsson, B. O. (1992). Effects of ammonia and lactate on Hybridoma growth, metabolism, and antibody production. *Biotechnol. Bioeng.* 39, 418–431. doi: 10.1002/bit.260390408

Pfizenmaier, J., Junghans, L., Teleki, A., and Takors, R. (2016). Hyperosmotic stimulus study discloses benefits in ATP supply and reveals miRNA/mRNA targets to improve recombinant protein production of CHO cells. *Biotechnol. J.* 11, 1037–1047. doi: 10.1002/biot.201500606

Pfizenmaier, J., Matuszczyk, J. C., and Takors, R. (2015). Changes in intracellular ATP-content of CHO cells as response to hyperosmolality. *Biotechnol. Prog.* 31, 1212–1216. doi: 10.1002/btpr.2143

Pieper, L. A., Strotbek, M., Wenger, T., Olayioye, M. A., and Hausser, A. (2017). ATF6β-based fine-tuning of the unfolded protein response enhances therapeutic antibody productivity of Chinese hamster ovary cells. *Biotechnol. Bioeng.* 114, 1310–1318. doi: 10.1002/bit.26263

Roos, A., and Boron, W. F. (1981). Intracellular pH. *Physiol. Rev.* 61, 296–434. doi: 10.1152/physrev.1981.61.2.296

Russell, J. B. (2007). The energy spilling reactions of bacteria and other organisms. *J. Mol. Microbiol. Biotechnol.* 13, 1–11. doi: 10.1159/000103591

Selvarasu, S., Ho, Y. S., Chong, W. P., Wong, N. S., Yusufi, F. N., Lee, Y. Y., et al. (2012). Combined *in silico* modeling and metabolomics analysis to characterize fed-batch CHO cell culture. *Biotechnol. Bioeng.* 109, 1415–1429. doi: 10.1002/bit.24445

Shukla, A. A., and Thömmes, J. (2010). Recent advances in large-scale production of monoclonal antibodies and related proteins. *Trends Biotechnol.* 28, 253–261. doi: 10.1016/j.tibtech.2010.02.001

Sieblist, C., Hägeholz, O., Aehle, M., Jenzsch, M., Pohlscheidt, M., and Lübbert, A. (2011). Insights into large-scale cell-culture reactors: II. Gas-phase mixing and CO_2 stripping. *Biotechnol. J.* 6, 1547–1556. doi: 10.1002/biot.201100153

Sou, S. N., Sellick, C., Lee, K., Mason, A., Kyriakopoulos, S., Polizzi, K. M., et al. (2015). How does mild hypothermia affect monoclonal antibody glycosylation? *Biotechnol. Bioeng.* 112, 1165–1176. doi: 10.1002/bit.25524

Takuma, S., Hirashima, C., and Piret, J. M. (2003). Effects of glucose and CO_2 concentrations on CHO cell physiology. *Anim. Cell Technol. Basic Appl. Aspects* 13, 99–103. doi: 10.1007/978-94-017-0726-8_17

Teleki, A., Sánchez-Kopper, A., and Takors, R. (2015). Alkaline conditions in hydrophilic interaction liquid chromatography for intracellular metabolite quantification using tandem mass spectrometry. *Anal. Biochem.* 475, 4–13. doi: 10.1016/j.ab.2015.01.002

Templeton, N., Dean, J., Reddy, P., and Young, J. D. (2013). Peak antibody production is associated with increased oxidative metabolism in an industrially relevant fed-batch CHO cell culture. *Biotechnol. Bioeng.* 110, 2013–2024. doi: 10.1002/bit.24858

Thiele, I., Price, N. D., Vo, T. D., and Palsson, B. Ø. (2005). Candidate metabolic network states in human mitochondria impact of diabetes, ischemia, and diet. *J. Biol. Chem.* 280, 11683–11695. doi: 10.1074/jbc.M409072200

Trummer, E., Fauland, K., Seidinger, S., Schriebl, K., Lattenmayer, C., Kunert, R., et al. (2006). Process parameter shifting: part I. Effect of DOT, pH, and temperature on the performance of Epo-Fc expressing CHO cells cultivated in controlled batch bioreactors. *Biotechnol. Bioeng.* 94, 1033–1044. doi: 10.1002/bit.21013

Vielhauer, O., Zakhartsev, M., Horn, T., Takors, R., and Reuss, M. (2011). Simplified absolute metabolite quantification by gas chromatography–isotope dilution mass spectrometry on the basis of commercially available source material. *J. Chromatogr. B* 879, 3859–3870. doi: 10.1016/j.jchromb.2011.10.036

Wahrheit, J., Nicolae, A., and Heinzle, E. (2014). Dynamics of growth and metabolism controlled by glutamine availability in Chinese hamster ovary cells. *Appl. Microbiol. Biotechnol.* 98, 1771–1783. doi: 10.1007/s00253-013-5452-2

Walsh, G. (2014). Biopharmaceutical benchmarks 2014. *Nat. Biotechnol.* 32, 992–1000. doi: 10.1038/nbt.3040

Wu, P., Ray, N., and Shuler, M. (1993). A computer model for intracellular pH regulation in Chinese hamster ovary cells. *Biotechnol. Prog.* 9, 374–384. doi: 10.1021/bp00022a004

Xing, Z., Kenty, B. M., Li, Z. J., and Lee, S. S. (2009). Scale-up analysis for a CHO cell culture process in large-scale bioreactors. *Biotechnol. Bioeng.* 103, 733–746. doi: 10.1002/bit.22287

Xu, S., Jiang, R., Mueller, R., Hoesli, N., Kretz, T., Bowers, J., et al. (2018). Probing lactate metabolism variations in large-scale bioreactors. *Biotechnol. Prog.* 34, 756–766. doi: 10.1002/btpr.2620

Yoon, S. K., Choi, S. L., Song, J. Y., and Lee, G. M. (2005). Effect of culture pH on erythropoietin production by Chinese hamster ovary cells grown in suspension at 32.5 and 37.0 C. *Biotechnol. Bioeng.* 89, 345–356. doi: 10.1002/bit.20353

Zalai, D., Koczka, K., Párta, L., Wechselberger, P., Klein, T., and Herwig, C. (2015). Combining mechanistic and data-driven approaches to gain process knowledge on the control of the metabolic shift to lactate uptake in a fed-batch CHO process. *Biotechnol. Prog.* 31, 1657–1668. doi: 10.1002/btpr.2179

Zanghi, J. A., Schmelzer, A. E., Mendoza, T. P., Knop, R. H., and Miller, W. M. (1999). Bicarbonate concentration and osmolality are key determinants in the inhibition of CHO cell polysialylation under elevated pCO_2 or pH. *Biotechnol. Bioeng.* 65, 182–191.

Zimmermann, M., Sauer, U., and Zamboni, N. (2014). Quantification and mass isotopomer profiling of α-keto acids in central carbon metabolism. *Anal. Chem.* 86, 3232–3237. doi: 10.1021/ac500472c

Conflict of Interest Statement: JB was employed by company Boehringer Ingelheim Pharma GmbH and Co. KG.

The remaining authors declare that the research was conducted in the absence of any commercial or financial relationships that could be construed as a potential conflict of interest.

B Manuscript II

The following manuscript was published in Biotechnology and Bioengineering, 116, 951 – 960 in 2019 and reproduced with permission of John Wiley and Sons (copyright holders).

Becker, M., Junghans, L., Teleki, A., Bechmann, J., Takors, R. (2019b). Perfusion cultures require optimum respiratory ATP supply to maximize cell-specific and volumetric productivities. *Biotechnology and bioengineering, 116(5)*, 951–960.

Received: 9 November 2018 | Revised: 12 January 2019 | Accepted: 16 January 2019

DOI: 10.1002/bit.26926

ARTICLE

WILEY BIOTECHNOLOGY & BIOENGINEERING

Perfusion cultures require optimum respiratory ATP supply to maximize cell-specific and volumetric productivities

Max Becker[1] | Lisa Junghans[1] | Attila Teleki[1] | Jan Bechmann[2] | Ralf Takors[1]

[1]Institute of Biochemical Engineering, University of Stuttgart, Stuttgart, Germany

[2]Boehringer Ingelheim Pharma GmbH & Co. KG, Biberach, Germany

Correspondence
Ralf Takors, Institute of Biochemical Engineering, University of Stuttgart, Allmandring 31, 70569 Stuttgart, Germany.
Email: takors@ibvt.uni-stuttgart.de

Funding information
Ministerium für Wissenschaft, Forschung und Kunst Baden-Württemberg, Grant/Award Number: 32–7546.31/1/4

Abstract

Perfusion processes are an emerging alternative to common fed-batch processes in the growing biopharmaceutical industry. However, the challenge of maintaining high cell-specific productivities remains. In this study, glucose limitation was applied to two perfusion steady states and compared with a third steady state without any detectable limitation. The metabolic phenotype was enhanced under glucose limitation with a decrease of 30% in glucose uptake and 75% in lactate formation. Cell-specific productivities were substantially improved by 50%. Remarkably, the productivities showed a strong correlation to respiratory adenosine triphosphate (ATP) supply. As less reduced nicotinamide adenine dinucleotide (NADH) remained in the cytosol, the ATP generation from oxidative phosphorylation was increased by almost 30%. Consequently, the efficiency of carbon metabolism and the resulting respiratory ATP supply was crucial for maintaining the highly productive cellular state. This study highlights that glucose limitation can be used for process intensification in perfusion cultures as ATP generation via respiration is significantly increased, leading to elevated productivities.

KEYWORDS
ATP, CHO, flux analysis, perfusion, productivity

1 | INTRODUCTION

In the past decade, the international market for biopharmaceuticals has grown steadily (Gaughan, 2016; Walsh, 2014) with rising shares of so-called "biosimilars" generated through optimized manufacturing conditions. Therefore, the need to develop novel production processes with minimized manufacturing costs is imminent. Although the modern biopharmaceutical industry focuses primarily on fed-batch processes (Shukla & Thömmes, 2010), perfusion processes are a substantial part of upcoming manufacturing technologies as they can provide multiple advantages. In addition to their economic feasibility (Croughan, Konstantinov, & Cooney, 2015), continuous processes using cell retention can provide higher cell densities, prolonged cultivation times, both removal of inhibitory by-products, and continuous substrate addition (Bielser, Wolf, Souquet, Broly, & Morbidelli, 2018; Voisard, Meuwly, Ruffieux, Baer, & Kadouri, 2003). Alternating tangential flow (ATF) and tangential flow filtration (TFF) using filtration via hollow fiber modules can potentially reach cell densities of well above 100×10^6 cells/ml (Clincke, Mölleryd, Zhang, et al., 2013) and stable long-term operation with high viabilities (Warikoo et al., 2012; Xu, Hoshan, & Chen, 2016). Nevertheless, additionally maintaining high cell-specific productivities during operation is crucial to maximize volumetric productivities and facilitate downstream processing (Bausch, Schultheiss, & Sieck, 2018; Steinebach et al., 2017). Recent approaches to intensify perfusion processes include temperature reduction (Wolf et al., 2018) and glucose limitation (Takuma, Hirashima, & Piret, 2007). The latter is based on the variation of perfusion and bleed rates, which is one way to decouple substrate availability and cell density (Clincke, Mölleryd, Zhang, et al., 2013; Takuma et al., 2007). Possible improvements in metabolic efficiency including the switch from lactate production to consumption have only been previously analyzed in distinct fed-batch phases using tools such as flux analysis (Brunner, Doppler, Klein, Herwig, & Fricke, 2018; Ivarsson, Noh,

Morbidelli, & Soos, 2015; Mulukutla, Gramer, & Hu, 2012) and measurements of intracellular metabolite pools (Luo et al., 2012). Although beneficial effects of glucose limitation on the cellular phenotype have been described for perfusion processes, the influence on the underlying metabolism and the connection between adenosine triphosphate (ATP) supply and productivity has not yet been unravelled.

In this study, the effect of glucose limitation on cells in perfusion mode was analyzed in three distinct steady states. Whereas similar cell densities were installed in all conditions, growth was controlled by glucose limitation in two approaches. To investigate putative impacts of inhibition or limitation impacts by products or substrates, two different perfusion rates were applied for the two glucose-limited approaches. As a reference, a non-glucose-limited perfusion steady state was installed by applying high saturating bleeding and feeding conditions with the glucose-containing feed medium. Conditions were then compared with respect to carbon metabolism and ATP availability. Furthermore, flux balance analysis (FBA) and intracellular quantification of nucleotides were used to complement phenotypic studies. In particular, respiratory ATP production was observed to be essential for optimizing antibody productivity.

2 | MATERIALS AND METHODS

2.1 | Seed train, bioreactor cultivation, and perfusion settings

The CHO cell line producing an IgG1 monoclonal antibody was provided by Boehringer Ingelheim. Proprietary chemically defined medium with a glucose concentration of 25 mM was used for all cultivation steps. For the seed train, an expansion medium was used, whereas batch and perfusion medium was identical. An additional glucose feed was prepared for non-glucose-limited conditions. The seed train was performed in a humidified incubator (Infors HT, Bottmingen, Switzerland) set to 37°C, 5% CO_2 overlay and shaking at 120 rpm. The cells were thawed and passaged six times in shaking flasks (Corning, New York) with liquid volumes of 125–500 ml before inoculating the bioreactor. Perfusion cultivation was performed in a single reactor of a four-fold parallel bioreactor system DS1500ODSS (DASGIP, Hamburg, Germany). To achieve perfusion mode using TFF, the bioreactor was connected to two Xampler CFP-4-E-3X2MA hollow fiber modules (GE Healthcare, Munich, Germany) with a pore size of 0.45 µm, an inner diameter of 1 mm and a membrane area of 230 cm^2. One of the modules was used, whereas the other was clamped as a backup in the event of clogging. The inlets of the modules were connected to a dip tube inside the bioreactor using a 505S peristaltic pump (Watson Marlow, Falmouth, UK). The outlet was connected to the bioreactor again to ensure the continuous flow of the biosuspension. The cell-free harvest was drained off via a 101U peristaltic pump (Watson Marlow) and collected in an additional bottle. The tangential flow rate through the hollow fiber module was kept constant at 150 ml/min. The temperature was fixed to 36.5°C and pH was controlled at 6.80 with a deadband of 0.05 through the addition of either CO_2 or 1 M Na_2CO_3. Agitation was set to 250 rpm and the setpoint of dissolved oxygen was fixed at 60%. The seed density was 0.7×10^6 cells/ml in 1.0 L liquid volume. After 24 hr of batch mode cultivation, the perfusion mode was started. For analysis, three steady states with the setpoints 15×10^6 (SS1), 25×10^6 (SS2), and 20×10^6 (SS3) cells/ml were installed subsequently with the perfusion rates 1.03, 1.28, and 1.5 L/d, respectively. SS1 and SS2 were reached with minimum bleeding rates of 0.03 L/d. The different perfusion rates in SS1 and SS2 should exclude any obvious by-product inhibition or further limitation besides glucose. In SS3, a bleeding rate of 0.25 L/d was applied. Bleeding was performed manually by replacing cell-containing bioreactor medium with fresh medium on a daily basis. In the case of SS3, the bleed was replaced with medium combined with the additional glucose feed to regain glucose concentrations of 35 mM after bleeding. Therefore, glucose concentrations were constantly above limiting thresholds until the next bleeding procedure. An offline measurement of cell density and glucose concentration was done before the bleeding procedure to determine the cell density and glucose concentration. Sampling and bleeding were performed in <30 min. After bleeding, a second sample was analyzed to ensure setpoint values were matched. Each steady state was kept for at least 4 days.

2.2 | Extracellular analytics

Cell density and extracellular metabolites (Supporting Information Table 2) were measured daily during the growth phase, SS1, and SS2. To compensate for the effect of the high bleeding rates in SS3, additional sampling was performed after bleeding with fresh medium. The cell density was determined with a Cedex XS cell counter (Roche, Mannheim, Germany) using an aliquot of 100 µl for each sample. The remaining solution was centrifuged for 5 min at 800 g and 4°C in a Megafuge 1.0R (Heraeus, Hanau, Germany). Glucose and lactate concentrations were then measured in technical triplicates with a Labotrace automatic analyzer (TraceAnalytics, Braunschweig, Germany). The remaining supernatants were stored in aliquots at −70°C before measuring antibody titers with enzyme-linked immunosorbent assay (Pfizenmaier, Matuszczyk, & Takors, 2015). Amino acid concentrations were determined via reversed phase high-performance liquid chromatography (HPLC) with an Agilent 1200 (Agilent, Santa Clara, CA) according to the protocol of Buchholz et al. (2013) with L-ornithine as an internal standard.

2.3 | Intracellular analytics

Samples for the determination of intracellular metabolite concentrations (Supporting Information Table 2) were taken in triplicate every 48 hr, starting at 72 hr of process time. To ensure sampling of 30×10^6 cells, the cell density was measured before sampling and the needed sample volume was calculated. The fast filtration protocol of Matuszczyk, Teleki, Pfizenmaier, and Takors (2015) was then applied with minimal amendments. The cell suspension was placed on a glass fiber filter A/D with a pore size of 3 µm (Pall, Port Washington, NY)

installing a vacuum of 60 mbar. After an additional washing step, ice-cold quenching buffer was added immediately after the previous liquid phase was drained off by vacuuming. After removal of the quenching buffer, the filters were stored in sample cups, immediately frozen in liquid nitrogen, and stored at −70°C. Subsequent extraction was performed according to the protocol of Pfizenmaier et al. (2015). Intracellular adenosine phosphate concentrations were measured with HPLC according to the protocol of Pfizenmaier, Junghans, Teleki, and Takors (2016).

2.4 | Calculation of cell-specific rates

The extracellular cell-specific rates were derived from mass balance equations and calculated in 24-hr intervals using the daily measured concentrations of metabolites and viable cell densities. The rates were averaged for the last 3 days of each steady state.

$$\mu = \frac{B}{V} + \frac{1}{X_V}\frac{dX_V}{dt}. \quad (1)$$

Equation (1) defines the apparent growth rate μ, where B is the bleed rate, V is the liquid bioreactor volume, and X_V is the bioreactor viable cell density. Under the assumption of complete cell retention and no cells in the harvest stream.

$$q_{\mathrm{mAb}} = \frac{1}{X_V}\left(\frac{c_{\mathrm{mAb}}P}{V} + \frac{dc_{\mathrm{mAb}}}{dt}\right). \quad (2)$$

The cell-specific antibody productivity, where c_{mAb} is the bioreactor antibody concentration and P the perfusion rate is defined in Equation (2). Under the assumption of the same antibody concentrations in bioreactor and harvest.

$$q_{\mathrm{Glc,cons}} = \frac{1}{X_V}\left(\frac{(c_{\mathrm{Glc,M}} - c_{\mathrm{Glc}})P}{V} + \frac{dc_{\mathrm{Glc}}}{dt}\right). \quad (3)$$

The cell-specific glucose consumption rate, where $c_{\mathrm{Glc,M}}$ is the medium glucose concentration and c_{Glc} is the bioreactor glucose concentration is defined in Equation (3). For SS3 the rate was calculated in the intervals from after bleeding until before next day bleeding with P = 1.25 L/d (as B = 0 L/d) to account for the additional glucose feeding and varying glucose concentrations.

$$q_{\mathrm{Lac,prod}} = \frac{1}{X_V}\left(\frac{c_{\mathrm{Lac}}P}{V} + \frac{dc_{\mathrm{Lac}}}{dt}\right). \quad (4)$$

Equation (4) indicates the cell-specific lactate production rate, where c_{Lac} is the bioreactor lactate concentration.

2.5 | Flux balance analysis

FBA was performed in MATLAB Version 2013a (Mathworks, Natick, MA) using the Cobra Toolbox. For each of the three steady states, a flux distribution was determined using the model of Sou et al. (2015) and the biomass composition of Selvarasu et al. (2012). The model was expanded by oxidative phosphorylation reactions to consider ATP formation rates. *P/O* ratios of 2.5 and 1.5 were assumed for reduced nicotinamide adenine dinucleotide (NADH) and reduced flavin adenine dinucleotide (FADH2), respectively. In total, 240 metabolites located in the cytosol and extracellular regions were considered, composing 99 intracellular and 114 exchange reactions. The cellular transport involving antibody production, glucose and amino acid uptake, lactate formation, and growth rates were constrained by experimental observations. Measurement errors of the cellular transport limited the solution space of FBA selecting ATP formation as an objective function of the optimization. The solution space was sampled using the Monte Carlo approach developed by Thiele, Price, Vo, and Palsson (2005) to assign error bars to each output flux (total number of sampling points: 2.5×10^6 using 2,500 randomly distributed starting points).

The redox variable R was calculated as described in Nolan and Lee (2011). NADH generating fluxes of glycolysis were divided by the NADH equivalent fluxes entering mitochondria. Therefore, the flux of NADH produced in the tricarboxylic acid cycle (TCA) ($v_{\mathrm{TCA}\rightarrow\mathrm{NADH}}$) was subtracted from the total flux of NADH being transformed in oxidative phosphorylation ($v_{\mathrm{NADH}\rightarrow\mathrm{oxPhos}}$):

$$R = \frac{v_{\mathrm{glycolysis}\rightarrow\mathrm{NADH}}}{v_{\mathrm{NADH}\rightarrow\mathrm{oxPhos}} - v_{\mathrm{TCA}\rightarrow\mathrm{NADH}}}.$$

3 | RESULTS

3.1 | Cell densities and metabolic rates

Table 1 lists the settings of the perfusion studies regarding flow rates and actual steady state values for viable cell density, glucose, and antibody concentrations. Glucose concentrations were below 1 mM in SS1 and SS2 as a consequence of minimal bleeding rates of 0.03 L/d. Accordingly, cells were limited by glucose availability. No other metabolite concentration decreased below 40% of the initial medium concentration at either of the perfusion rates in SS1 and SS2,

TABLE 1 Overview of the viable cell densities, glucose concentrations, antibody concentrations, and flow rates in the three steady states

	SS1	SS2	SS3
Viable cell density (10^6 cells/ml)	16.37 ± 0.43	25.28 ± 0.95	22.10 ± 2.52 18.97 ± 0.74
Glucose concentration (mmol/L)	0.96 ± 0.33	0.52 ± 0.24	6.58 ± 0.77 34.29 ± 0.59
Antibody concentration (g/L)	0.22 ± 0.02	0.28 ± 0.02	0.14 ± 0.03 0.12 ± 0.01
Perfusion rate (L/d)	1.03	1.28	1.5
Bleed rate (L/d)	0.03	0.03	0.25
Harvest rate (L/d)	1.00	1.25	1.25

Note. Concentration values are averaged for the last 3 days of each steady state. For SS3 concentration values before and after daily bleeding are given.

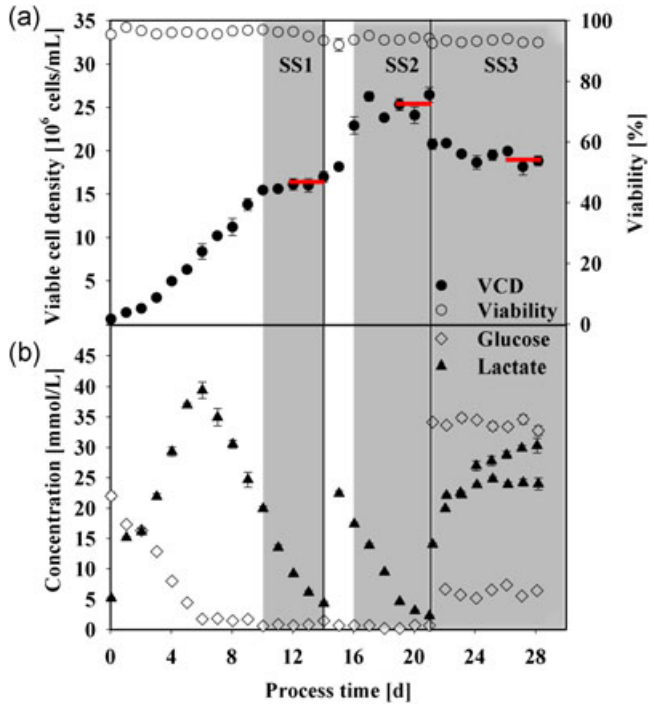

FIGURE 1 Viable cell density and viability (a) and glucose and lactate concentrations (b) over process time. The shifts of perfusion rates are shown by solid vertical lines and the three steady states with constant cell densities are marked in gray. The horizontal red lines mark the steady-state conditions for which cell-specific rates were calculated. For SS3 only values after manual bleeding are shown. Error bars indicate the error of technical triplicates [Color figure can be viewed at wileyonlinelibrary.com]

therefore any further detectable limitation was excluded (Supporting Information Table 1). In SS3, the glucose concentration exceeded 6 mM when the high bleeding rate of 0.25 L/d was installed. We report here that the cell density was limited by the applied bleeding. The resulting viable cell densities and viabilities are highlighted in Figure 1a. The cell density was constantly increasing until SS1 was reached with about 16×10^6 cells/ml after 10 days. After 14 days, the perfusion rate was increased to 1.28 L/d leading to the cell density of 25×10^6 cells/ml in SS2 after 16 days. After 21 days, the perfusion rate was elevated to 1.5 L/d and remained constant until the end of the cultivation. Contrary to SS1 and SS2, the bleed rate shifted substantially to 0.25 L/d on average. Consequently, cell densities were artificially diluted to 20×10^6 cells/ml, which ranges between SS1 and SS2. The viability was maintained above 90% throughout the cultivation. Glucose concentrations (Figure 1b) were close to zero after about 6 days. At the same time, lactate concentrations started decreasing from 40 mM towards an average of 6.5 mM in the last three days of SS1 (cf. Supporting Information Table 1). The average lactate concentration at the end of SS2 was 3.3 mM. In the non-glucose-limited SS3 lactate concentrations ranged from 24 to 31 mM.

Figure 2 shows a set of averaged key metabolic rates representing the three steady states. The cell-specific rates were similar in SS1 and SS2 but differed significantly from SS3. Glucose consumption was increased by 30–60% in SS3 with values of 2,000 fmol·cell^{-1}·d^{-1} compared with 1,500 fmol·cell^{-1}·d^{-1} in SS1 and 1,250 fmol·cell^{-1}·d^{-1} in SS2. Accordingly, lactate production was similarly elevated. Whereas lactate was secreted with 250–750 fmol·cell^{-1}·d^{-1} in SS1 and SS2, respectively, the rate increased to 2100 fmol·cell^{-1}·d^{-1} in SS3. The growth rate was reduced to 0.05 L/d in SS1 and 0.07 L/d in SS2 due to the glucose-limited state. In contrast, the growth rate reached 0.3 L/d in SS3 thereby compensating the strong dilution via bleeding. However, the growth rate was highest in the early growth phase of the perfusion with 0.4 L/d. Interestingly, the cell-specific antibody production was 50% higher in SS1 and SS2, showing values of 14 pg·cell^{-1}·d^{-1} compared with only 9.5 pg·cell^{-1}·d^{-1} in the non-glucose-limited SS3.

3.2 | FBA, ATP formation, and balancing of carbon

The results of FBA are depicted in Figure 3. According to the extracellular glucose uptake rates, the glycolytic flux was approximately 30% higher in SS3 than in SS1 and SS2 and approximately 50% of the glycolytic carbon flux was converted to lactate. Given that 400 fmol·cell^{-1}·d^{-1} of alanine were additionally produced via alanine transaminase, only 40% of pyruvate fueled the TCA. For SS1 and SS2, the yields amounted to 70% and 84%, respectively. By-product formation was significantly decreased, resulting in a 25% rise in TCA flux despite the lowered glycolytic flux. The uptake rates of glutamine as a second major carbon source were similar for all steady states with values of approximately 200 fmol·cell^{-1}·d^{-1}. The flux through the pentose phosphate pathway was elevated in SS3, whereas only marginal fluxes in SS1 and SS2 were observed. This coincides with the increased growth rate of SS3 (Table 1) and the attributed role of the pentose phosphate pathway to provide NADPH for biomass generation.

The ATP formation rates in Figure 4 were derived from the FBA. Values of the total produced ATP sum up to approximately 22,000 fmol·cell^{-1}·d^{-1} in all steady states, revealing only a minimally lower rate in SS3. However, the fractional distribution of ATP formation differs between SS1, SS2, and SS3. In SS1 and SS2, glycolysis accounted for 25% of produced ATP, succinyl-CoA synthetase in TCA for 10%, and oxidative phosphorylation for the remaining 65%. By contrast, glycolysis contributed 40% in SS3 whereas the fraction of oxidative phosphorylation was reduced to

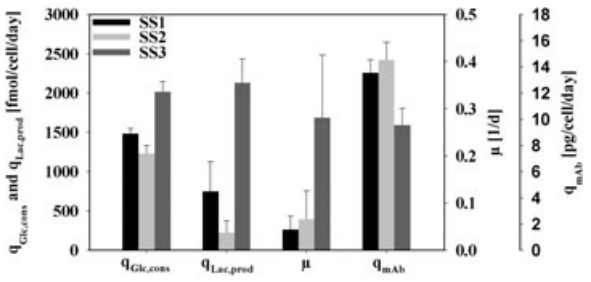

FIGURE 2 Cell-specific rates of glucose consumption, lactate production, growth and antibody production in the three steady states. Average values and errors are derived from the last three days of each steady state

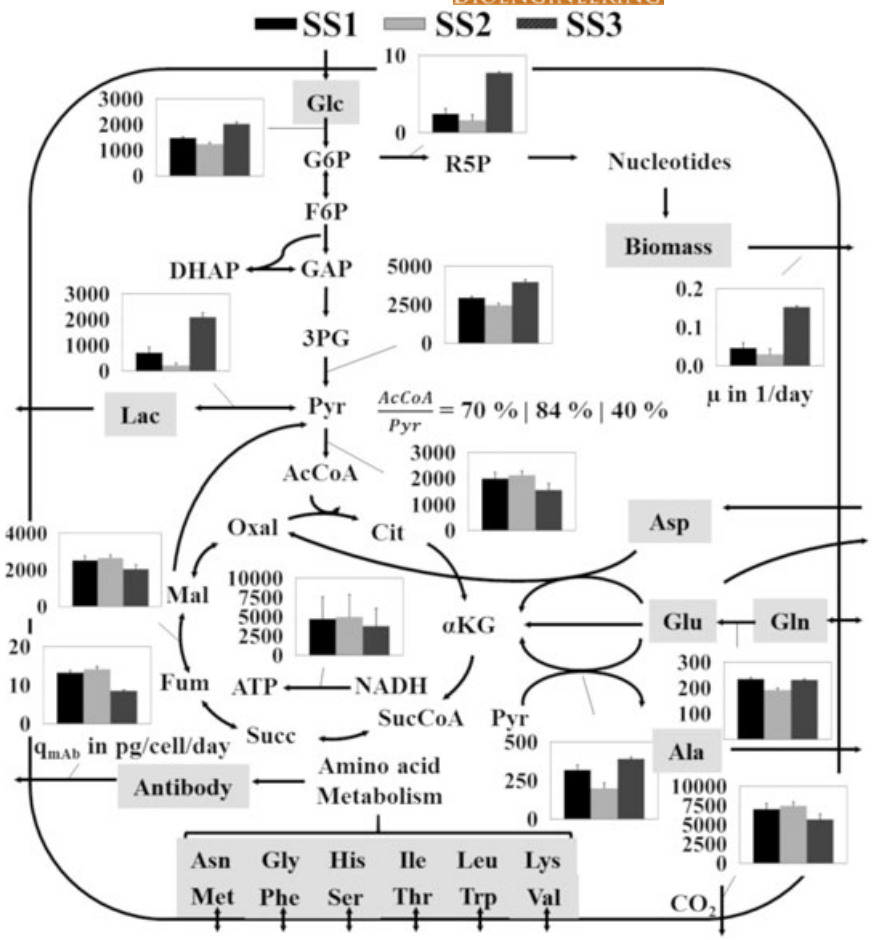

FIGURE 3 Scheme of the main carbon metabolism showing the results of the flux balance analysis for the three steady states. The three bars of each flux are sorted as marked at the top. Fluxes are given in fmol·cell^{-1}·d^{-1} unless otherwise stated. Errors were determined through Monte Carlo sampling as described in the materials and methods section

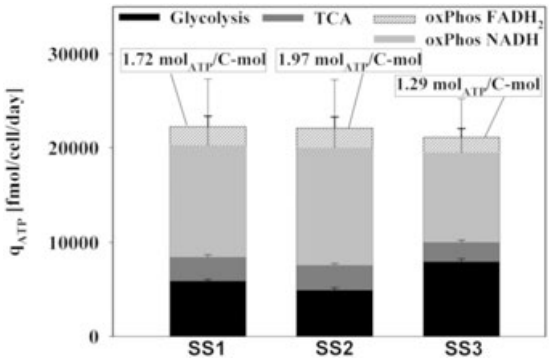

FIGURE 4 ATP formation rates at the three steady states. The source of ATP formation is indicated in the legend. Accordingly, ATP may be generated by oxidation of NADH (oxPhos NADH) or $FADH_2$ (oxPhos $FADH_2$), both being produced in TCA and glycolysis. Additionally, ATP may be derived energy equivalent from succinyl-CoA synthetase (indicated as TCA) or directly from glycolysis (indicated as Glycolysis). Results were obtained from the flux balance analysis. Errors were determined through Monte Carlo sampling as described in the materials and methods section. ATP: adenosine triphosphate; $FADH_2$: reduced flavin adenine dinucleotide; NADH: reduced nicotinamide adenine dinucleotide

50%. Again, approximately 10% were derived from succinyl-CoA synthetase. Furthermore, the yield of ATP generated per C-mol was only 1.29, whereas in SS1 and SS2 the yields were estimated to be 1.72 and 1.97, respectively.

Figure 5 shows the dependence of cell-specific (q_{mAb}) and volumetric (Q_{mAb}) productivities on the ATP formation rates from oxidative phosphorylation ($q_{ATP,\ oxPhos}$). Interestingly, a strong correlation between q_{mAb} and $q_{ATP,\ oxPhos}$ could be found for both this perfusion process and a previously performed reference fed-batch (figure 5a). Although $q_{ATP,\ oxPhos}$ exceeded the perfusion values of SS1 and SS2 by 5,000–8,000 fmol·cell^{-1}·d^{-1} in the growth and stationary phase of the fed-batch, q_{mAb} was the same or only slightly increased by approximately 2.5 pg·cell^{-1}·d^{-1}. Q_{mAb} (Figure 5b) was about 0.2 g·L^{-1}·d^{-1} for SS1 and the fed-batch decline and stationary phase with similar cell densities of 15×10^6 cells/ml. Although higher cell densities of 25×10^6 cells/ml were reached in SS3, Q_{mAb} was nearly identical due to diminished cell-specific productivity. SS2 had the highest volumetric productivity of 0.36 g·L^{-1}·d^{-1} resulting from a combination of high cell densities and high q_{mAb}.

The dependency of antibody productivity and lactate formation on the redox variable R for all three steady states is presented in Figure 6. Notably, SS3 showed the highest R of 2.37, followed by the substrate limited steady states with R being 1.39 in SS1 and 1.08 in SS2. Whereas the antibody productivity was negatively correlated and decreased with

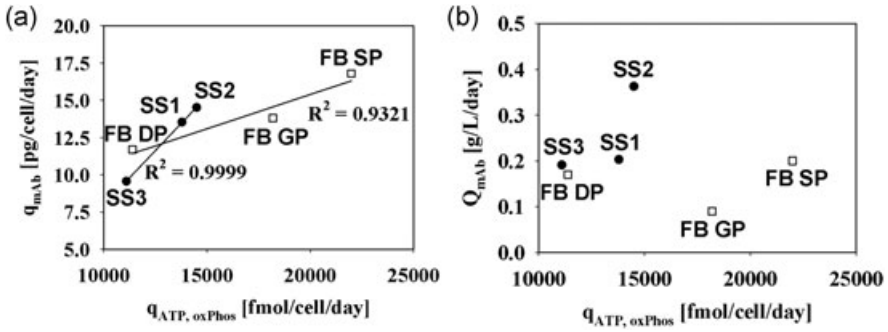

FIGURE 5 Cell-specific productivity (a) and volumetric productivity (b) as a function of ATP formation rates of oxidative phosphorylation ($q_{ATP, oxPhos}$). Depicted are the three perfusion (●) steady states (SS1, SS2, and SS3) and values from growth phase (GP), stationary phase (SP) and decline phase (DP) of a reference fed-batch (FB); (□) from previous experiments. ATP: adenosine triphosphate

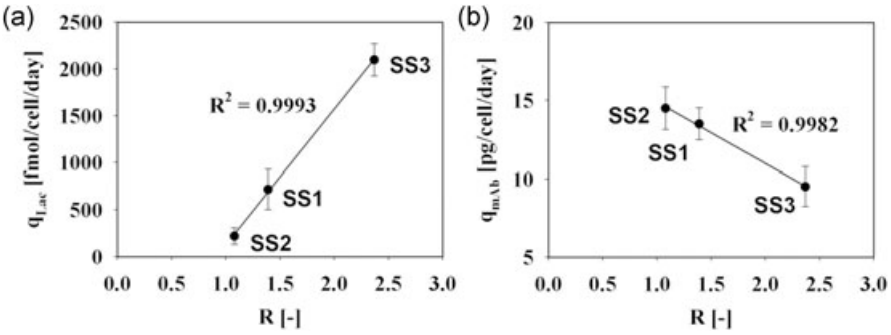

FIGURE 6 Cell-specific lactate production (a) and cell-specific antibody productivity (b) for the three steady states as a function of the redox variable R, which was calculated from the results of flux balance analysis. Average values and errors of the cell-specific rates are derived from the last three days of each steady state

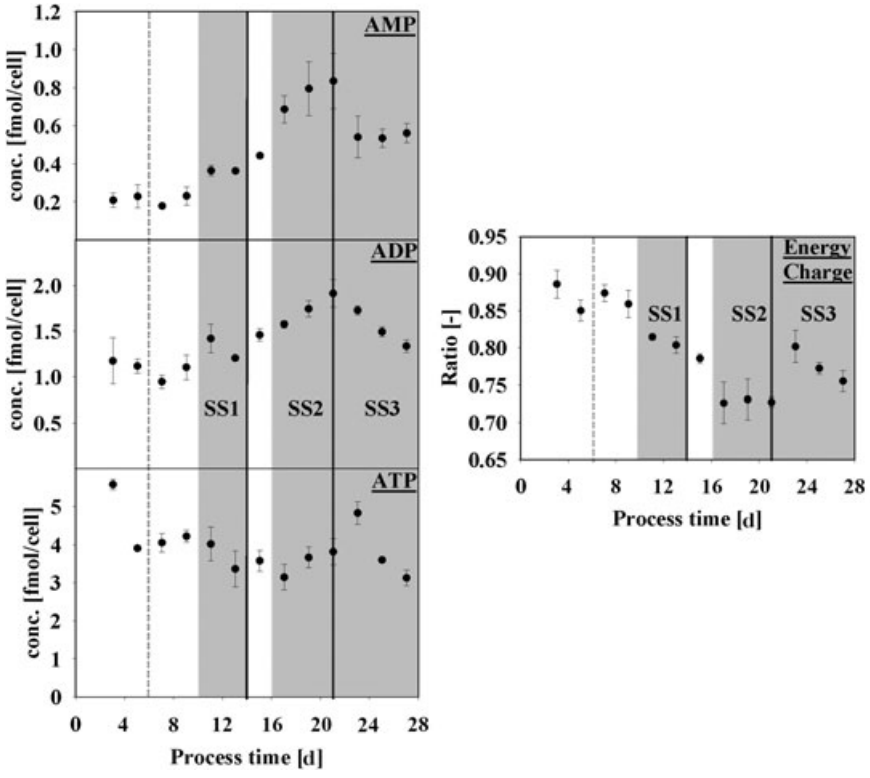

FIGURE 7 Intracellular concentrations of nucleotides as well as adenylate energy charge. Samples were taken every second day. The dashed vertical line indicates sinking extracellular glucose levels below 4 mM. The shifts of perfusion rates are shown by solid vertical lines and the three steady states with constant cell densities are marked in gray. Error bars indicate the error of technical triplicates

increasing R (Figure 6b), the lactate formation was positively correlated to R (Figure 6a). According to the regression line, the state of no lactate formation or uptake ($q_{Lac} = 0$) is estimated as R = 0.92 and agrees with the theoretical value of 1.0.

3.3 | Intracellular levels of adenosine phosphates

Nucleotide levels and the adenylate energy charge are depicted in Figure 7. Highest ATP concentrations of 5.5 fmol/cell were present at the very beginning of the process after 3 days. In the following, nucleotide concentrations were not severely affected by glucose limitation and changed only marginally until the end of SS1. Adenosine monophosphate (AMP) and Adenosine diphosphate (ADP) levels were 1.25 fmol/cell and 0.4 fmol/cell, respectively, whereas ATP concentrations diminished slightly towards 3.5 fmol/cell. After the first increase in perfusion rate, all nucleotide pool sizes increased, with ATP levels of 3.9 fmol/cell at the end of SS2. Due to the rise in AMP and ADP, the adenylate energy charge decreased to the lowest value of 0.73. In SS3, the energy charge was regenerated through the degradation of AMP and ADP and reached values of above 0.80 until finally decreasing to 0.76. Interestingly, the ATP concentrations improved only shortly after extracellular glucose was available in excess again and started falling towards the final value of 3.0 fmol/cell.

4 | DISCUSSION

4.1 | Effect of perfusion mode and substrate level on growth and main metabolic rates

As depicted in Figure 1, all three settings (Table 1) reached a steady state for a minimum of 4 days showing constant viable cell densities. SS1 and SS2 were growth limited due to glucose limitation. Two different perfusion rates were set to rule out any detectable limitations in amino acids or inhibition by lactate (Supporting Information Table 1). Cell densities in SS3 were kept constant through daily bleeds without any obvious substrate limitation. Stable operation of perfusion processes using similar cell densities of about 20×10^6 cells/ml and perfusion rates of approximately one reactor volume per day has been shown to be useful perfusion modes (Clincke, Mölleryd, Zhang, et al., 2013; Karst, Serra, Villiger, Soos, & Morbidelli, 2016). Although much higher cell densities can be reached using concentrated media (Clincke, Mölleryd, Zhang, et al., 2013; Xu et al., 2016), the goal of this study was to investigate the effect of glucose limitation on productivity and cellular metabolism. Such studies do not necessarily require further elevated high cell density steady states.

Lu, Sun, and Zhang (2005) defined a glucose concentration below 1.2 mM as growth limiting, which is well above the values in SS1 and SS2 (Table 1 and Figure 1). By contrast, glucose concentrations were always clearly above 1.2 mM in SS3. Lactate concentrations never reached inhibiting concentrations of 60 mM (Lao & Toth, 1997) in the course of the whole cultivation. The glucose-limited environment in SS1 and SS2 proved to be beneficial for the cellular phenotype as $q_{Glc,\ cons}$ and $q_{Lac,\ prod}$ decreased (25% and 75%), whereas q_{mAb} increased by 50% in comparison to the non-glucose-limited SS3 (Figure 2). Indications that antibody titers may be artificially increased due to the unwanted product retention in the hollow fiber membrane (Clincke, Mölleryd, Samani, et al., 2013; Karst et al., 2016) cannot be completely ruled out due to missing harvest titer measurements. However, the measured bioreactor titers were constant over each steady state.

The phenotypic effect of glucose limitation on cell-specific antibody formation has been previously investigated. Although some publications describe a negative effect on productivity (Altamirano et al., 2001) or product quality (Chee Furng Wong, Tin Kam Wong, Tang Goh, Kiat Heng, & Gek Sim Yap, 2005), others stress constant product formation rates (Europa, Gambhir, Fu, & Hu, 2000; Takuma et al., 2007). However, all of these publications outline declining glucose uptake and lactate formation. Accordingly, carbon metabolism turned into highly efficient modes, preventing overflow metabolism as indicated in Figure 2. The phenotype may be triggered by cell-cycle arrest in the G1 phase, which is caused by glucose limitation (Dalm, Cuijten, van Grunsven, Tramper, & Martens, 2004). Growth rates in SS1 and SS2 decreased sharply, indicating the cell-cycle arrest. Multiple approaches, such as temperature reduction and osmotic shift, have been shown to result in growth inhibition and cell-cycle arrest in the G1 phase, along with beneficial adaptations of cellular metabolism. Similar to glucose limitation, cells exposed to temperature reduction showed lower glucose uptake rates in perfusion processes whereas specific productivity increased by 50–60% (Ahn, Jeon, Jeong, Lee, & Yoon, 2008; Furukawa & Ohsuye, 1999; Wolf et al., 2018). Notably, osmotic shifts led to highly productive cell-cycle arrest, although a rise in $q_{Glc,\ cons}$ and $q_{Lac,\ prod}$ was observed (Pfizenmaier et al., 2015; Pfizenmaier et al., 2016). The latter is in contrast to the phenotypes of glucose limitation or temperature reduction. The decreased glucose uptake and lactate production due to glucose limitation observed in this study suggest a strong increase in the efficiency of carbon metabolism.

4.2 | Adjustments of carbon and energy metabolism to different substrate availabilities

FBA was used to unravel the connection between intracellular fluxes, ATP availability, and elevated productivity. We observed that cells adapted their carbon metabolism according to the glucose supply. Intracellular flux distributions (Figure 3) showed an increase of efficiency in SS1 and SS2, as the fraction of pyruvate being fueled into TCA nearly doubled to approximately 80% compared with that of the non-glucose-limited SS3. In SS3, the elevated glycolytic flux towards pyruvate shifted to the by-products lactate and alanine. Remarkably, fluxes through TCA were highest under limited conditions and coincided with the highest antibody productivities. Similar changes in carbon metabolism were observed for the transition from exponential to stationary phase in fed-batch processes when growth rates decreased (Ahn et al., 2008; Mulukutla

et al., 2012; Templeton, Dean, Reddy, & Young, 2013). Besides, similar findings were reported for batch processes after glucose depletion (Martínez et al., 2013). Strong positive correlations have been previously reported between growth and glycolytic flux, and between antibody productivity and TCA flux (Templeton et al., 2013). More recently, Templeton, Xu, Roush, and Chen (2017) compared fed-batch and perfusion processes and reported that the total protein productivity was the same in both process modes. However, the fractions of biomass protein and antibody protein differed. In contrast to the stationary phase of the fed-batch process, cells in perfusion mode showed higher growth rates, which resulted in increased biomass protein formation. Consequently, it is likely beneficial to keep cells in a nongrowing state, as in SS1 and SS2, to shift protein formation from biomass demands to antibody production.

Dalm et al. (2007) recommended the installation of glucose-limited perfusion processes to increase TCA fluxes. Consequently, one may anticipate reduced lactate production coinciding with elevated ATP formation. In our study, ATP formation rates under conditions of glucose excess (SS3; Figure 4) showed only a slight reduction of q_{ATP} in SS3 compared with SS1 and SS2. However, remarkable differences were observed for the origin of ATP. Although ATP formation via oxidative phosphorylation accounted for the major part (about two-thirds) in SS1 and SS2, glycolytic ATP formation was much more pronounced in SS3 and nearly equilibrated with the sum of glycolytic and TCA-based ATP formation of SS1 and SS2. In total, ATP formation efficiency of SS3 was far below the efficiency of SS1 and SS2. Specifically, ATP perC-mol was about 35% less in SS3 than in SS1 and SS2.

Interestingly, Templeton et al. (2013) showed a strong connection between CO_2 producing TCA reactions and antibody production for a fed-batch process, stating that oxidative metabolism could promote productivity. The strong correlation between q_{mAb} and $q_{ATP,\ oxPhos}$ (Figure 5a) found in our study underlines the apparent influence of respiratory ATP supply on cellular productivity. Regarding the elevated $q_{ATP,\ oxPhos}$ in the fed-batch, cells likely spent additional ATP for maintenance due to the stress factors such as lactate inhibition, but also increased pCO_2 and osmolality, leading to a different correlation. This finding opens the door for further process improvements. In particular, significantly higher volumetric productivities (Figure 5b) could be reached in perfusion mode compared with the fed-batch process if cell densities were increased further. To be precise, proper glucose limitations must be installed to ensure optimum ATP formation. This notion is particularly relevant for the efficient metabolic state in SS1 and SS2 with high respiratory ATP supply.

As NADH is oxidized to NAD^+ either via the formation of lactate or via oxidative phosphorylation, the relative use of the two reactions plays a crucial role setting the cellular carbon efficiency and the ATP generation. The finding is also reflected by the redox variable R (Brunner et al., 2018; Nolan & Lee, 2011) revealing a negative correlation between R and q_{mAb} for each steady state (Figure 6). The more NADH is produced in glycolysis and not transported into mitochondria for oxidative phosphorylation, the fewer antibodies are produced. Consequently, the redox balance is extremely important for maintaining high oxidative phosphorylation and therefore high ATP availability, which ultimately is required for the energy-demanding process of antibody synthesis.

4.3 | Intracellular pools change with extracellular steady-state conditions

Intracellular AMP and ADP concentrations in Figure 7 increased towards the end of SS2, whereas the final ATP concentrations in SS1, SS2, and SS3 achieved very similar levels irrespective of the steady state. In contrast, AMP and ADP levels were highest during most challenging glucose limitation. Apparently, cells managed to keep ATP formation high despite carbon limitation which is in agreement with previous findings of Matuszczyk et al. (2015). Similar to the findings in our study, Moore et al. (1997) showed constant ATP levels over time for cells arrested in the G1 phase, given that viability was constant. Furthermore, pool sizes of ATP were comparable with CHO cultivations performed by Pfizenmaier et al. (2015, 2016). The resulting adenylate energy charge decreased initially but regenerated by the degradation of AMP and ADP. However, final steady-state values ranged from 0.73 to 0.80 and showed no significant deviations. Although higher energy charges of 0.9 were reported for nonlimited perfusion processes (Karst et al., 2017), values were in physiological ranges throughout the process (Chapman & Atkinson, 1973).

In conclusion, we report a strong effect of glucose limitation on carbon metabolism and ATP supply resulting in elevated productivities. Differences in metabolic efficiency could be tracked in distinct steady states. Undoubtedly, glucose limitation led to beneficial changes in the metabolic phenotype in terms of both lower glucose uptake and lactate formation. We observed that increased product formation rates were induced by significantly elevated ATP supply from oxidative phosphorylation. The correlation between q_{mAb} and $q_{ATP,\ oxPhos}$ underlines the need for high ATP availability for antibody synthesis, preferably generated from respiration and not from glycolysis. R correlated positively with q_{Lac} and negatively with q_{mAb}. In other words, the more NADH is available in the cytosol, the more lactate will be formed and the less ATP can be generated via respiration. Given that the latter outcome supports q_{mAb} production, low R values are preferred.

ACKNOWLEDGMENT

The authors gratefully acknowledge the funding by the Ministerium für Wissenschaft, Forschung und Kunst Baden-Württemberg (MWK, Grant 32–7546.31/1/4).

CONFLICTS OF INTEREST

Author Jan Bechmann was employed by the company Boehringer Ingelheim Pharma GmbH & Co. KG. All other authors declare that there are no conflicts of interests.

ORCID

Max Becker http://orcid.org/0000-0002-1180-1888

REFERENCES

Ahn, W. S., Jeon, J. J., Jeong, Y. R., Lee, S. J., & Yoon, S. K. (2008). Effect of culture temperature on erythropoietin production and glycosylation in a perfusion culture of recombinant CHO cells. *Biotechnology and Bioengineering*, *101*(6), 1234–1244. https://doi.org/10.1002/bit.22006.

Altamirano, C., Illanes, A., Casablancas, A., Gamez, X., Cairo, J. J., & Godia, C. (2001). Analysis of CHO cells metabolic redistribution in a glutamate-based defined medium in continuous culture. *Biotechnology Progress*, *17*(6), 1032–1041.

Bausch, M., Schultheiss, C., & Sieck, J. B. (2018). Recommendations for comparison of productivity between fed-batch and perfusion processes. *Biotechnology Journal*, e1700721. https://doi.org/10.1002/biot.201700721.

Bielser, J. M., Wolf, M., Souquet, J., Broly, H., & Morbidelli, M. (2018). Perfusion mammalian cell culture for recombinant protein manufacturing–A critical review. *Biotechnology Advances*, *36*(4), 1328–1340. https://doi.org/10.1016/j.biotechadv.2018.04.011.

Brunner, M., Doppler, P., Klein, T., Herwig, C., & Fricke, J. (2018). Elevated pCO2 affects the lactate metabolic shift in CHO cell culture processes. *Engineering in Life Sciences*, *18*(3), 204–214.

Buchholz, J., Schwentner, A., Brunnenkan, B., Gabris, C., Grimm, S., Gerstmeir, R., … Blombach, B. (2013). Platform engineering of Corynebacterium glutamicum with reduced pyruvate dehydrogenase complex activity for improved production of L-lysine, L-valine, and 2-ketoisovalerate. *Applied and Environmental Microbiology*, *79*(18), 5566–5575.

Chapman, A. G., & Atkinson, D. E. (1973). Stabilization of adenylate energy charge by the adenylate deaminase reaction. *Journal of Biological Chemistry*, *248*(23), 8309–8312.

Chee Furng Wong, D., Tin Kam Wong, K., Tang Goh, L., Kiat Heng, C., & Gek Sim Yap, M. (2005). Impact of dynamic online fed-batch strategies on metabolism, productivity and N-glycosylation quality in CHO cell cultures. *Biotechnology and Bioengineering*, *89*(2), 164–177. https://doi.org/10.1002/bit.20317.

Clincke, M. F., Mölleryd, C., Samani, P. K., Lindskog, E., Fäldt, E., Walsh, K., & Chotteau, V. (2013). Very high density of Chinese hamster ovary cells in perfusion by alternating tangential flow or tangential flow filtration in WAVE Bioreactor-part II: Applications for antibody production and cryopreservation. *Biotechnology Progress*, *29*(3), 768–777. https://doi.org/10.1002/btpr.1703.

Clincke, M. F., Mölleryd, C., Zhang, Y., Lindskog, E., Walsh, K., & Chotteau, V. (2013). Very high density of CHO cells in perfusion by ATF or TFF in WAVE bioreactor. Part I. Effect of the cell density on the process. *Biotechnology Progress*, *29*(3), 754–767. https://doi.org/10.1002/btpr.1704.

Croughan, M. S., Konstantinov, K. B., & Cooney, C. (2015). The future of industrial bioprocessing: Batch or continuous?. *Biotechnology and Bioengineering*, *112*(4), 648–651.

Dalm, M. C. F., Cuijten, S. M. R., van Grunsven, W. M. J., Tramper, J., & Martens, D. E. (2004). Effect of feed and bleed rate on hybridoma cells in an acoustic perfusion bioreactor: Part I. Cell density, viability, and cell-cycle distribution. *Biotechnology and Bioengineering*, *88*(5), 547–557. doi: . https://doi.org/10.1002/bit.20287.

Dalm, M. C. F., Lamers, P. P., Cuijten, S. M. R., Tjeerdsma, A. M., Van Grunsven, W. M. J., Tramper, J., & Martens, D. E. (2007). Effect of feed and bleed rate on hybridoma cells in an acoustic perfusion bioreactor: Metabolic analysis. *Biotechnology Progress*, *23*(3), 560–569.

Europa, A. F., Gambhir, A., Fu, P. C., & Hu, W. S. (2000). Multiple steady states with distinct cellular metabolism in continuous culture of mammalian cells. *Biotechnology and Bioengineering*, *67*(1), 25–34.

Furukawa, K., & Ohsuye, K. (1999). Enhancement of productivity of recombinant α-amidating enzyme by low temperature culture. *Cytotechnology*, *31*(1-2), 85–94.

Gaughan, C. L. (2016). The present state of the art in expression, production, and characterization of monoclonal antibodies. *Molecular Diversity*, *20*(1), 255–270.

Ivarsson, M., Noh, H., Morbidelli, M., & Soos, M. (2015). Insights into pH-induced metabolic switch by flux balance analysis. *Biotechnology Progress*, *31*(2), 347–357.

Karst, D. J., Serra, E., Villiger, T. K., Soos, M., & Morbidelli, M. (2016). Characterization and comparison of ATF and TFF in stirred bioreactors for continuous mammalian cell culture processes. *Biochemical Engineering Journal*, *110*, 17–26. https://doi.org/10.1016/j.bej.2016.02.003.

Karst, D. J., Steinhoff, R. F., Kopp, M. R. G., Serra, E., Soos, M., Zenobi, R., & Morbidelli, M. (2017). Intracellular CHO cell metabolite profiling reveals steady-state dependent metabolic fingerprints in perfusion culture. *Biotechnology Progress*, *33*, 879–890. https://doi.org/10.1002/btpr.2421.

Lao, M. S., & Toth, D. (1997). Effects of ammonium and lactate on growth and metabolism of a recombinant Chinese hamster ovary cell culture. *Biotechnology Progress*, *13*(5), 688–691.

Lu, S., Sun, X., & Zhang, Y. (2005). Insight into metabolism of CHO cells at low glucose concentration on the basis of the determination of intracellular metabolites. *Process Biochemistry*, *40*(5), 1917–1921. https://doi.org/10.1016/j.procbio.2004.07.004.

Luo, J., Vijayasankaran, N., Autsen, J., Santuray, R., Hudson, T., Amanullah, A., & Li, F. (2012). Comparative metabolite analysis to understand lactate metabolism shift in Chinese hamster ovary cell culture process. *Biotechnology and Bioengineering*, *109*(1), 146–156.

Martínez, V. S., Dietmair, S., Quek, L. E., Hodson, M. P., Gray, P., & Nielsen, L. K. (2013). Flux balance analysis of CHO cells before and after a metabolic switch from lactate production to consumption. *Biotechnology and Bioengineering*, *110*(2), 660–666.

Matuszczyk, J. C., Teleki, A., Pfizenmaier, J., & Takors, R. (2015). Compartment-specific metabolomics for CHO reveals that ATP pools in mitochondria are much lower than in cytosol. *Biotechnology Journal*, *10*(10), 1639–1650.

Moore, A., Mercer, J., Dutina, G., Donahue, C. J., Bauer, K. D., Mather, J. P., … Ryll, T. (1997). Effects of temperature shift on cell cycle, apoptosis, and nucleotide pools in CHO cell batch cultues. *Cytotechnology*, *23*(1-3), 47–54.

Mulukutla, B. C., Gramer, M., & Hu, W.-S. (2012). On metabolic shift to lactate consumption in fed-batch culture of mammalian cells. *Metabolic Engineering*, *14*(2), 138–149.

Nolan, R. P., & Lee, K. (2011). Dynamic model of CHO cell metabolism. *Metabolic Engineering*, *13*(1), 108–124. https://doi.org/10.1016/j.ymben.2010.09.003.

Pfizenmaier, J., Junghans, L., Teleki, A., & Takors, R. (2016). Hyperosmotic stimulus study discloses benefits in ATP supply and reveals miRNA/mRNA targets to improve recombinant protein production of CHO cells. *Biotechnology Journal*, *11*(8), 1037–1047.

Pfizenmaier, J., Matuszczyk, J. C., & Takors, R. (2015). Changes in intracellular ATP-content of CHO cells as response to hyperosmolality. *Biotechnology Progress*, *31*(5), 1212–1216.

Selvarasu, S., Ho, Y. S., Chong, W. P. K., Wong, N. S. C., Yusufi, F. N. K., Lee, Y. Y., … Lee, D. Y. (2012). Combined in silico modeling and metabolomics analysis to characterize fed-batch CHO cell culture. *Biotechnology and Bioengineering*, *109*(6), 1415–1429.

Shukla, A. A., & Thömmes, J. (2010). Recent advances in large-scale production of monoclonal antibodies and related proteins. *Trends in Biotechnology*, *28*(5), 253–261.

Sou, S. N., Sellick, C., Lee, K., Mason, A., Kyriakopoulos, S., Polizzi, K. M., & Kontoravdi, C. (2015). How does mild hypothermia affect monoclonal

antibody glycosylation?. *Biotechnology and Bioengineering*, *112*(6), 1165–1176.

Steinebach, F., Ulmer, N., Wolf, M., Decker, L., Schneider, V., Wälchli, R., … Morbidelli, M. (2017). Design and operation of a continuous integrated monoclonal antibody production process. *Biotechnology Progress*, *33*(5), 1303–1313. https://doi.org/10.1002/btpr.2522.

Takuma, S., Hirashima, C., & Piret, J. M. (2007). Dependence on glucose limitation of the pCO2 influences on CHO cell growth, metabolism and IgG production. *Biotechnology and Bioengineering*, *97*(6), 1479–1488. https://doi.org/10.1002/bit.21376.

Templeton, N., Dean, J., Reddy, P., & Young, J. D. (2013). Peak antibody production is associated with increased oxidative metabolism in an industrially relevant fed-batch CHO cell culture. *Biotechnology and Bioengineering*, *110*(7), 2013–2024.

Templeton, N., Xu, S., Roush, D. J., & Chen, H. (2017). ^{13}C metabolic flux analysis identifies limitations to increasing specific productivity in fed-batch and perfusion. *Metabolic Engineering*, *44*, 126–133. https://doi.org/10.1016/j.ymben.2017.09.010.

Thiele, I., Price, N. D., Vo, T. D., & Palsson, B. O. (2005). Candidate metabolic network states in human mitochondria impact of diabetes, ischemia, and diet. *Journal of Biological Chemistry*, *280*(12), 11683–11695.

Voisard, D., Meuwly, F., Ruffieux, P. A., Baer, G., & Kadouri, A. (2003). Potential of cell retention techniques for large-scale high-density perfusion culture of suspended mammalian cells. *Biotechnology and Bioengineering*, *82*(7), 751–765. https://doi.org/10.1002/bit.10629.

Walsh, G. (2014). Biopharmaceutical benchmarks 2014. *Nature Biotechnology*, *32*(10), 992–1000.

Warikoo, V., Godawat, R., Brower, K., Jain, S., Cummings, D., Simons, E., … Konstantinov, K. (2012). Integrated continuous production of recombinant therapeutic proteins. *Biotechnology and Bioengineering*, *109*(12), 3018–3029.

Wolf, M. K. F., Closet, A., Bzowska, M., Bielser, J. M., Souquet, J., Broly, H., & Morbidelli, M. (2018). Improved performance in mammalian cell perfusion cultures by growth inhibition. *Biotechnology Journal*, e1700722. https://doi.org/10.1002/biot.201700722.

Xu, S., Hoshan, L., & Chen, H. (2016). Improving lactate metabolism in an intensified CHO culture process: Productivity and product quality considerations. *Bioprocess and Biosystems Engineering*, *39*(11), 1689–1702. https://doi.org/10.1007/s00449-016-1644-3.

SUPPORTING INFORMATION

Additional supporting information may be found online in the Supporting Information section at the end of the article.

How to cite this article: Becker M, Junghans L, Teleki A, Bechmann J, Takors R. Perfusion cultures require optimum respiratory ATP supply to maximize cell-specific and volumetric productivities. *Biotechnology and Bioengineering*. 2019;116:951–960. https://doi.org/10.1002/bit.26926

C List of Publications and Author Contribution

This chapter specifies my (Max Becker) contribution to manuscripts which have already been published in peer-reviewed international journals during the time at the IBVT. Manuscript I and II were prepared as a first author and are provided in the appendices A and B.

Manuscript I

Becker, M., Junghans, L., Teleki, A., Bechmann, J., Takors, R. (2019). The less the better: How suppressed base addition boosts production of monoclonal antibodies with Chinese Hamster Ovary Cells. Frontiers in Bioengineering and Biotechnology, 7, 76.

Max Becker (MB) performed the cultivations, extracellular analytics and modeling, and participated in designing the study, preparing the manuscript and performing the intracellular metabolomics.

Manuscript II

Becker, M., Junghans, L., Teleki, A., Bechmann, J., Takors, R. (2019). Perfusion cultures require optimum respiratory ATP supply to maximize cell-specific and volumetric productivities. Biotechnology and bioengineering, 116, 951 – 960.

MB performed the cultivations, extracellular analytics and modeling, and participated in designing the study, preparing the manuscript and performing the intracellular metabolomics.

Manuscript III

Junghans, L., Teleki, A., Wijaya, A. W., **Becker, M.**, Schweikert, M., Takors, R. (2019). From nutritional wealth to autophagy: In vivo metabolic dynamics in the cytosol, mitochondrion and shuttles of IgG producing CHO cells. Metabolic Engineering, 54, 145 - 159.

MB participated in performing the cultivations and intracellular metabolomics.

Manuscript IV

Sánchez-Kopper, A., **Becker, M.**, Pfizenmaier, J., Kessler, C., Karau, A., Takors, R. (2016). Tracking dipeptides at work-uptake and intracellular fate in CHO culture. AMB Express, 6(1), 48.

MB participated in performing the cultivations, extracellular analytics and data analysis.